

THE UNIVERSITY OF CALGARY

Nonlinearities in Biodielectrics

by

Stephen John Paddison

A DISSERTATION

**SUBMITTED TO THE FACULTY OF GRADUATE STUDIES
IN PARTIAL FULFILMENT OF THE REQUIREMENTS FOR THE
DEGREE OF DOCTOR OF PHILOSOPHY**

DEPARTMENT OF CHEMISTRY

CALGARY, ALBERTA

JULY, 1996

© Stephen John Paddison 1996

THE UNIVERSITY OF CALGARY
FACULTY OF GRADUATE STUDIES

The undersigned certify that they have read, and recommend to the Faculty of Graduate Studies for acceptance, a dissertation entitled "Nonlinearities in Biodielectrics" submitted by Stephen John Paddison in partial fulfillment of the requirements for the degree of Doctor of Philosophy.

R Paul

Supervisor, Dr. R. Paul, Chemistry

Wm G. Laidlaw

Dr. W.G. Laidlaw, Chemistry

A. Rauk

Dr. A. Rauk, Chemistry

K.V.I.S. Kaler

Dr. K.V.I.S. Kaler, Electrical and Computer Engineering

Peter Gascoyne

External Examiner, Dr. P.R.C. Gascoyne

M.D. Anderson Cancer Center, University of Texas

96/9/4

Date

Abstract

A mathematical model involving a nonlinear electric displacement vector at the interface of a spherical particle with a linear medium, has been derived to explain experimental observations of multiple Clausius–Mossotti factors in the low frequency (10Hz. – 1kHz.) domain in the dielectrophoretic spectrum of *tobacco* protoplasts. The developed model clearly demonstrates the active role of the electric field on influencing the physical properties of the medium–particle interface. Suitable choice of the second order parameters in permittivity and conductivity result in good qualitative agreement with the experimentally observed low frequency hysteresis loops.

These charged dielectrophoretically levitated particles (both *tobacco* and *canola* protoplasts) have also been observed to display stable periodic micro–motion within the same regime of the spectrum. An existing dynamical model, a highly nonlinear second order differential equation, constructed on the basis of Newton’s second law, has been extended to include: (a) cubic nonlinearity in the dielectrophoretic forces; (b) convective flow contributions as described by Oseen’s equation; and (c) a novel mathematical model to describe the nonlinear dependence of the particle surface charge on the electric field based on the solution of a Langevin equation. Numerical integration of the vector field by means of a Runge–Kutta sixth order algorithm, when evaluated over several frequencies and represented in phase plane portraits, provides an excellent means of estimating the surface charge, an important, and difficult to ascertain, fundamental cell property. Fast Fourier transforms of the numerical solutions show the experimentally observed higher harmonics in the micro-motion attesting to the significance of the electric field dependent dissociation constant of the carboxylic groups in the surface proteins. Application of Melnikov’s method to the dynamical system has shown that deterministic chaos is present, but is not realizable within

the experimental parameter space.

Acknowledgements

At the onset of this dissertation it is appropriate that several individuals be acknowledged for their significant contributions in my doctoral program here at the University of Calgary.

First, I wish to sincerely thank my supervisor , Professor Reginald Paul for his oversight, direction, patience, and mathematical skill.

I would also like to acknowledge Dr. William George Laidlaw for my original introduction into the area of deterministic chaos through a graduate course I took early in my program.

The opportunity to do experimental work in the laboratory of Dr. K.V.I.S. Kaler is experience I very much value; and I do thank him for the invitation to use his equipment.

I appreciated the profitable discussions in nonlinear dynamics with Dr. David Rod of the Mathematics and Statistics department here at the University of Calgary, and also for the use of his extensive mathematical library.

I would also like to thank Ms. Tanya Hooker for her work in the planting and preparation of the canola plants; and in the isolation of the protoplast samples used in the micromotion studies.

Finally, I wish to acknowledge the financial support of the Natural Sciences and Engineering Research Council (NSERC) of Canada through a Postgraduate Scholarship B, and the University of Calgary through a Silver Anniversary Fellowship.

to
the love of my life,
Joan Elaine

Table of Contents

Approval page	ii
Abstract	iii
Acknowledgements	v
Dedication	vi
Table of Contents	vii
List of Tables	xii
List of Figures	xiii
List of Symbols	xv
1 Introduction	1
1.1 Context of Research	1
1.2 Purpose of Research	1
1.3 Definitions	3
1.3.1 Nonlinear Phenomena	3
1.3.2 Biodielectrics	4
1.4 Properties of Nonlinear Dielectrics	4
1.5 Electrical Measurement Techniques	7
1.5.1 Cell Suspension Method	8
1.5.2 Micropipette Technique	8
1.5.3 Electrorotation Method	9
1.6 Electrophoresis and Dielectrophoresis	9
1.7 Single-Cell DEP Levitation Methods	11
1.7.1 Passive Levitation	12

1.7.2	Active Levitation	12
1.7.3	Dual-Frequency Levitation Scheme	13
1.8	Dissertation Outline	14
2	Theory	15
2.1	The Dielectrophoretic Force	15
2.1.1	The Net Force on an Infinitesimal Dipole	16
2.1.2	Derivation of the Effective Dipole Moment for a Lossless System	17
2.1.3	Extension of the Effective Dipole Moment to a Conducting System	23
2.1.4	Effective Moment Calculation of the DEP Force	24
2.1.5	Comparison of DEP Force Derivations	26
2.2	Shell Model Treatments	27
2.3	Polarization Mechanisms	29
2.3.1	Electronic, Atomic, and Dipolar Polarization	29
2.3.2	Maxwell-Wagner Polarization	30
2.3.3	Counterion Polarization	30
2.4	Theoretically Generated DEP Spectra	31
2.4.1	The DEP Spectrum of a Homogeneous Dielectric Sphere	32
2.4.2	The DEP Spectrum of a Homogeneous Concentric Dielectric Shell	33
3	Hysteresis	35
3.1	Introduction	35
3.2	Experimental Observations	35
3.3	Theoretical Thrust	36
3.4	Introduction of the Nonlinearity	37
3.5	Analytical Solutions of Quadratic Equation	47
3.6	Extraction of Real Clausius-Mossotti Factors	49
3.7	Numerical Computations and Comparison with Experiment	52

3.8	Conclusions	56
4	Micromotion	58
4.1	Introduction	58
4.2	Experimental	59
4.2.1	Measurement and Detection of Micromotion	62
4.2.2	Protoplast Preparation	63
4.3	Dynamical Equation of Study	64
4.3.1	Derivation	64
4.3.2	Approximations	66
4.3.3	Dimensionless Form	68
4.3.4	Comparison with Duffing Equation	69
4.4	Numerical Investigations	71
4.4.1	Initial Numerical Results	73
4.5	Additional Modelling	76
4.5.1	Nonlinear Hydrodynamic Interactions	76
4.5.2	Field-Dependent Surface Charge Model	77
4.6	Final Numerical Results	83
4.7	Conclusions	85
5	The Melnikov Method	88
5.1	Introduction	88
5.2	Definitions	88
5.2.1	The Vector Field	89
5.2.2	Phase Space	89
5.2.3	Initial Condition(s)	89
5.2.4	Solution(s)	89
5.2.5	Integral Curve	90

5.2.6	Orbit	90
5.2.6.1	Homoclinic Orbit	90
5.2.6.2	Heteroclinic Orbit	90
5.2.7	Manifold	90
5.2.8	Equilibrium Solution	90
5.2.9	Stability (of the fixed point)	91
5.2.10	Determination of Stability: Linearization	91
5.2.11	Stability Classification	92
5.2.11.1	Hyperbolic	92
5.2.11.1	Saddle Point	92
5.2.11.3	Stable Node (Sink)	93
5.2.11.4	Unstable Node (Source)	93
5.2.11.5	Center or Elliptic Point	93
5.2.12.1	Stable Manifold	93
5.2.12.2	Unstable Manifold	93
5.3	Derivation of the Melnikov Method	93
5.3.1	Perturbed Vector Field	94
5.3.2	Computation of the Separation Distance of the Stable and Unstable Manifolds	96
5.3.3	Melnikov Function	98
5.3.4	Final Remarks	98
5.4	Application of Melnikov's Method	99
5.5	Discussion of Results	110
6	Concluding Remarks	112
6.1	Connection	112
6.2	Future Research	112

References	114
Appendix	121

List of Tables

2.1	The first few Legendre polynomial terms	20
4.1	Micromotion Equation Parameters	73
5.1	Variable Transformations	110

List of Figures

2.1	Force on a dipole in a nonuniform electric field.	16
2.2	Schematic of lossless system consisting of dielectric particle and medium.	17
2.3	Spherical concentric dielectric shell with distinct shell and core permittivities.	27
2.4	DEP spectrum of a homogeneous dielectric sphere.	32
2.5	DEP spectrum of a homogeneous concentric dielectric shell.	33
3.1	Experimental DEP spectrum showing double valued Clausius–Mossotti factor in the low frequency region.	35
3.2	Representation of nonlinear boundary condition at particle–medium interface.	40
3.3	Behavior of the two Clausius–Mossotti factors for different values of the second–order parameters.	55
4.1	Sample FFT spectrum from the centroid detector obtained for a 45 μm –diameter protoplast excited by a 20 Hz., 1.0 V–rms AC signal.	60
4.2	Sample FFT spectrum from the centroid detector obtained for a 45 μm –diameter protoplast excited by a 2 Hz., 1.0 V–rms AC signal.	61
4.3	Cross–sectional view of the levitation chamber, showing the axisymmetric electrodes and the dual–frequency excitation scheme used to measure the DEP spectra of a lone protoplast.	62
4.4	Experimentally measured Canola protoplast DEP spectrum.	71
4.5	Mathematically generated phase plane portraits: (a) @ 100 Hz.; (b) @ 50 Hz.; and (c) @ 10 Hz.	74

4.6	Phase plane portrait solution from Eq. (4.18) with spring constants set to 0.	75
4.7	Diagram geometry for electric field frequency dependent surface charge model.	78
4.8	Phase plane portrait from numerical solution of Eq. (4.52) @ 20 Hz.; $G'_{11} = G_{10} = 2.69 \times 10^{-5}$.	85
4.9	Fourier transform of the displacement for the numerical solution displayed in Fig. 4.8.	86
4.10	Fourier transform of the displacement from the solution of Eq. (4.53) @ 10 Hz., with $G'_{12} = 1/2 \times G'_{11}$ and $G'_{11} = G_{10} = 2.69 \times 10^{-5}$.	87
5.1	Integration contour diagram.	106

List of Symbols

Operators:

d	<i>derivative</i>
D	<i>Jacobian space derivative</i>
∂	<i>partial derivative</i>
$O()$	<i>order of</i>
$\vec{\nabla}$	<i>gradient operator</i>
∇^2	<i>Laplacian (a scalar)</i>
\cdot	<i>dot or scalar product</i>
\times	<i>cross or vector product</i>
$\text{Re}\{ \}$	<i>real part</i>
$\text{Im}\{ \}$	<i>imaginary part</i>
$ $	<i>modulus, magnitude of</i>
$\langle \rangle$	<i>average (defined in context)</i>

Superscripts:

\sim	<i>dimensionless quantity</i>
\rightarrow	<i>vector quantity</i>
$*$	<i>complex conjugated quantity</i>
T	<i>transpose of the vector (a row vector)</i>
—	<i>time average</i>

Subscripts:

l	<i>liquid</i>
-----	---------------

m	<i>medium</i>
p	<i>particle</i>
s	<i>surface or solid</i>
$\underline{\quad}$	<i>complex quantity</i>
$\underline{\underline{\quad}}$	<i>dyadic tensor</i>

Notation:

$A_{1,m}$	<i>dipolar coefficient (general solution of Laplace's equation)</i>
α	<i>polarizability</i>
\vec{B}	<i>magnetic induction</i>
c	<i>speed of light</i>
\underline{C}_{mb}	<i>complex capacitance of the membrane</i>
\vec{D}	<i>electric field displacement vector (electric flux density)</i>
δ_{ij}	<i>Kronecker delta</i>
\vec{e}_i	<i>i^{th} unit vector in Cartesian space</i>
$e_{1,2}$	<i>charge of designated ion (1,2)</i>
\vec{E}	<i>electric field intensity</i>
E_0	<i>magnitude of applied electric field</i>
E_{rms}	<i>root-mean-square magnitude of applied electric field</i>
ϵ	<i>relative electric permittivity, dielectric constant</i>
ϵ_0	<i>permittivity of free space = $8.854 \times 10^{-12} \text{Fm}^{-1}$</i>
ϵ_m	<i>permittivity of medium</i>
ϵ_p	<i>permittivity of particle</i>
$\underline{\epsilon}$	<i>complex permittivity</i>

ε'	<i>real part of the complex permittivity</i>
ε''	<i>imaginary part of the complex permittivity</i>
$\underline{\varepsilon}^{(n)}(\omega)$	<i>n^{th} order complex permittivity tensor</i>
f	<i>frequency (Hz.)</i>
\vec{f}_e	<i>electromagnetic body force</i>
f	<i>unperturbed part of vector field</i>
\vec{F}_{DEP}	<i>dielectrophoretic force</i>
g	<i>perturbed part of vector field</i>
g_{mb}	<i>transmembrane conductance</i>
H	<i>Hamiltonian</i>
\vec{H}	<i>magnetic field intensity</i>
i	<i>complex number $\equiv \sqrt{-1}$</i>
\vec{J}	<i>current density vector</i>
k	<i>Boltzmann constant</i>
K	<i>dissociation/equilibrium/ionization constant</i>
\underline{K}_e	<i>complex Clausius–Mossotti factor</i>
$L(a)$	<i>Langevin function</i>
μ_D	<i>dipole moment</i>
$\underline{\mu}$	<i>complex magnetic permeability</i>
μ'	<i>real part of the complex magnetic permeability</i>
μ''	<i>imaginary part of the complex magnetic permeability</i>
\vec{n}_s	<i>unit normal vector to surface</i>
\vec{p}	<i>dipole moment</i>
\vec{p}_{eff}	<i>effective dipole moment</i>

$\vec{P}(t)$	<i>total polarization vector</i>
$P_n(\cos \theta)$	<i>n^{th} order Legendre polynomial</i>
$\underline{\underline{P}}$	<i>pressure tensor</i>
\vec{p}_e	<i>electromagnetic momentum density</i>
$\underline{\underline{\Pi}}$	<i>Maxwell stress tensor</i>
q	<i>net charge on particle surface</i>
Q	<i>Onsager's effective association length</i>
Q_{pw}	<i>dissipated power</i>
R	<i>radius of particle or cell</i>
\mathbb{R}^n	<i>n^{th} dimensional real space</i>
ϱ	<i>charge density</i>
σ	<i>conductivity</i>
$\sigma^{(n)}(\omega)$	<i>n^{th} order conductivity tensor</i>
Σ	<i>surface section</i>
\vec{t}_{ex}	<i>external force density vector</i>
\vec{t}_{sl}	<i>surface force density vector</i>
T	<i>period</i>
T	<i>temperature (K)</i>
τ	<i>mass density</i>
$\underline{\underline{U}}$	<i>unit tensor, identity matrix</i>
u	<i>mobility</i>
u_e	<i>electromagnetic field energy density</i>
$\chi^{(n)}(\omega)$	<i>n^{th} order susceptibility tensor</i>
ψ	<i>electric field potential</i>
V	<i>volume of spherical particle</i>

\vec{v}	<i>velocity</i>
\mathbf{x}	<i>time dependent position vector, vector field</i>
ω	<i>radian frequency of electric field</i>
z	<i>complex number</i>

Chapter 1: Introduction

1.1 Context of Research

The determination and study of the electric and dielectric properties of biological cells is actively pursued because of their importance in several areas including physiology, biophysics, and biomedical engineering (1). These properties determine the various pathways of current flow in the human body, and are therefore important in the experimental measurement of physiological parameters using impedance techniques, the study of the effects of electromagnetic fields on biological materials, nerve transmission, muscle contraction, and electrocardiography (2).

Precise measurement of the electrical cellular parameters can be used as a diagnostic tool to assess the effects of chemical agents, various drugs, and even nuclear radiation on living cells. In addition, they may be used to establish protocols to sort cells (3) and distinguish malignant cells from healthy cells (4). An understanding of the dielectric properties of the cells, along with cell–medium and cell–cell interactions is also crucial in modern biotechnology; where, in techniques such as electrofusion (5) and electroporation, it is very important to know the optimal applied field parameters including field strength and field frequency.

As biological cells are typically immersed in an electrolyte or suspension medium, the electrical properties are a function of the electrical makeup of the cellular components (i.e. the membrane and cytoplasm), and to some extent, the electrical properties of the medium. Thus, the underlying polarization mechanism(s) may be understood through monitoring the dielectric response of the cell.

1.2 Purpose of Research

Of the many experimental techniques developed to study and probe the dielectric properties of particles or biological cells (several, of which, will be discussed later in this chapter), the single cell dual–frequency feedback–controlled dielectrophoretic levita-

tion has proven to be a non-invasive technique, that has emerged as a powerful method for investigating the frequency-dependent polarization of living biological cells (6). Along with the various experimental approaches, a number of theoretical models have been proposed to explain and predict the electrical properties, the most popular being the shelled model (see §2.2) and its various analogues. Although the shelled model has been successful in providing an adequate explanation of high frequency (>100Hz.) polarizability, it has utterly failed in the low frequency regime.

Because of this discrepancy between experiment and theory, the dielectrophoretic response in the low frequency region has been referred to as *anomalous dielectrophoresis* (7), (8). Typically in this region, the DEP spectrum is characterized by a rise in the polarizability as the frequency is decreased; the real part of the Clausius–Mossotti factor (Eq. (2.36)) often exceeding a magnitude of 1. This anomalous response has been investigated in several recent papers (7), (9), (10), but still lacks a complete explanation.

More recently, hysteresis loops (see Fig. 3.1) in this same low frequency region of the DEP spectrum, have been observed from dual-frequency levitation experiments involving plant protoplasts upon reversing the direction of the frequency scan (the first scan proceeds in the direction of decreasing frequency; the reverse in the direction of increasing frequency); thus further complicating the polarizability of this region.

Because of the shortcomings of conventional theory in either predicting or explaining the occurrence of multiple valued Clausius–Mossotti factors in the low-frequency region of the spectra, it was the purpose of the initial investigation to model the observed hysteresis in order to obtain insight into the origin of the phenomena; and as well, if possible, offer some insight into the cause of the anomalous dielectrophoresis.

In addition to anomalous dielectrophoresis, a number of other related and unexplained experimental observations have been reported which include: batch-type DEP measurements on Friend murine erythroleukaemic cells (11), (12) and yeast cells (13); and electrorotation measurements on latex particles (14). Very recently, another significant

anomaly, in the low frequency regime, has been observed (9), (10); this being the oscillatory motion of single DEP levitated plant protoplasts. This motion has been referred to as *micromotion* (8), and has received intensive investigation both experimentally (9) and theoretically (10). Perhaps the most interesting observation reported by the authors was the fact that the micromotion was not simple harmonic motion at applied electric field frequencies below 20 Hz., but possessed significant higher harmonic components (see Figs. 4.1 and 4.2).

The previous investigations ((9), (10)) failed to explain the physical origins of the phenomena; and in addition, the micromotion models proposed by the authors, did not reproduce the experimentally observed higher harmonics. It was clear, however, that the observed dynamics were nonlinear, and thus, it is not surprising that the linear response theory previously proposed, did not provide an explanation for the origins of the phenomena.

Therefore, it was the intent of the second part of the research, to determine the physical mechanism of the observed higher harmonics in the micromotion of the particles in the very low frequency regime of the spectrum.

1.3 Definitions

The title of this dissertation, "Nonlinearities in Biodielectrics", involves two "big words", or perhaps more correctly, two specific concepts: these being: *nonlinear* and *biodielectric*. Thus, it is fitting that at the onset, concise definitions be given so as to make clear the context of the research.

1.3.1 Nonlinear Phenomena

The use of the word "nonlinear" to describe phenomena or observable dynamics of physical variables, identifies that the underlying processes are understood to be governed by nonlinear equations. Thus the classification of phenomena as being nonlinear, is the result of an observer's or theorist's description and physical insight (which is only an approximate rationale for what is seen) into that specific phenomena through mathematical modelling. Jackson (15) in his excellent text: "Perspectives of Nonlinear dynamics" suggests an operational definition for nonlinear phenomena as: "*Physical phenomena concern*

the interrelationship of a set of physical variables which are deterministic (within some accuracy). Nonlinear phenomena involve those sets of variables such that an initial change of one variable does not produce a proportional change in the behavior of that variable, or some other variable. In other words, the ratio (action/reaction) is not constant.” It should be realized that the interrelationship between the physical variables of a nonlinear process need not always be related in a nonlinear fashion; but for some situations may be related linearly.

1.3.2 Biodielectrics

Bodielectrics involves the study and investigation into the dielectric behavior of biological materials. Dielectrics, in contrast with conductors, are materials where all charges are attached to specific atoms or molecules; and thus the motion or movement of charge is constrained within the bulk of the material. The principal mechanisms by which electric fields can distort the charge distribution of a dielectric atom or molecule are two fold: stretching and rotating.

1.4 Properties of Nonlinear Dielectrics

It should be fairly apparent from the definitions presented thus far, that dielectric materials, whether biological or not, where the properties of the material are dependent on the intensity of an input signal (e.g. an electric field) are classified as nonlinear. Furthermore, it has been observed that the onset of nonlinearity also depends on the magnitude of the dipole moment and the stability of the individual molecules in the material. Several important mechanisms have been proposed to explain nonlinear electric polarization, and these will be discussed in this section.

The first theory of electric polarization of polar molecules was developed by Debye (16) who suggested that the mean dipole moment $\langle \mu_D \rangle$ of a group of molecules possessing a dipole moment μ_D , when subjected to an electric field, was:

$$\langle \mu_D \rangle = \mu_D \left[\frac{1}{3} \left(\frac{\mu_D E}{kT} \right) - \frac{1}{45} \left(\frac{\mu_D E}{kT} \right)^3 + \frac{2}{945} \left(\frac{\mu_D E}{kT} \right)^5 - \dots \right] \quad (1.1)$$

where E is the electric field intensity, k the Boltzmann constant, T the temperature, and the expansion in the square brackets, the Langevin function ($L(a)$) with argument $a = \mu_D E/kT$.

This expression (Eq. (1.1)) demonstrates that the mean moment is a function of the field intensity. The behavior of the Langevin function is plotted in Fig. 1.1. Examination of Fig. 1.1 shows that $\langle \mu_D \rangle$ increases linearly for small intensity fields but becomes nonlinear for large field intensities. Furthermore, for very large field intensities, the mean dipole moment approaches asymptotically the value of the dipole moment for the molecule; implying complete orientation or *dielectric saturation*. However, if the intensity of the applied field is small then all the higher-order terms in Eq. (1.1) may be neglected; and under these conditions, the polarizability $\alpha \equiv \langle \mu_D \rangle / E$, becomes:

$$\alpha = \frac{\langle \mu_D \rangle}{E} = \frac{\mu_D^2}{3kT} \quad (1.2)$$

It is clear from this equation that under conditions of a low intensity field, the polarizability is independent of E . It should also be realized that the onset of nonlinearity is also a function of the magnitude of μ_D ; i.e. nonlinear dielectric behavior may be observed for molecules possessing very large dipole moments with relatively small electric fields.

In addition to the mechanism of dielectric saturation for nonlinear electric polarization, several other causes of nonlinearity have been suggested. Wien (17) observed that Ohm's law is applicable to fields of only moderate intensity; that is, the resistance of strong or weak electrolytes may be independent of the voltage at low field intensities, but becomes voltage dependent at high field intensities. An additional effect observed by Wien, was the enhancement of the ionization of weak electrolytes upon subjection to strong electrical fields. Onsager (18) derived an equation that described the relative increase of the dissociation constant in the presence of a strong field:

$$\frac{K(E)}{K(0)} = 1 + 2\beta Q + \frac{(4\beta Q)^2}{2!3!} + \frac{(4\beta Q)^3}{3!4!} + \dots \quad (1.3)$$

where $K(E)$ is the ionization constant in the presence of a strong field; $K(0)$ the dissociation

constant in the absence of the applied field; and Q the effective association length defined by:

$$Q = -\frac{e_1 e_2}{2\epsilon kT} \quad (1.4)$$

where ϵ is the dielectric constant of the solvent; and e_1 and e_2 are the charges of the ions.

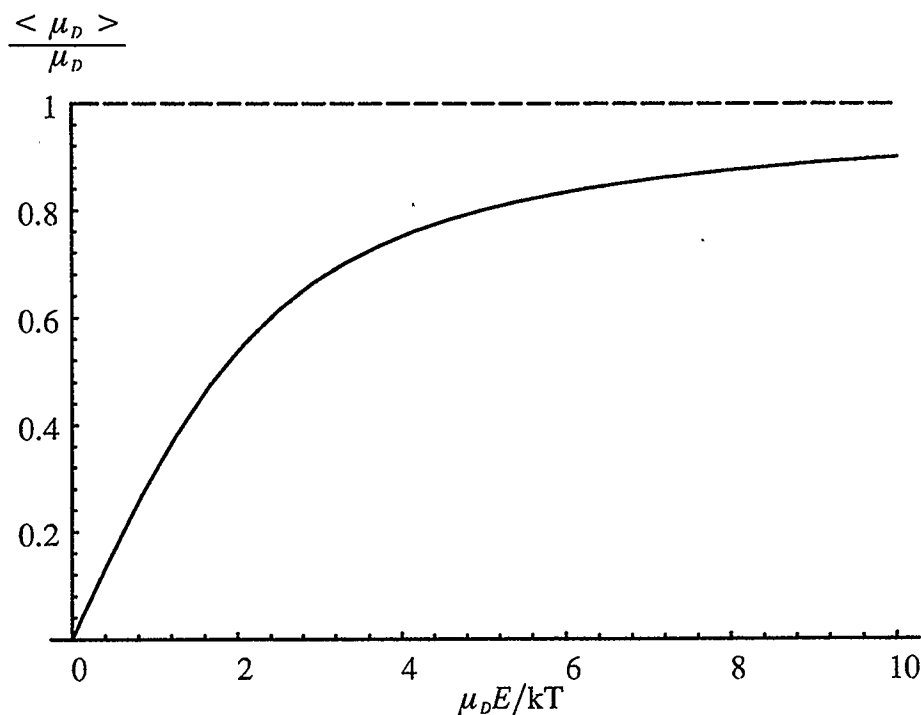


Fig. 1.1 The behavior of the Langevin function.

His theory was formulated such that if the distance r between two ions is larger than the association length Q , then the ions are considered separated and, if $r < Q$, the ions are considered paired. The quantity 2β in Eq. (1.3) is defined as follows:

$$2\beta \equiv \frac{|E(e_1 u_1 - e_2 u_2)|}{kT(u_1 + u_2)} \quad (1.5)$$

where u_1 and u_2 are the mobilities of the ions. In agreement with Onsager's theoretical predictions, he observed experimentally that the effect of an applied field was more pronounced when the dielectric constant of the solvent is small. Thus, he concluded that the field induced enhancement of the ionization of weak electrolytes was much more pronounced if the dielec-

tric constant of the solvent was small.

Further work was done on Onsager's theoretical formulation by Bass (19); who treated q as a field dependent quantity and assumed that the contour of the potential barrier surrounding an ion would be altered by the application of an electrical field. In this sense, the basic formulation proposed by Bass is distinct from the work of Onsager, although his derived ratio of $K(E)/K(0)$ is quite similar to Eq. (1.3). Takashima (20) has suggested that Bass' theory may be closer to the physical reality of nonlinear ionic processes.

Nonlinear polarization effects giving rise to positive and negative increments in the dielectric constant of polar molecules, were reported by Piekara (21) and Malecki (22). These nonlinear effects were attributed to changes of the dipole moment and/or the polarizability of the molecules by strong electric fields. They suggested that changes in the dipole moment may be due to conformation changes of the molecule or due to the realignment of dipoles causing enhancement or partial cancellation of effective moments. Piekara derived a correlation parameter to account for the nonlinear effects attributed to the interaction between a molecule and its near neighbors. Additional work was done by Böettcher and Bordewijk (23) who derived an extension to the second-order dielectric constant term.

Very little work has been done on the study of the nonlinear dielectric behavior of biological macromolecules. Block and Hayes (24) and Gregson *et al* (25) investigated dielectric saturation effects in poly-benzyl-L-glutamate; and Jones (26) measured the voltage dependent dielectric constant of myoglobin.

The discussion and survey of previous work on the observation and elucidation of the properties of nonlinear dielectrics has focused on the microscopic/molecular level. This dissertation is concerned with nonlinear dielectric properties of biological cells; and hence attention is now turned to the mesoscopic/cellular scale.

1.5 Electrical Measurement Techniques

As mentioned in the opening section of this dissertation, various techniques have been derived to quantify the characteristic dielectric response; and each is applicable

for a limited or specific set of circumstances and conditions. A brief discussion of the most common approaches is presented in this section.

1.5.1 Cell Suspension Method

The "cell suspension" method, a commonly employed technique in the study and determination of the frequency-dependent dielectric properties of both suspended biological cells and tissue (2), (27), involves the application of an electrical potential across a chamber in which a collection of cells are suspended in a conducting medium. The resistance is higher for the suspension than for the pure suspending medium, and this allows the determination of cellular properties such as volume and membrane capacitance (28). The capacitance and conductance are both measured using a sensitive impedance bridge technique over a wide frequency range. From such measurements, the effective permittivity of the cells may be extracted by invoking the applicable dielectric mixture formulae (2), (29), (30); and in addition, valuable insight into the frequency-dependent polarization response mechanisms of the intact cells may also be obtained.

There are, however, some deficiencies in the suspension method. As the measurements are performed on a collection of cells, the cellular parameters are only "averaged" values and the variation of individual cell characteristics can not be assessed. In addition, since the measurements are all based on the relative change of impedance of the suspension chamber, a relatively high concentration of cells is required in order to observe a change, which results in cell-cell interactions that introduce error into the derived effective permittivity.

1.5.2 Micropipette Technique

The micropipette technique was devised by several investigators (31) to measure the membrane conductance and capacitance of a selected individual cell for the purpose of studying the ion transport properties of the cell membrane. The micropipette, a borosilicate glass capillary, is filled with a brine solution and functions as a probing electrode. During a typical conductance measurement, a tight seal is maintained between the cell and the

tip of the micropipette through the application of a weak suction. A measuring bridge is set up between this tip electrode and the reference electrode immersed in the suspending medium. The measurements are limited to low frequency (~ 4 Hz. – 1000 Hz.) due to the large parasitic impedance of the micropipette.

1.5.3 Electrorotation Method

An additional technique developed to investigate the dielectric properties of single cells is the electrorotation method (32), (33). This technique examines the rotational response of biological cells induced by a rotating AC electric field. Sauer (34) has shown that the torque exerted on a polarized particle is related to the imaginary part of the excess effective polarizability \underline{K}_e (see § 2.1.3 for a derivation of this quantity). The rotational velocity, in turn, may be related to $\text{Im}\{\underline{K}_e\}$ when the particle rotation reaches a steady-state. By measuring the cell rotation rate as a function of the applied field frequency the imaginary part of the effective polarization spectrum may be plotted. By fitting this experimentally determined rotation spectrum to a suitable theoretical model, the dielectric properties of membrane capacitance and conductance may be extracted. A practical drawback to this method is the difficulty arising in the data collection. Quite recently, Kaler and Sheng (35) have developed a new approach for detecting the velocity of the rotating cell using a digital image processing method.

Prior to discussing additional single cell dielectric measurement methods, it is needful to interject a description of the physical phenomena on which these techniques are based; namely, electrophoresis and dielectrophoresis.

1.6 Electrophoresis and Dielectrophoresis

Electrophoresis is the phenomenon where a charged particle responds to Coulombic forces induced by an externally applied electric field. The electrophoretic response is dependent on both the magnitude and sign of the net charge on the particle, and also on the field polarity. Consequently, the behavior differs for DC and AC electric fields, but is unaffected by field inhomogeneities.

The majority of cell types maintain a net negative surface charge under normal physiological conditions (36), (37). Thus, when placed in a DC electrostatic field, the cells tend to move toward the anode electrode. Through measurement of this electrophoretic velocity, the net surface charge has been estimated (see §4.4 for numerical values). Electrophoresis has also been used for cell separation (38).

Dielectrophoresis (DEP), in contrast to electrophoresis, is the translational response of electrically polarizable particles (charged or uncharged) when subjected to an inhomogeneous electric field (39). As this phenomenon is operable on neutral particles, it is independent of the electric field polarity. Here, this dielectrophoretic force is a function of the excess effective polarizability of the particle with respect to the surrounding medium, the frequency of the applied field, the local field magnitude and gradient, and the particle shape and volume (for the exact mathematical details the reader is referred to Chapter 2).

The phenomenon of dielectrophoresis has been successfully used in various industrial applications including the pumping of liquids and powders, the classification and separation of minerals, the removal of particulate matter in liquid or gas suspensions, and the anchoring of toner particles in xerography. Dielectrophoresis has primarily been applied to biological cells in the following three ways: (a) the measurement of the polarization spectrum of various cells over a wide frequency range; (b) the separation of cells differing in polarization characteristics; and (c) the manipulation and interrogation of cells. Since the 1970's, several investigations have been conducted on the behavior of bio-particles under nonuniform electric fields with various methods, based on the principles of DEP, being developed (40). Most of these approaches and techniques are based on an indirect measurement of the DEP force, performed on a sample containing a large quantity of cells; and therefore, the methods are inevitably subject to error and an averaged effect. However, these problems have largely been circumvented through the introduction of DEP levitation (41).

Return is now made to the discussion of additional dielectric measurement techniques; the following been based on DEP levitation schemes.

1.7 Single-Cell DEP Levitation Methods

Levitation is a very effective method of studying small particle properties and interactions. Techniques have been successfully developed to levitate particles with several types of fields including: magnetic fields, acoustic fields, and electric fields. DEP levitation is the three dimensional confinement of a single particle, where the gravitational and buoyant (due to the presence of the suspending medium) forces are balanced by the dielectrophoretic force. This is achieved by suspending a single particle between two electrodes constructed in such a manner as to produce an inhomogeneous electric field. Therefore, it offers the opportunity to investigate the polarization response of single particles with much improved accuracy over the other techniques outlined above.

All of the DEP levitation techniques discussed below exploit both the voltage dependence and the frequency dependence of the DEP force (see §2.1.4 for explicit functionality details). Essential to this is the fact that both parameters (V, f) may be varied independently of one another. The DEP force changes as the the applied electric field frequency is varied, while the gravitational–buoyancy force remains fixed. This results in the particle being displaced from its initial position and thus, the DEP force must be adjusted accordingly through the voltage dependence to return the particle to its equilibrium position at the new frequency. Provided that a force balance is maintained, the equation describing the equilibrium situation can be manipulated to yield the excess effective polarization of the particle as a function of the frequency; with the result being the construction of DEP spectrum (see §2.1.4)

In the following sections, three experimental methods of obtaining DEP spectra are outlined. All three techniques are based on the principles outlined above. The distinctions between them arises as a result of the equilibrium stability requirements. For stable equilibrium situations, no feedback control is required. However, for cases where an unstable equilibrium exists, there is the requirement of externally (typically through the electronic instrumentation) establishing and maintaining the stability of the particle at a fixed

point. It should be noted that biological cells suspended in aqueous media, typically exhibit both positive and negative DEP depending on the particular regime of the frequency spectrum.

1.7.1 Passive Levitation

The most straightforward situation is where the particle exhibits only *negative* DEP (see §2.1.4 for further description), that is the displacement of the particle under the action of the external inhomogeneous field is to the region of lower field intensity. Jones and Bliss (42) generated an axisymmetric electric field using a ring–disk electrode geometry, by which they successfully stably levitated bubbles, droplets, and dielectric particles in three dimensions. With this geometry, localized minima in the electric field exist which are detached from the electrode surfaces. The electric field gradients in both the axial and radial directions are sufficiently strong so as to center the particle along the vertical axis, counteracting the buoyant force. This type of levitation that requires no feedback to maintain the particle at a fixed position is referred to as *passive levitation*.

1.7.2 Active Levitation

The levitation of particles that exhibit *positive* DEP (see §2.1.4 for further description) is complicated by the fact that to stably levitate the particle in a similar manner as described in passive levitation would require an isolated maximum in the field. This requirement is not possible for divergence and curl–free electrostatic fields, as a maximum can only occur at an electrode surface. This situation is therefore one of unstable equilibrium; that is, any slight displacement is greatly magnified and the particle will inherently move toward one of the electrode surfaces where the maximum (positive DEP) or minimum (negative DEP) exists. Practically, the focused electric field is not capable of simultaneously ensuring both radial and axial stability; the details of the analysis which may be found in the paper by Holmes (43). Therefore, stable levitation may only be achieved for particles exhibiting positive DEP where feedback–control is implemented (44), (45). This technique involves the use of an axisymmetric cusped shaped electrode with a plate electrode (the com-

plete details of the apparatus may be found in §4.2). Radial stability is passively achieved using the focused electric field produced by the conic electrode; and axial stability is achieved through feedback control.

1.7.3 Dual-Frequency Levitation Scheme

As was alluded to previously, a biological cell will exhibit both positive and negative DEP: positive DEP in the intermediate and high frequency regions; and negative DEP at low frequencies. This fact makes it impossible to obtain dielectrophoretic measurements over the entire frequency spectrum when using the same experimental apparatus as described in §1.7.2. The reason for this is that in the region of negative DEP, both the DEP and the net gravitational–buoyancy force act in the same direction (this is assuming, of course, that the density of the particle is greater than the density of the suspending medium) with the result that a balance of forces is impossible. Therefore, to obtain data in the negative DEP region (the low frequency region) using the same electrode configuration and feedback control as was used in the positive DEP region, a *dual-frequency levitation* technique was devised (6).

The principle behind the dual-frequency levitation scheme is to utilize a positive DEP force to balance the negative DEP force and the net gravitational–buoyancy force when levitating a biological cell in regions of negative DEP. This is achieved by synthesizing two AC voltages of distinct frequencies ($f_1 < f_2$). It has been shown (46) that the mean-square of the sum of two sinusoids is approximately equal to the sum of the mean-squares of each sinusoid if and only if the two frequencies are well separated. The situation is the same as for feedback-controlled levitation in the frequency region for which positive DEP exists; that is, a balance is maintained between the positive DEP and the net gravitational–buoyancy force by adjusting a single frequency voltage. When the frequency has been reduced to where a cross over occurs to negative DEP, the second field component, driven at the higher fixed frequency (f_2), is added. The low field frequency voltage (V_1) is fixed and the high field frequency voltage (V_2) is adjusted by the feedback-controller to achieve and

maintain levitation.

1.8 Dissertation Outline

In this dissertation, the anomalous observations of hysteresis and higher harmonic components in the micromotion have been theoretically explored with the intent of obtaining insight into the underlying mechanism(s). Chapter 2 reviews in some detail the basic conventional theory of dielectrophoresis: including a derivation of the DEP force and discussion of typical models and polarization mechanisms. The novel experimental observation of hysteresis loops in the DEP spectrum of levitated plant protoplasts are presented in Chapter 3, along with the derivation and results of the mathematical modelling. Chapter 4 begins with a discussion of the experimental setup and measurement technique implemented in the detection of the micromotion of levitated plant protoplasts; followed with an overview of previous modelling; and concluding with a presentation of the new modelling investigations. The Melnikov method is derived and applied to the micromotion system in Chapter 5. The final chapter, Chapter 6, connects the two theoretical investigations together, and makes suggestion of possible future research.

Chapter 2: Theory

As was alluded to in the introductory chapter of this dissertation, there is a significant amount of basic theory lying at the foundation of dielectrophoresis. The review and presentation of this material is both useful and beneficial if the specific theoretical contributions of the modelling done on hysteresis (Chapter 3) and micromotion (Chapter 4) are to be understood. The material presented in this chapter is based primarily on: the venerable and excellent tome of Stratton on electromagnetic theory (47); Pohl's monograph on dielectrophoresis (39); and the very recent engineer's text on the electromechanics of particles by Jones (48).

2.1 The Dielectrophoretic Force

An appropriate starting point is to be realized in the derivation of the DEP force experienced by a spherical, polarizable, and homogeneous particle immersed in a homogeneous dielectric medium subjected to a nonuniform electric field. The DEP force is, in essence, the force experienced by a dipole (permanent or induced) in a nonuniform electric field and hence it is convenient to consider its derivation in 3 steps: (1) the net force on an infinitesimal dipole subject to a nonuniform field; (2) the derivation of the effective dipole moment in a lossless system consisting of a dielectric sphere in a dielectric medium; and (3) the effective moment method calculation of the DEP force. The results will then be extended to the more physically realistic situation allowing for dielectric losses in both the particle and the medium. This type of approach shows the basic assumptions that are involved in obtaining an expression for the ponderomotive force experienced by dielectrics in an inhomogeneous electrostatic field. This rather straight forward result for the DEP force is then compared to the result of the DEP force rigorously derived by Sauer (49), (34) based on the Maxwell stress tensor and the principle of the conservation of electromagnetic momentum density; the full details, which are to be found in the Appendix.

2.1.1 The Net Force on an Infinitesimal Dipole

Consider a finite dipole consisting of oppositely charged point charges of equal magnitude $+q$ and $-q$ separated by a distance \vec{d} located in an electric field \vec{E} ; shown pictorially in Fig. 2.1.

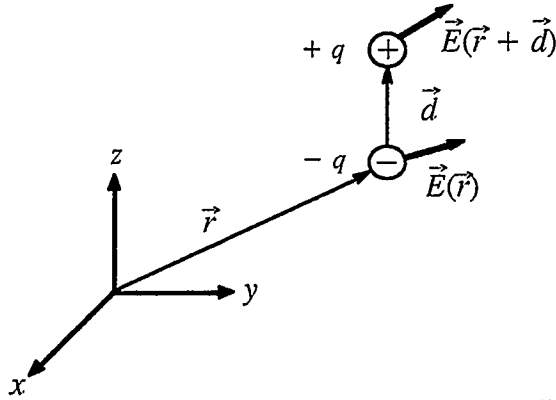


Fig. 2.1 Force on a dipole in a nonuniform electric field.

As the electric field is not uniform, the two point charges experience different values of the electric field with the net effect being that the dipole itself experiences a net force, \vec{F}_{dipole} given by:

$$\vec{F}_{dipole} = q\vec{E}(\vec{r} + \vec{d}) + (-q)\vec{E}(\vec{r}) \quad (2.1)$$

where \vec{r} is the position vector of the negative point charge ($-q$). Now if the magnitude of \vec{d} is small compared to the characteristic dimension of electric field nonuniformity, then the electric field experienced by the positive point charge may be expanded according to the Taylor expansion:

$$\vec{E}(\vec{r} + \vec{d}) = \vec{E}(\vec{r}) + \vec{d} \cdot \vec{\nabla} \vec{E}(\vec{r}) + \dots \quad (2.2)$$

If the higher order terms (terms that express the contribution of higher order poles) in Eq. (2.2) are neglected (being small) and the result substituted into Eq. (2.1), one obtains for the net force of this finite dipole:

$$\vec{F}_{dipole} = q\vec{d} \cdot \vec{\nabla} \vec{E} \quad (2.3)$$

After conventional formalism, the dipole moment may be defined according to:

$$\vec{p} \equiv q\vec{d} \quad (2.4)$$

and if the limit $|\vec{d}| \rightarrow 0$ is taken with the constraint that the dipole moment remains finite, then Eq. (2.3) becomes the net force of an infinitesimal dipole in a nonuniform electric field:

$$\vec{F}_{dipole} = \vec{p} \cdot \vec{\nabla} \vec{E} \quad (2.5)$$

It should be noted that this approximation for the net force, referred to as the *dielectrophoretic approximation*, is fairly good for typical conditions where the electric field nonuniformity is large compared to the particle dimensions.

2.1.2 Derivation of the Effective Dipole Moment for a Lossless System

Consider an insulating dielectric sphere of radius R and permittivity ϵ_p suspended in a fluid medium of permittivity ϵ_m and subjected to a *uniform* electric field $\vec{E}(\vec{r}) = E_0\vec{e}_z$; it may be conveniently represented by Fig. 2.2.

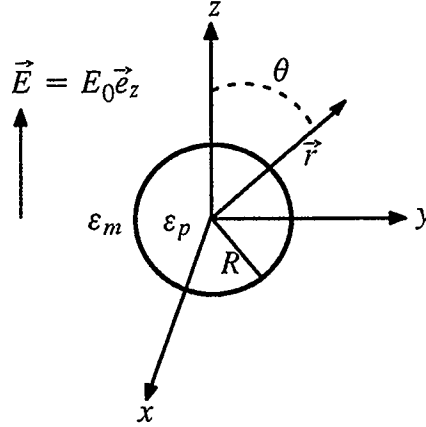


Fig. 2.2 Schematic of lossless system consisting of dielectric particle and medium.

Initially, expressions for the electric potentials of both the particle and the medium, must be derived. It should be realized that the higher order multipoles will make no contribution because of the insistence that the field be uniform in the initial phase of the derivation. An appropriate starting point for this electrostatic problem is the Maxwell's equations:

$$\vec{\nabla} \times \vec{E} + \frac{\partial \vec{B}}{\partial t} = 0 \quad (2.6)$$

$$\vec{\nabla} \times \vec{H} - \frac{\partial \vec{D}}{\partial t} = \vec{J} \quad (2.7)$$

where \vec{E} and \vec{H} are the intensities of the electric and magnetic fields respectively, \vec{D} the electric field displacement, \vec{B} the magnetic field induction, and \vec{J} the current density vector. The divergence of Eq. (2.7) yields the important result:

$$\frac{\partial}{\partial t}(\vec{\nabla} \cdot \vec{D}) + \vec{\nabla} \cdot \vec{J} = 0 \quad (2.8)$$

where use has been made of: (a) the divergence of the curl of any vector vanishes identically; and (b) the commutability of the two operators $\vec{\nabla}$ and $\frac{\partial}{\partial t}$. Recognition of the significance of Eq. (2.8) is made by recalling the definition of the current, I :

$$I \equiv \int_S \vec{J} \cdot \vec{n}_s \, da \quad (2.9)$$

where S is the surface, \vec{n}_s the normal vector to the surface, and da an infinitesimal surface element; and realizing the obvious relationship between the current with the charge density, ρ :

$$I = - \frac{d}{dt} \int_V \rho \, dv = - \int_V \frac{\partial \rho}{\partial t} \, dv \quad (2.10)$$

where V is the volume, dv the infinitesimal volume element, and the second equality is the result of assuming that the surface through which charge passes is fixed and that the integral is convergent. Applying Gauss' divergence theorem to Eq. (2.9) gives:

$$\int_S \vec{J} \cdot \vec{n} \, da = \int_V \vec{\nabla} \cdot \vec{J} \, dv \quad (2.11)$$

and therefore equating the results of Eqs. (2.10) and (2.11) yields:

$$\int_V \left(\vec{\nabla} \cdot \vec{J} + \frac{\partial \rho}{\partial t} \right) \, dv = 0 \quad (2.12)$$

Now if this integral is to vanish for arbitrary volumes V , it is necessary that the integrand be identically zero, i.e.:

$$\vec{\nabla} \cdot \vec{J} + \frac{\partial \rho}{\partial t} = 0 \quad (2.13)$$

Now the differential equation given in Eq. (2.13) is a continuity equation expressing the principle of the conservation of charge in the neighborhood of a point. Substitution of Eq. (2.13) into Eq. (2.8) gives:

$$\frac{\partial}{\partial t} (\vec{\nabla} \cdot \vec{D} - \rho) = 0 \quad (2.14)$$

and with the assumption that at some time in its past or future the field may have or may vanish, one obtains the following result:

$$\vec{\nabla} \cdot \vec{D} = \rho \quad (2.15)$$

which is a familiar result and implies that the sources of the electric displacement are the result of the distribution of charges with density ρ .

It should be clear that the results derived so far, are completely general and thus apply for any system lossy or otherwise. For the problem, described above in Fig. 2.2, it has been assumed that there is no free charge anywhere in the sphere or the dielectric medium; and therefore ρ , in Eq. (2.15), can assumed to be equal to zero. If, in addition, it is assumed that the displacement vector in both dielectric regions has only a linear dependence on the electric field intensity, i.e.:

$$\vec{D}_p = \epsilon_p \vec{E}_p \quad \vec{D}_m = \epsilon_m \vec{E}_m \quad (2.16)$$

then from Eq. (2.15) the following two equalities hold:

$$\vec{\nabla} \epsilon_p \cdot \vec{E}_p + \epsilon_p \vec{\nabla} \cdot \vec{E}_p = 0 \quad \vec{\nabla} \epsilon_m \cdot \vec{E}_m + \epsilon_m \vec{\nabla} \cdot \vec{E}_m = 0 \quad (2.17)$$

If both the sphere and the medium are homogeneous then:

$$\vec{\nabla} \epsilon_p = \vec{\nabla} \epsilon_m = 0 \quad (2.18)$$

and hence Eq. (2.17) becomes:

$$\vec{\nabla} \cdot \vec{E}_p = 0 \quad \vec{\nabla} \cdot \vec{E}_m = 0 \quad (2.19)$$

which expresses, of course, that the electric field is divergence-free. Now if the electric field

in both regions is also curl-free, then the electric field must be the gradient of some scalar function:

$$\vec{E}_p = -\vec{\nabla}\psi_p, \quad \vec{E}_m = -\vec{\nabla}\psi_m \quad (2.20)$$

where $\psi_{p,m}$ are the electric field potentials of the particle or sphere and the medium respectively; and therefore with substitution into Eq. (2.19) gives Laplace's equation for each region:

$$\nabla^2\psi_p = 0 \quad \text{and} \quad \nabla^2\psi_m = 0 \quad (2.21)$$

where because of the azimuthal symmetry, the Laplacian has the form:

$$\nabla^2 = \frac{\partial}{\partial r} \left(r^2 \frac{\partial}{\partial r} \right) + \frac{1}{\sin \theta} \frac{\partial}{\partial \theta} \left(\sin \theta \frac{\partial}{\partial \theta} \right) \quad (2.22)$$

The solution of Laplace's equation in polar coordinates is, of course:

$$\psi(r, \theta) = \sum_{n=1} \frac{A_n}{r^{n+1}} P_n(\cos \theta) + \sum_{n=1} B_n r^n P_n(\cos \theta) \quad (2.23)$$

where A_n and B_n are arbitrary constants and $P_n(\cos \theta)$ the standard Legendre polynomials, the first few terms of which are given in Table 2.1.

Table 2.1 *The first few Legendre polynomial terms*

n	$P_n(\cos \theta)$
0	1
1	$\cos \theta$
2	$\frac{1}{2}[3 \cos^2 \theta - 1]$
3	$\frac{1}{2}[5 \cos^3 \theta - 3 \cos \theta]$

As Eq. (2.23) expresses a superposition of solutions, i.e. $\psi(r, \theta) = \sum_{n=1} \psi_n$, then, for simplicity, the first term in the summation ($n=1$) is chosen as an appropriate solution. Thus, acceptable solutions of Eq. (2.21) are:

$$\psi_p(r, \theta) = \frac{A_{1,p}}{r^2} \cos \theta + B_{1,p} r \cos \theta \quad \psi_m(r, \theta) = \frac{A_{1,m}}{r^2} \cos \theta + B_{1,m} r \cos \theta \quad (2.24)$$

Physical constraints to the problem impose the two conditions:

$$\begin{aligned} \lim_{r \rightarrow \infty} \psi(r, \theta) &= -E_0 r \cos \theta \\ -\infty &< \lim_{r \rightarrow 0} \psi(r, \theta) < \infty \end{aligned} \quad (2.25)$$

where the first condition is the requirement that at distances far away from the particle, the electric field is simply the applied field; and the second condition, that the electric field must remain finite at all places within the particle. Thus, with application of these two conditions to the electric field potentials of the two regions (Eq. (2.24)), one obtains:

$$\psi_p(r, \theta) = B_{1,p} r \cos \theta \quad (2.26)$$

$$\psi_m(r, \theta) = \frac{A_{1,m}}{r^2} \cos \theta - E_0 r \cos \theta \quad (2.27)$$

In addition to the constraints of Eq. (2.25), there are also the following important boundary conditions which occur at the particle–medium interface:

$$\psi_p(R, \theta) = \psi_m(R, \theta) \quad (2.28)$$

$$\vec{D}_p(R, \theta) \cdot \vec{n}_s = \vec{D}_m(R, \theta) \cdot \vec{n}_s \quad (2.29)$$

where Eq. (2.28) expresses the principle of the continuity of the electric field potential across the particle–medium boundary; and Eq. (2.29) declares that the normal component of the electric flux density vector must be continuous across the uncharged surface separating the two regions (\vec{n}_s is the unit normal vector at the surface). Now if the linear relations of Eq. (2.16) are again assumed, then Eq. (2.29) becomes:

$$\epsilon_p \vec{E}_p(R, \theta) \cdot \vec{n}_s = \epsilon_m \vec{E}_m(R, \theta) \cdot \vec{n}_s \quad (2.30)$$

Applying the boundary conditions, Eqs. (2.28) and (2.30), to the derived electric field potential solutions, Eqs. (2.26) and (2.27), gives the electric field potentials for the two regions:

$$\psi_p(r, \theta) = - \left(\frac{3\epsilon_m}{\epsilon_p + 2\epsilon_m} \right) E_0 r \cos \theta \quad (2.31)$$

$$\psi_m(r, \theta) = \left(\frac{\epsilon_p - \epsilon_m}{\epsilon_p + 2\epsilon_m} \right) \frac{R^3 E_0 \cos \theta}{r^2} - E_0 r \cos \theta \quad (2.32)$$

Of the two derived potentials, it is Eq. (2.32) that is of particular significance, as the first term on the right hand side has the form of a dipolar potential. It is the result of the dipole induced on the sphere as a consequence of an applied external electric field. The electrostatic potential Ψ due to a finite dipole consisting of two point charges $+q$ and $-q$, separated by a distance d and aligned on the z -axis, immersed in a linear dielectric of permittivity ϵ_m , is:

$$\Psi(r, \theta) = \frac{qdP_1(\cos\theta)}{4\pi\epsilon_m r^2} + \frac{qd^3P_3(\cos\theta)}{16\pi\epsilon_m r^4} + \dots \quad (2.33)$$

where the first term is the dipole term and the second is the octupolar term; with higher order terms following. Recognizing that the product qd is the effective dipole moment p_{eff} , the dipole potential in Eq. (2.33) may be written in terms of an effective dipole moment:

$$\psi_{dipole}(r, \theta) = \frac{|\vec{p}_{eff}| \cos\theta}{4\pi\epsilon_m r^2} \quad (2.34)$$

Comparison of Eq. (2.34) to the induced electric dipole term in Eq. (2.32) yields the result for the effective dipole moment of the homogeneous, dielectric sphere:

$$|\vec{p}_{eff}| = 4\pi\epsilon_m \left(\frac{\epsilon_p - \epsilon_m}{\epsilon_p + 2\epsilon_m} \right) R^3 E_0 \quad (2.35)$$

It is worth recognizing at this point, that the ratio of permittivities in Eq. (2.35) is the so called *Clausius–Mossotti factor* or function, K_e :

$$K_e(\epsilon_p, \epsilon_m) \equiv \frac{\epsilon_p - \epsilon_m}{\epsilon_p + 2\epsilon_m} \quad (2.36)$$

The Clausius–Mossotti factor provides a measure of the magnitude of the effective polarization of the spherical particle as a function of ϵ_p and ϵ_m . If one recalls that for an isotropic dielectric sphere, that is one in which the electrical properties at a particular point are independent of the direction of the applied field, the induced dipole moment is related to the electric field through the polarizability α , according to:

$$\vec{p} = \frac{4}{3}\pi R^3 \alpha \vec{E} \quad (2.37)$$

then the Clausius–Mossotti factor is essentially a measure of the *excess effective polarizability*

ty of the sphere; comparison of Eq. (2.37) with Eq. (2.35) and use of the definition in Eq. (2.36) reveals the following relationship between the Clausius–Mossotti factor and the polarizability:

$$K_e = \frac{\alpha}{3\epsilon_m} \quad (2.38)$$

2.1.3 Extension of the Effective Dipole Moment to a Conducting System

Now the derivation in §2.1.2 began with the explicit assumption that both the sphere and the medium were non-conducting and that the applied electric field was a constant DC field. The derivation is extended to the situation where conductive losses occur in both the particle and the medium and the electric field is a sinusoidal steady-state AC electric field. The ohmic loss is incorporated into the system through making the permittivities complex:

$$\underline{\epsilon}_p = \epsilon'_p + \frac{\sigma_p}{i\omega} \quad \underline{\epsilon}_m = \epsilon'_m + \frac{\sigma_m}{i\omega} \quad (2.39)$$

where the underscoring indicates a complex quantity; $\sigma_{p,m}$ are the conductivities of the particle and the medium, respectively; and ω the radian frequency of the AC electric field ($i = \sqrt{-1}$). The applied field is uniform and periodic, with a magnitude of E_0 , and therefore may be represented as:

$$\vec{E}(t) = \text{Re}\{E_0 \vec{e}_z e^{-i\omega t}\} \quad (2.40)$$

The same geometry as represented in Fig 2.2 is assumed, and thus all the governing and constraining equations are the same with the exception that the second boundary condition becomes:

$$\underline{\epsilon}_p \vec{E}_p(R, \theta, t) \cdot \vec{n}_s = \underline{\epsilon}_m \vec{E}_m(R, \theta, t) \cdot \vec{n}_s \quad (2.41)$$

where the electric fields are now explicitly time dependent and the permittivities complex. This leads to similar results as before except the Clausius–Mossotti factor becomes complex:

$$\underline{K}_e(\underline{\epsilon}_p, \underline{\epsilon}_m) \equiv \frac{\underline{\epsilon}_p - \underline{\epsilon}_m}{\underline{\epsilon}_p + 2\underline{\epsilon}_m} \quad (2.42)$$

and thus the effective moment in Eq. (2.35) becomes complex:

$$\vec{p}_{eff} = 4\pi\epsilon_m K_e R^3 \vec{E} \quad (2.43)$$

It is important to note that the measured effective moment $\vec{p}_{eff}(t) = \text{Re}\left\{\vec{p}_{eff} e^{-i\omega t}\right\}$ may be envisaged as the moment of a time-varying equivalent free charge dipole that produces the same electrostatic field in the same dielectric medium. Furthermore, because the Clausius–Mossotti factor is complex, both its magnitude and phase are functions of the field frequency. This phase angle represents the lag between the applied electric field and the induced dipole moment. Jones (48) points out that such ohmic, dispersive behavior is the result of the finite time required to build up a surface charge at the interface. It should also be realized that the permittivity of the medium appearing explicitly in Eq. (2.43) can *not* be complex because its origin is based on Gauss’s law of charge interaction relating the charge to the electric field.

2.1.4 Effective Moment Calculation of the DEP Force

Attention is now given to the problem of calculating the dielectrophoretic force on the homogeneous, dielectric, spherical particle immersed in a dielectric medium (fluid) as represented in Fig 2.2. The effective moment method of calculating the DEP force is based on the assumption that the force may be related to the effective moments identified from the calculated induced electrostatic field due to the particle. Thus within this framework, it may be assumed from Eq. (2.5) that the DEP force can be calculated from the relation:

$$\vec{F}_{DEP}(t) = \vec{p}_{eff}(t) \cdot \vec{\nabla}\vec{E}(t) \quad (2.44)$$

where all quantities are real and instantaneous functions of time. It should be realized that there will be higher-order moment contributions to this force which will be significant if the nonuniformity of the applied electric field is made substantial. Furthermore, Eq. (2.44), strictly speaking, only applies to systems that are *lossless*. For the more physically realistic situation where conductive losses occur in either or both the particle and medium, potential energy is not conserved and thus the foundations of this method of force calculation is not

tenable. Hence for the lossless system of §2.1.2, in combining Eqs. (2.35) and (2.44) one obtains:

$$\vec{F}_{DEP} = 2\pi\epsilon_m R^3 \left(\frac{\epsilon_p - \epsilon_m}{\epsilon_p + 2\epsilon_m} \right) \vec{\nabla}(E_0)^2 \quad (2.45)$$

Now this expression for the dielectrophoretic force, is the traditional one that was first derived by Pohl (50) and is a good approximation for spherical particles with no dielectric losses and subject to only slightly nonuniform fields.

For the extension described in §2.1.3 involving a sinusoidal steady-state AC electric field applied to a system with ohmic conduction, Eq. (2.44) is modified according to:

$$\vec{F}_{DEP}(t) = \text{Re} \left\{ \vec{p}_{eff} e^{-i\omega t} \right\} \cdot \vec{\nabla} \text{Re} \left\{ \vec{E}(\vec{r}) e^{-i\omega t} \right\} \quad (2.46)$$

Applying the Cycle Average Theorem to Eq. (2.46), one obtains for the time average dielectrophoretic force:

$$\overline{\vec{F}_{DEP}(t)} = \frac{1}{2} \text{Re} \left\{ \vec{p}_{eff}(t) \cdot \vec{\nabla} \vec{E}^*(r, t) \right\} \quad (2.47)$$

where the bar indicates time average and the * signifies the complex conjugated quantity. Substitution of Eq. (2.43) into Eq. (2.47) gives:

$$\begin{aligned} \overline{\vec{F}_{DEP}(t)} &= \frac{1}{2} \text{Re} \left\{ 4\pi\epsilon_m R^3 \underline{K}_e E_0 \vec{e}_z e^{-i\omega t} \cdot \vec{\nabla} E_0 \vec{e}_z e^{i\omega t} \right\} \\ &= 2\pi R^3 \epsilon_m \text{Re} \left\{ \underline{K}_e \vec{\nabla} \left(\frac{1}{2} (E_0)^2 \right) \right\} \\ &= \pi R^3 \epsilon_m \text{Re} \{ \underline{K}_e \} \vec{\nabla} (E_0)^2 \end{aligned} \quad (2.48)$$

Now the maximum amplitude of the AC electric field may be related to the root-mean-square magnitude of the externally applied AC electric field through the definition:

$$E_{rms} \equiv \frac{E_0}{\sqrt{2}} \quad (2.49)$$

Thus substitution of Eq. (2.49) into Eq. (2.48) gives for the time average of the DEP force:

$$\overline{\vec{F}_{DEP}(t)} = 2\pi R^3 \varepsilon_m \operatorname{Re}\{\underline{K}_e\} \vec{\nabla}(E_{rms})^2 \quad (2.50)$$

Examination of Eq. (2.50) shows that the time average DEP force is a function of the real part of the Clausius–Mossotti factor which itself is a function of the field frequency. From Eq. (2.42) it is clear that the complex Clausius–Mossotti factor, a function of the complex permittivities of both particle and medium, will be positive when $\varepsilon_p > \varepsilon_m$, and negative when $\varepsilon_p < \varepsilon_m$; and therefore when $\operatorname{Re}\{\underline{K}_e\} > 0$, we have *positive dielectrophoresis* and when $\operatorname{Re}\{\underline{K}_e\} < 0$, *negative dielectrophoresis*. Positive DEP manifests itself in movement of the particle to a region of greater electric field intensity; and negative DEP, movement to a region of lower field intensity.

2.1.5 Comparison of DEP Force Derivations

As was alluded to earlier, the derivation of the DEP force using the effective moment method for lossy systems is not really correct in its methodology because the potential energy is not conserved. The first rigorous derivation of the DEP force for a lossy system consisting of a dielectric spherical particle in a dielectric medium was published by Sauer in 1983 (49) and with the same formulation extended to derive the electrical torque in 1985 (51). The derivation is based on the principle of the conservation of electromagnetic momentum (rather than energy) and therefore involves the evaluation of the net force on the particle through integration of the Maxwell stress tensor over the surface of the sphere. The formalism is quite complicated and since many of the details were omitted in Sauer’s paper, the full derivation is included in this dissertation (see the Appendix). Comparison of Sauer’s final result, Eq. (A.66):

$$\vec{F}_{ex} = -\pi R^3 \operatorname{Re}\{\underline{\varepsilon}_l\} \operatorname{Re}\{\underline{K}_e\} \vec{\nabla}|\vec{E}_{ex}|^2 \quad (2.51)$$

with the result from the effective dipole method, Eq. (2.48):

$$\overline{\vec{F}_{DEP}(t)} = \pi R^3 \varepsilon_m \operatorname{Re}\{\underline{K}_e\} \vec{\nabla}(E_0)^2$$

indicates that the general form is essentially the same. The negative sign appearing in Sauer’s expression is a result of his choice of sign convention of the net force: the electromagnet-

ic force being directed towards the center of the particle. It should also be realized that the Clausius–Mossotti factors are slightly different in the two expressions; the permittivities in Sauer’s expression containing complex components $-i\epsilon_m''$ and $-i\epsilon_p''$ which express dielectric loss mechanisms in the medium and particle that are not just the result of a phase lag induced through ohmic losses between the applied external field and the induced dipole in the particle. It is worth remarking on the fact that a very similar derivation, to that of Sauer’s, of the electromagnetic forces on dissipative dielectric media has appeared very recently by Giner *et al* (52). They calculated the electromagnetic force for three different systems: (a) an oscillating charge facing a semi–infinite dielectric; (b) the rise of a liquid between parallel charged plates; and (c) the DEP force on a spherical particle. Their results are in complete agreement to that of Sauer.

2.2 Shell Model Treatments

The treatment of the particle up to this point has been to consider the particle as simply a homogeneous sphere (either lossless or lossy). However, this is really an oversimplification for most real particles as they do possess structure, and even more importantly, an interface or surface of finite thickness with dielectric properties distinct from the main bulk of the interior of the particle. Biological cells, the particles with which this dissertation is concerned, are very clear examples of layered particles possessing either a cell wall (as in the case of plant cells) or a cell membrane (found on animal cells). Thus, to model a layered particle various so called “shelled models” have been constructed; the first probably being that of Pauly and Schwan (53). The simplest dielectric shell model consisting of a single concentric layer is shown in Fig. 2.3.

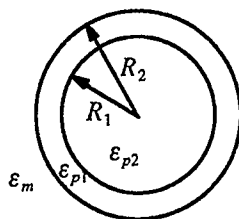


Fig. 2.3 Spherical concentric dielectric shell with distinct shell and core permittivities.

It may be assumed, as was done in §2.1.2, that Laplace's equation holds for the electric potentials in each of the three regions. Now after solution of these equations followed by application of similar constraints and boundary conditions (for both interfaces) one obtains for the DEP force under the hypotheses of the effective moment method:

$$\vec{F}_{DEP} = 2\pi\epsilon_m R_2^3 K(\epsilon_m, \epsilon_{p1}, \epsilon_{p2}) \vec{\nabla}(E_0)^2 \quad (2.52)$$

where the Clausius–Mossotti factor has the explicit form:

$$K_e(\epsilon_m, \epsilon_{p1}, \epsilon_{p2}) = \frac{\epsilon_p^\dagger - \epsilon_m}{\epsilon_p^\dagger + 2\epsilon_m} \quad (2.53)$$

with the effective permittivity, ϵ_p^\dagger , being defined according to:

$$\epsilon_p^\dagger \stackrel{\text{def}}{=} \epsilon_{p1} \left[\frac{a^3 + 2\left(\frac{\epsilon_{p2} - \epsilon_{p1}}{\epsilon_{p2} + 2\epsilon_{p1}}\right)}{a^3 - \left(\frac{\epsilon_{p2} - \epsilon_{p1}}{\epsilon_{p2} + 2\epsilon_{p1}}\right)} \right] \quad (2.54)$$

where $a = \frac{R_1}{R_2}$. For a similar shell where ohmic losses take place in both the medium and the particle, and where the the applied field is an AC electric field, the results are the same as the lossless system equations above (Eqs. (2.52) – (2.54)), except that all permittivities become complex; i.e.:

$$\underline{K}_e(\underline{\epsilon}_m, \underline{\epsilon}_{p1}, \underline{\epsilon}_{p2}) = \frac{\underline{\epsilon}_p^\dagger - \underline{\epsilon}_m}{\underline{\epsilon}_p^\dagger + 2\underline{\epsilon}_m} \quad (2.55)$$

and $\underline{\epsilon}_p^\dagger$ is:

$$\underline{\epsilon}_p^\dagger \stackrel{\text{def}}{=} \underline{\epsilon}_{p1} \left[\frac{a^3 + 2\left(\frac{\underline{\epsilon}_{p2} - \underline{\epsilon}_{p1}}{\underline{\epsilon}_{p2} + 2\underline{\epsilon}_{p1}}\right)}{a^3 - \left(\frac{\underline{\epsilon}_{p2} - \underline{\epsilon}_{p1}}{\underline{\epsilon}_{p2} + 2\underline{\epsilon}_{p1}}\right)} \right] \quad (2.56)$$

The model of a particle or biological cell consisting of a single concentric shell or membrane is the most basic attempt at modelling the surface. Other more sophisticated models have been proposed including: models consisting of additional layers; special

cases of very thin films involving either *series* or *shunt admittance* elements; and specific biological models such as the walled cell model and the protoplast model. The reader is referred to the text of Jones (48) for specific details concerning these models.

2.3 Polarization Mechanisms

Having derived expressions for the excess effective polarization for systems experiencing ohmic losses when subjected to AC fields; namely Eq. (2.42) of §2.1.3 for a simple spherical dielectric particle, and Eq. (2.56) of §2.2 for a spherical concentric dielectric shell, it is appropriate to briefly outline the various mechanisms attributed to the induced polarization (see Chapter 3 in reference (39) for a full description). There are essentially three types of mechanisms; the first being microscopic which includes electronic, atomic, and dipolar polarization; the second, interfacial, referred to as Maxwell–Wagner polarization; and the last, counterion polarization. All polarization mechanisms are very much dependent on the frequency of the applied electric field; some operable at low frequency while others being evident only at high frequencies.

2.3.1 Electronic, Atomic, and Dipolar Polarization

Electronic polarization is the result of the *distortion* of the positive and negative charge centres within atoms due to the application of an external electrical field. At sufficiently high field frequencies a polarization dispersion occurs as a result of the inability of the distortion to follow the alternating field. This dispersion is typically observed in the very high regime of the frequency spectrum, i.e. the ultraviolet.

Atomic polarization, to be distinguished from electronic polarization, arises from the actual physical *displacement* or shift of differently charged atoms within a molecule or complex. This dispersion is usually seen at infrared frequencies.

The third microscopic mechanism is dipolar or orientational polarization and comes into play as a result of the orientational responses of molecules due to an applied field. This mechanism is realized in molecules possessing a permanent dipole and is driven by the effort of the molecules to minimize their potential energy by realignment. This polarization

dispersion is characterized by a Debye type relaxation process (54).

2.3.2 Maxwell–Wagner Polarization

Interfacial or Maxwell–Wagner polarization is the result of charge accumulation at the structural interfaces of heterogeneous materials. The characteristic relaxation time constant for this process, τ_{MW} , may be realized by recasting Eq. (2.42) in the following form:

$$\underline{K}_e(\varepsilon_p, \varepsilon_m) = \frac{\sigma_p - \sigma_m}{\sigma_p + 2\sigma_m} \left[\frac{i\omega\tau_0 + 1}{i\omega\tau_{MW} + 1} \right] \quad (2.57)$$

where $\tau_0 \equiv \frac{\varepsilon_p - \varepsilon_m}{\sigma_p - \sigma_m}$ and $\tau_{MW} \equiv \frac{\varepsilon_p + 2\varepsilon_m}{\sigma_p + 2\sigma_m}$. Therefore, from this expression it is quite evident that the Maxwell–Wagner interfacial polarization is a first order process, and is seen as the dispersive response of a homogeneous ohmic dielectric sphere immersed in an ohmic dielectric medium. The frequency regime to which this type of mechanism is operable may be determined by examining both the low and high frequency limits of the Clausius–Mossotti factor expressed in Eq. (2.57):

$$\lim_{\omega \rightarrow 0} [\underline{K}_e] = \frac{\sigma_p - \sigma_m}{\sigma_p + 2\sigma_m} \quad (2.58)$$

$$\lim_{\omega \rightarrow \infty} [\underline{K}_e] = \frac{\varepsilon_p - \varepsilon_m}{\varepsilon_p + 2\varepsilon_m} \quad (2.59)$$

From these limits it is clear that the Maxwell–Wagner polarization mechanism, and hence charge accumulation at the particle/medium interface, occurs on the long time scale, $t \gg \tau_{MW}$, at low electric field frequencies. The ratio in Eq. (2.58) confirms the physical intuition that surface charge accumulation is governed by DC conduction. On the other hand, Eq. (2.59) indicates that at high frequencies the response is simply that for a lossless or insulating dielectric sphere, Eq. (2.36).

2.3.3 Counterion Polarization

Counterion polarization is the result of ionic diffusion within the *electrical double layer* created by the charge accumulation at the interface of two heterogeneous mate-

rials. The double layer consists of a layer of counterions that encompass the surface charge ions in a spherically symmetric fashion providing there is no outside perturbation. Upon the application of an external electric field, the symmetry of the counterionic cloud will be broken resulting in a "dipole" or induced polarization. The effects of counterion polarization have been observed in a number of different systems including: emulsions (55), charged polystyrene sphere suspensions (56), micro-organisms (57), and linear macromolecules including DNA (58). The effects of this type of polarization are manifest significantly at low frequencies and are difficult to quantify in a rigorous manner because of the phenomena being governed by nonlinear hydrodynamic-electrical equations (1). Many theories and models have been proposed to explain and describe this phenomena; the first due to Schwarz (59) who successfully described the amplitude of the dispersion. Schurr (60) extended the theory of Schwarz to include tangential surface flux with the bulk medium while still maintaining the features of a tightly bound layer of charges. This aspect of Schwarz's original model was abandoned by Fixman (61) and Chew and Sen (62); both groups incorporating the Guoy-Chapman model of a diffuse double layer with a potential for the ionic charge cloud described by a Boltzmann distribution. These exceedingly complicated models were simplified while maintaining their characteristic features by Grosse (63). More recently yet, Paul *et al* (7) proposed a nonequilibrium statistical mechanical model to account for anomalies in the surface conductance of the double layer for very low field frequencies.

2.4 Theoretically Generated DEP Spectra

Through the derivation of the DEP force in §2.1.4 and the discussion of the various polarization mechanisms, in particular Maxwell-Wagner polarization in §2.3.2, it should be clear that the dielectric properties of the particle are contained in the expression of the Clausius-Mossotti factor; and in particular, for lossy systems the real part of this expression. The derived expressions for the Clausius-Mossotti factor for both the homogeneous dielectric sphere, Eq. (2.42), and the concentric dielectric shell, Eq. (2.55), are intrinsically frequency dependent through the complex permittivities. Thus, the frequency

dependence of a particular theoretical model is displayed in a DEP spectral plot of the $\text{Re}\{\underline{K}_e\}$. The suitability of a specific theoretical model may be determined by comparison of theoretically generated DEP spectra with those obtained experimentally. The results for the two models are examined separately in the following two sections.

2.4.1 The DEP Spectrum of a Homogeneous Dielectric Sphere

The DEP spectrum, that is a plot of the real part of the Clausius–Mossotti factor versus the frequency ($f = \frac{\omega}{2\pi}$) of the applied electric field, for a lossy system consisting of a homogeneous dielectric sphere in a homogeneous dielectric medium is displayed in Fig. 2.4.

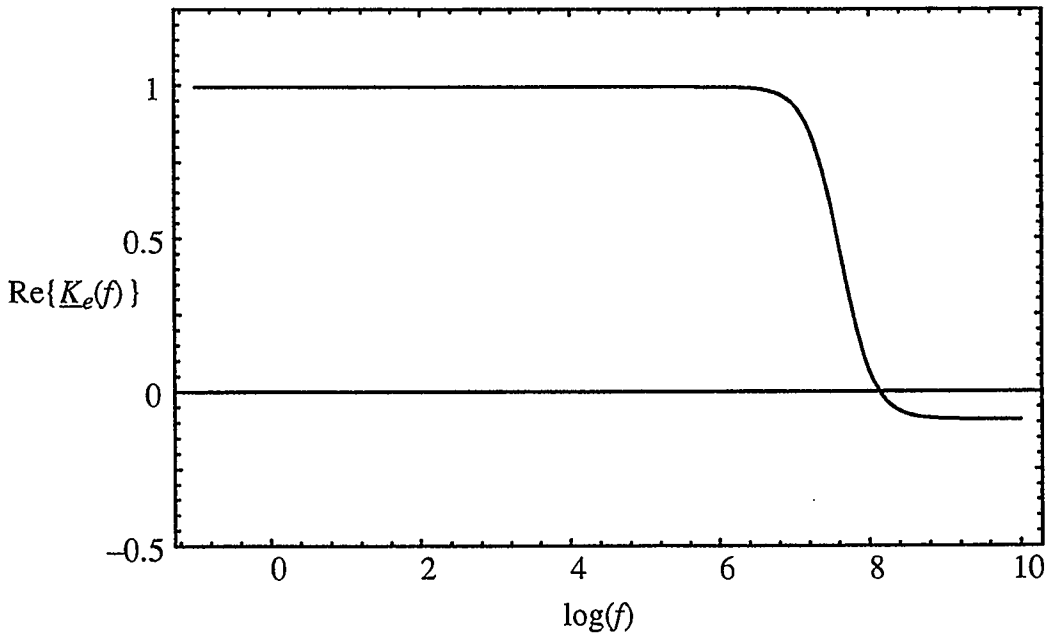


Fig. 2.4 DEP spectrum of a homogeneous dielectric sphere.

$$(\varepsilon_m = 80\varepsilon_o, \varepsilon_p = 60\varepsilon_o, \sigma_m = 0.001\text{Sm}^{-1}, \sigma_p = 0.5\text{Sm}^{-1}) \quad (44)$$

The selected permittivities and conductivities (45) are typical values (or estimates) for a plant protoplast suspended in a dilute electrolyte solution (essentially water). The effective polarizability plot shows that the polarization of the particle remains at a constant maximum value for the low frequencies indicating that in this region the induced dipole is synchronized with the oscillating electric field. Beyond a frequency of approximately 1 MHz, the fluctuating dipole (movement of charges within the particle) lags behind the AC field resulting in

a polarization dispersion; energy is lost within the particle. For sufficiently high frequencies ($> 10^8$ Hz.) charge movement essentially ceases and a constant minimum value in the effective polarizability is observed.

2.4.2 The DEP Spectrum of a Homogeneous Concentric Dielectric Shell

As was alluded to in §2.2, the concentric dielectric shell was developed to better model the physical reality of a biological cell with its distinct cell membrane. The cell membrane for a plant protoplast consists of a very thin (that is, when compared to the overall dimensions of the cell) lipid protein bi-layer (64). The membrane capacitance c_{mb} is typically $\sim 0.005 Fm^{-2}$ and the transmembrane conductance g_{mb} , very small, in fact negligible except at very low frequencies. Thus, the theoretically generated DEP spectrum (where the real part of the Clausius–Mossotti factor is evaluated from Eqs. (2.55) and (2.56)) for a plant protoplast modelled as a lossy concentric dielectric shell, is plotted in Fig. 2.5.

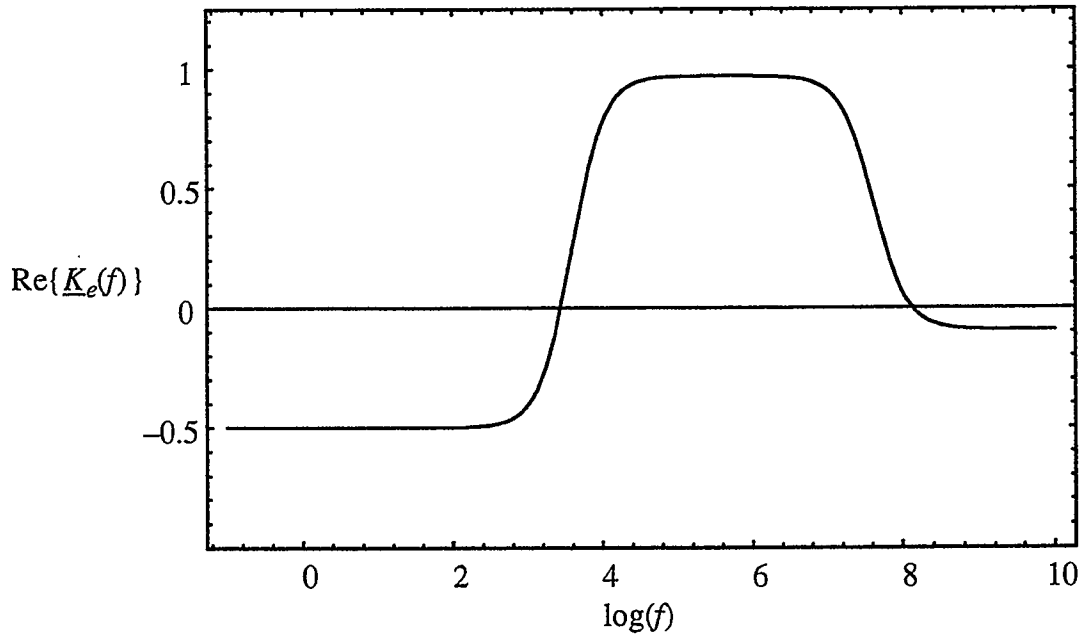


Fig. 2.5 DEP spectrum of a homogeneous concentric dielectric shell.

$$(\epsilon_m = 80\epsilon_o, \epsilon_{p2} = 60\epsilon_o, \sigma_m = 0.001 Sm^{-1}, \sigma_{p2} = 0.5 Sm^{-1}, \epsilon_{p1} = 5.6\epsilon_o, \\ \sigma_{p1} = 0 Sm^{-1}, R_2 = 17.5 \times 10^{-6} m, R_2 - R_1 = 0.01 \times 10^{-6} m)$$

Now the parameters listed in Fig. 2.5 are related to the specific membrane parameters of the capacitance and conductance through the following relations:

$$c_{mb} = \frac{\varepsilon_{p1}}{R_2 - R_1} \qquad g_{mb} = \frac{\sigma_{p1}}{R_2 - R_1}$$

It is perhaps worth noting that these results obtained through the simple shelled model treatment of §2.2 are essentially identical to the results obtained by the previously alluded to *series admittance model* (48), which specifically introduces the conditions of a finite potential drop, $E_m(R_2 - R_1)$, across the thin shell through modifying the boundary condition (see Eq. (2.28)) requiring continuity in electric field potential to be:

$$\underline{c}_{mb}(\psi_m(R_2, \theta) - \psi_{p2}(R_2, \theta)) = \underline{\varepsilon}_m E_m(R_2, \theta) \qquad (2.60)$$

where the complex capacitance of the membrane \underline{c}_{mb} is defined according to:

$$\underline{c}_{mb} \equiv c_{mb} + \frac{g_{mb}}{i\omega}$$

and both the electric field potentials and the electric field intensities are, of course, complex after the fashion of Eq. (2.40). The effective permittivity $\underline{\varepsilon}'_p$ in Eq. (2.55) is now replaced by:

$$\underline{\varepsilon}'_p = \underline{c}_{mb} R_2 \left(\frac{\varepsilon_{p2}}{\underline{c}_{mb} R_2 + \varepsilon_{p2}} \right) \qquad (2.61)$$

This parallel to the series admittance model further attests to the insulating character of the membrane being incorporated into the shelled model; with the selected parameters given in Fig. 2.5. Examination of Fig. 2.5 indicates that the polarization of the particle at high frequencies is the same as was seen for the simple homogeneous sphere—high frequency dispersion. The low frequency behavior, however, is quite different in that a constant minimum value (−0.5) is observed. This low frequency result indicates that the membrane is effectively insulating the interior of the cell with the effective permittivity being less than the permittivity of the medium, and hence negative DEP is observed. The rise in the polarizability above 1000 Hz is the result of penetration by the electric field into the interior of the cell and corresponding charge build up at the interface (Maxwell–Wagner polarization).

Chapter 3: Hysteresis

3.1 Introduction

The previous two chapters have already made reference to the importance of the electrical properties of the particle–medium interface in determining the physicochemical properties of the particle, where the specific context has been that of the cell membrane of living intact plant protoplasts. As alluded to in Chapter 1, the anomalous observation of *hysteresis loops* in the low–frequency regime of experimentally measured DEP spectra, has suggested a nonlinear interaction of the external electric field with the cell membrane. Being that conventional theory has failed to explain or predict this phenomena, a careful theoretical investigation beginning from first principles, was deemed to be useful in suggesting the possible cause and physical mechanism of the hysteresis. Thus, this chapter presents the details of the theoretical modelling.

This author has recently reported the experimental observations along with a detailed theoretical analysis in the journal *Bioelectrochemistry and Bioenergetics* (65), and thus some of the material contained in this chapter has been published.

3.2 Experimental Observations

The DEP spectral results obtained from a typical dual–frequency levitation experiment involving a tobacco protoplast in 8% sorbitol is displayed in Fig. 3.1.

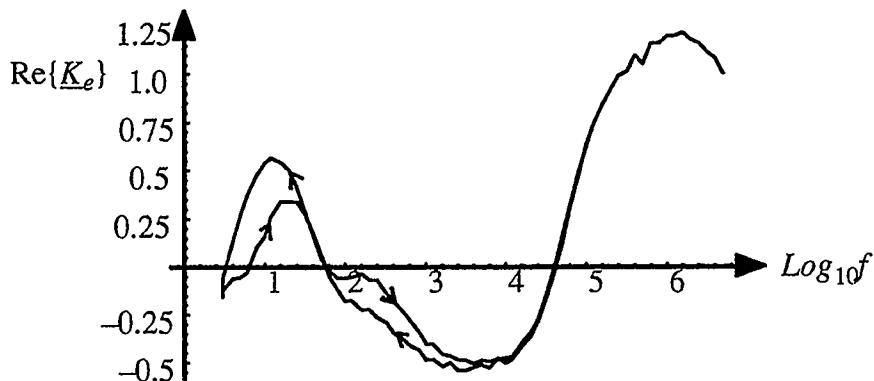


Fig. 3.1 Experimental DEP spectrum showing double valued Clausius–Mossotti factor in the low frequency region.

The complete experimental details, including the isolation and preparation of the protoplast sample, and experimental setup and technique are given in Chapter 4 (the context in which the author carried out his own experiments); however, there are a few important details pertaining to the hysteresis measurements.

The spectral scan was usually carried out starting from a high frequency, typically 5 MHz.; and the time averaged levitation voltage monitored at a minimum of 10 evenly spaced frequency points per decade. The downward sweep was halted when the frequency reached 1 Hz. and then the frequency scan was repeated on the same cell; the direction of the scan, however, was reversed (i.e. low to high). From the example (Fig. 3.1) of a typical Clausius–Mossotti response for an individual protoplast, it is seen that the polarizability is essentially independent of the scan direction over an appreciable frequency range (1 KHz. to 5 MHz.). In the low frequency region (< 1 KHz.), however, the Clausius–Mossotti factor is clearly sensitive to the scan direction.

One also notes, that in the up and down scan of the spectrum, a splitting of the value of the Clausius–Mossotti factor is exhibited in a manner that is clearly typical of a hysteresis effect. Furthermore, this characteristic splitting appears to be sensitive to the previous history of the sample. This is quite distinct from the high–frequency response region where even after repeated scans the characteristic features are retained. During the course of such prolonged levitation studies, usually about 20 minutes for 5 complete scans, no alteration was detected in either the cell size or shape. The occurrence of some cell leakage can not be entirely ruled out, and could probably be ascertained through electrorotation measurements (66). It is, however, unclear how cell leakage would relate to or explain the hysteresis.

3.3 Theoretical Thrust

As outlined in §2.1.3, the Clausius–Mossotti factor for systems exhibiting ohmic dielectric losses when subjected to an AC electric field, is a function of the complex, frequency–dependent permittivities. The permittivity arises through the relationship be-

tween the electric field intensity and the displacement vector; which for free space is:

$$\vec{D} = \varepsilon_o \vec{E} \quad (3.1)$$

where ε_o , a scalar constant, is the permittivity of free space. It is well known from the general theory of electrodynamics, that the choice of a linear relationship between the displacement vector and the local electric field is basically a phenomenological one. From a physical standpoint, this choice simply amounts to assuming that the complex permittivity may depend on the local field frequency, but is independent of the amplitude of the field. This assumption is valid so long as the local field does not alter the structure of the medium in which it is present. An examination of Fig. 3.1, however, shows that when the direction of the frequency scan is reversed, the value of the Clausius–Mossotti factor has been altered by the previous scan, thus indicating a change in the complex permittivity as a result of the presence of the field. This, of course, implies that the permittivity is a function of the electric field:

$$\underline{\varepsilon} = \underline{\varepsilon}(\vec{E})$$

3.4 Introduction of the Nonlinearity

The possibility of considering a displacement vector that is nonlinear in the local field has already been the subject of some interest in the topic of dielectric saturation, a good account of this work which may be found in Scaife's book (67). The permittivity in the context of dielectric saturation is taken to be quadratic in the local field:

$$\varepsilon(\vec{E}) \approx \varepsilon(0)(1 - \lambda E^2) \quad (3.2)$$

Here, the first term $\varepsilon(0)$ is the standard field independent permittivity, while the second term represents a quadratic correction, with λ a small parameter that measures the degree of nonlinearity. Substitution of Eq. (3.2) into Eq. (2.15) with the assumption of $\rho = 0$ gives for a curl-free electric field:

$$\left[1 - \lambda (\vec{\nabla}\psi \cdot \vec{\nabla}\psi) \right] \nabla^2 \psi = \lambda \left\{ \left[(\vec{\nabla}\psi) \cdot \vec{\nabla} \right] (\vec{\nabla}\psi \cdot \vec{\nabla}\psi) \right\} \quad (3.3)$$

Now Eq. (3.3) is a nonlinear extension of Laplace's equation (Eq. (2.21)) which for the lossy

system under consideration, must be solved within both the particle and the surrounding medium; subject to the boundary conditions of Eqs. (2.28) and (2.41). This highly nonlinear equation can not be solved exactly, and thus one is obliged to attempt solving it numerically or by means of a perturbative technique. Although the perturbation, as represented by the parameter λ , is small, the calculation of this type presented by Scaife does not reveal the multiplicity of solutions one would expect from a nonlinear theory.

Therefore, in order to obtain the multiplicity of solutions observed in the experimental plot (Fig. 3.1), it is essential that the model constructed be one that may be subject to analysis without any approximations. Such a model can not employ the sophisticated mathematics envisaged in Eq. (3.3), nor can it be a completely linear treatment as used in the traditional approach outlined in §2.1.2 and §2.1.3.

The model developed and presented here, avoids the necessity of solving a highly nonlinear partial differential equation by assuming that the material both inside the particle and in the surrounding medium continues to obey the standard linear Laplace equations (Eq. (2.21)). Consequently, the exact solutions obtained for the homogeneous sphere model (Eqs. (2.26) and (2.27)) can still be utilized along with the boundary condition invoking the continuity of the electric potential (Eq. (2.28)). The second boundary condition requiring continuity of the electric flux density across the boundary, must be reformulated beginning with its defining equation, Eq. (2.41). Thus, the constructed model essentially consists of taking two linear dielectrics and separating them by an infinitesimally thin nonlinear boundary. It should be pointed out, that such an approach in which the nonlinearity is introduced through the boundary conditions rather than the differential equation itself, is not unique, but in fact has been used in other areas of nonlinear dynamics (68).

The displacement vector is assumed to have the standard form (47) applicable for describing the electromagnetic state of a sample of matter:

$$\vec{D}(t) = \epsilon_0 \vec{E}(t) + \vec{P}(t) \quad (3.4)$$

where $\vec{P}(t)$ is the total polarization vector for the region of interest, which in the present case

is the particle–medium interface. For a completely general nonlinear case, the polarization vector may be expressed in terms of the local field (69) as follows:

$$\begin{aligned} \vec{P}(t) = & \left[\varepsilon_o \chi^{(1)}(\omega) + \frac{1}{i\omega} \sigma^{(1)}(\omega) \right] \cdot \vec{E}(t) + \left[\varepsilon_o \chi^{(2)}(\omega) + \frac{1}{2i\omega} \sigma^{(2)}(\omega) \right] : \vec{E}(t) \vec{E}(t) + \\ & \cdots + \left[\varepsilon_o \chi^{(n)}(\omega) + \frac{1}{ni\omega} \sigma^{(n)}(\omega) \right] | \vec{E}(t) \vec{E}(t) \vec{E}(t) \cdots \vec{E}(t) \end{aligned} \quad (3.5)$$

where $\chi^{(n)}(\omega)$ is the n^{th} order susceptibility tensor, $\sigma^{(n)}(\omega)$ the n^{th} order conductivity tensor, and ω the frequency of the electric field. Substitution of Eq. (3.5) into Eq. (3.4) gives for the general nonlinear displacement vector:

$$\begin{aligned} \vec{D}(t) = & \left[\varepsilon_o \{1 + \chi^{(1)}(\omega)\} + \frac{1}{i\omega} \sigma^{(1)}(\omega) \right] \cdot \vec{E}(t) + \left[\varepsilon_o \chi^{(2)}(\omega) + \frac{1}{2i\omega} \sigma^{(2)}(\omega) \right] : \vec{E}(t) \vec{E}(t) \\ & + \cdots + \left[\varepsilon_o \chi^{(n)}(\omega) + \frac{1}{ni\omega} \sigma^{(n)}(\omega) \right] | \vec{E}(t) \vec{E}(t) \vec{E}(t) \cdots \vec{E}(t) \end{aligned} \quad (3.6)$$

There are n terms in Eq. (3.6) and therefore, for the ease of keeping track of each of the terms, this general displacement vector may simply be written:

$$\vec{D}(t) = \vec{D}_1(t) + \vec{D}_2(t) + \cdots + \vec{D}_n(t) \quad (3.7)$$

In addition, one may further represent the general displacement vector in terms of permittivity tensors by employing the following definitions:

$$\begin{aligned} \underline{\varepsilon}^{(1)}(\omega) & \equiv \varepsilon_o \{1 + \chi^{(1)}(\omega)\} \\ \underline{\varepsilon}^{(n)}(\omega) & \equiv \varepsilon_o \chi^{(n)}(\omega) \\ \underline{\underline{\varepsilon}}^{(n)}(\omega) & \equiv \underline{\varepsilon}^{(n)}(\omega) + \frac{1}{ni\omega} \sigma^{(n)}(\omega) \end{aligned} \quad (3.8)$$

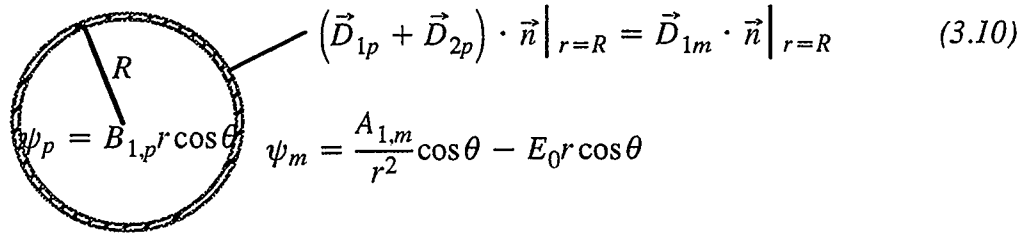
and therefore Eq. (3.6) may be written in terms of permittivity tensors:

$$\vec{D}(t) = \underline{\underline{\varepsilon}}^{(1)}(\omega) \cdot \vec{E}(t) + \underline{\underline{\varepsilon}}^{(2)}(\omega) : \vec{E}(t) \vec{E}(t) + \cdots + \underline{\underline{\varepsilon}}^{(n)}(\omega) | \vec{E}(t) \vec{E}(t) \cdots \vec{E}(t) \quad (3.9)$$

Butcher and Cotter (69) point out that $\chi^{(2)}(\omega)$ vanishes in media possessing inversion symmetry because the polarisation must change sign when the optical electric field

is reversed. Both the particle and the medium possess inversion symmetry. The particle–medium boundary or interface when considered over the entire spherical surface also has inversion symmetry. Hence, the even powered terms in Eq. (3.9) should be set to zero for the problem dealt with here. However, in the model that follows, the quadratic term is retained on the particle side of the interface (see Eq. (3.10)) on the assumption that the interface, though treated spherically, actually possesses intrinsic asymmetry.

Now as the simplest extension to the traditional linear model, a nonlinearity is introduced on the particle side of the interface by retaining both the linear and quadratic field dependent terms of Eq. (3.9); while on the medium side, only the linear term is retained. Thus, the model may be represented pictorially as shown in Fig. 3.2.



$$\left(\vec{D}_{1p} + \vec{D}_{2p} \right) \cdot \vec{n} \Big|_{r=R} = \vec{D}_{1m} \cdot \vec{n} \Big|_{r=R} \quad (3.10)$$

$$\psi_p = B_{1,p} r \cos \theta \quad \psi_m = \frac{A_{1,m}}{r^2} \cos \theta - E_0 r \cos \theta$$

Fig. 3.2 Representation of nonlinear boundary condition at particle–medium interface.

Such an assumption results in a nonlinear model that may be handled exactly and with a reasonable mathematical sophistication beyond that required in the linear; but also affords some attractive and interesting physical and chemical insights.

The membrane of biological cells is almost impervious to conduction current in the low–frequency regime; thus restricting most of the electrically measurable properties to the cell surface (70). It is also well understood that the cell membrane is a fairly complicated structure, and thus presents a surface that is capable of displaying a very rich and nonlinear response to the external field. In many treatments involving the computation of the Clausius–Mossotti factor, the cell surface is generally regarded as a charged object with an electrical double layer; hence performing a relatively passive role. Such a view is rather simplistic since the membrane lying immediately within the surface is a center of much activity (71). In the work of Kell and Harris (72), a much more active role has been ascribed to the

membrane in which the diffusional motion of the protein molecules affect the dielectric properties. Furthermore, if one considers the fact that an applied electric field is capable of altering the conformation of the proteins and influencing the equilibrium constants of the various chemical reactions, as discussed in Takashima (20), it is indeed reasonable to assume that the surface electrical properties will be dependent on the local field, and thus display the type of nonlinearities already alluded to in this chapter. The medium side of the interface, however, is further removed from the membrane, and thus a linear approximation may be considered adequate.

It should be noted that no attempt has been given in this dissertation to give a detailed account of the molecular mechanisms that could contribute towards the nonlinear response at the interface. It is possible, however, to relax the assumption made earlier regarding the uncharged nature of the cell surface, and to consider the nonlinearity as originating in the surface charge and its accompanying double layer. This feature is fully consistent with the model being presented here; and this aspect may be clearly seen by rewriting the boundary condition (Eq. (3.10)) given in Fig. 3.2 in the following manner:

$$(\vec{D}_{1p} - \vec{D}_{1m}) \cdot \vec{n} \Big|_{r=R} = \vec{D}_{2p} \cdot \vec{n} \Big|_{r=R} = \rho$$

where ρ is an equivalent surface charge density. This interpretation is more consistent with the fact that the surfaces of cells are charged objects.

Both the first-order, $\underline{\epsilon}^{(1)}(\omega)$, and the second-order, $\underline{\epsilon}^{(2)}(\omega)$, permittivities in Eq. (3.9) are tensors of the second and third rank respectively; since the formalism is completely general and thus the tensorial properties allow for the possibility that the displacement vector and the local electrical field may not be parallel. The first order permittivity may therefore be written:

$$\underline{\epsilon}^{(1)}(\omega) = \sum_{i=1}^3 \sum_{j=1}^3 \underline{\epsilon}^{(1)}_{ij} \vec{e}_i \vec{e}_j \quad (3.11)$$

where $\underline{\epsilon}^{(1)}_{ij}$ are the components of the second rank tensor, and $\vec{e}_i \vec{e}_j$ the dyadic product of two

arbitrary unit vectors. A comparison of Eq. (3.7) with Eq. (3.9), followed by the substitution of Eq. (3.11), gives for the linear displacement vector:

$$\vec{D}_1(t) = \sum_{i=1}^3 \sum_{j=1}^3 \underline{\epsilon}^{(1)}_{ij} \vec{e}_i \vec{e}_j \cdot \vec{E}(t) \quad (3.12)$$

With the assumption that both the particle and the medium behave isotropically under influence of the electric field, the first order complex permittivity tensor must reduce to a diagonal tensor of rank two possessing equal components, i.e.:

$$\begin{aligned} \vec{e}_i \vec{e}_j &= \delta_{ij} \\ \underline{\epsilon}^{(1)}_{11} &= \underline{\epsilon}^{(1)}_{22} = \underline{\epsilon}^{(1)}_{33} \end{aligned} \quad (3.13)$$

With this constraint, Eq. (3.12) becomes:

$$\vec{D}_1(t) = \underline{\epsilon}^{(1)} \sum_{i=1}^3 \sum_{j=1}^3 \vec{e}_i \vec{e}_j \cdot \vec{E}(t) \quad (3.14)$$

where $\underline{\epsilon}^{(1)} \equiv \underline{\epsilon}^{(1)}_{11} = \underline{\epsilon}^{(1)}_{22} = \underline{\epsilon}^{(1)}_{33}$. The linear displacement vector may be expressed in terms of the scalar electric field potential as given in Eq. (2.21), resulting in the following:

$$\begin{aligned} \vec{D}_1(t) &= -\underline{\epsilon}^{(1)} \sum_{i=1}^3 \vec{e}_i \vec{e}_i \cdot \vec{\nabla} \psi \\ &= -\underline{\epsilon}^{(1)} \sum_{i=1}^3 \vec{e}_i \vec{e}_i \cdot \sum_{k=1}^3 \frac{\partial \psi}{\partial x_k} \vec{e}_k \\ &= -\underline{\epsilon}^{(1)} \sum_{i=1}^3 \sum_{k=1}^3 \frac{\partial \psi}{\partial x_k} \vec{e}_i \delta_{ik} \\ &= -\underline{\epsilon}^{(1)} \sum_{i=1}^3 \frac{\partial \psi}{\partial x_i} \vec{e}_i \end{aligned} \quad (3.15)$$

where x_1 , x_2 , and x_3 are the cartesian coordinates x , y , and z , respectively. Now the quadratic term in the displacement vector, $\vec{D}_2(t)$, may be treated in a similar fashion. The complex frequency dependent permittivity tensor is a third rank tensor and so may be written:

$$\underline{\varepsilon}^{(2)}(\omega) = \sum_{i=1}^3 \sum_{j=1}^3 \sum_{k=1}^3 \underline{\varepsilon}^{(2)}_{ijk} \vec{e}_i \vec{e}_j \vec{e}_k$$

and therefore the quadratic term becomes:

$$\vec{D}_2(t) = \left[\sum_{i=1}^3 \sum_{j=1}^3 \sum_{k=1}^3 \underline{\varepsilon}^{(2)}_{ijk} \vec{e}_i \vec{e}_j \vec{e}_k \cdot \vec{E}(t) \right] \cdot \vec{E}(t) \quad (3.16)$$

The isotropicity condition requires that Eq. (3.16) be reduced to a diagonal second rank tensor with equivalent elements; and thus the quadratic term becomes:

$$\begin{aligned} \vec{D}_2(t) &= \left[\sum_{i=1}^3 \sum_{j=1}^3 \sum_{k=1}^3 \underline{\varepsilon}^{(2)}_{ijk} \vec{e}_i \vec{e}_j \vec{e}_k \cdot \sum_{l=1}^3 E_l \vec{e}_l \right] \cdot \vec{E}(t) \\ &= \left[\sum_{i=1}^3 \sum_{j=1}^3 \sum_{k=1}^3 \underline{\varepsilon}^{(2)}_{ijk} \vec{e}_i \vec{e}_j E_k \right] \cdot \vec{E}(t) \\ &= \left[\sum_{i=1}^3 \sum_{k=1}^3 \underline{\varepsilon}^{(2)}_{iik} \vec{e}_i \vec{e}_i E_k \right] \cdot \vec{E}(t) \\ &= \left[\left(\underline{\varepsilon}^{(2)}_{\alpha} E_1 + \underline{\varepsilon}^{(2)}_{\beta} E_2 + \underline{\varepsilon}^{(2)}_{\gamma} E_3 \right) \sum_{i=1}^3 \vec{e}_i \vec{e}_i \right] \cdot \vec{E}(t) \end{aligned} \quad (3.17)$$

where the last line of Eq. (3.17) is the result of the requirement of the diagonal elements being equal and the invoking of the definitions: $\underline{\varepsilon}^{(2)}_{\alpha} \equiv \underline{\varepsilon}^{(2)}_{111} = \underline{\varepsilon}^{(2)}_{221} = \underline{\varepsilon}^{(2)}_{331}$; $\underline{\varepsilon}^{(2)}_{\beta} \equiv \underline{\varepsilon}^{(2)}_{112} = \underline{\varepsilon}^{(2)}_{222} = \underline{\varepsilon}^{(2)}_{332}$; and $\underline{\varepsilon}^{(2)}_{\gamma} \equiv \underline{\varepsilon}^{(2)}_{113} = \underline{\varepsilon}^{(2)}_{223} = \underline{\varepsilon}^{(2)}_{333}$. And thus, $\vec{D}_2(t)$ maybe expressed in terms of the electric field potential:

$$\vec{D}_2(t) = \left[\underline{\varepsilon}^{(2)}_{\alpha} \frac{\partial \psi}{\partial x_1} + \underline{\varepsilon}^{(2)}_{\beta} \frac{\partial \psi}{\partial x_2} + \underline{\varepsilon}^{(2)}_{\gamma} \frac{\partial \psi}{\partial x_3} \right] \sum_{i=1}^3 \frac{\partial \psi}{\partial x_i} \vec{e}_i \quad (3.18)$$

The protoplast particles have obvious spherical symmetry and therefore a coordinate transformation to polar spherical coordinates is desirable. The transformation from cartesian coordinates to polar spherical coordinates is, of course, according to the relations:

$$x_1 = r \sin \theta \cos \phi \quad x_2 = r \sin \theta \sin \phi \quad x_3 = r \cos \theta$$

and the corresponding differential operators obtained from the equations:

$$\begin{aligned}
\frac{\partial}{\partial x_1} &= \sin \theta \cos \phi \frac{\partial}{\partial r} + \frac{\cos \theta \cos \phi}{r} \frac{\partial}{\partial \theta} - \frac{\sin \phi}{r \sin \theta} \frac{\partial}{\partial \phi} \\
\frac{\partial}{\partial x_2} &= \sin \theta \sin \phi \frac{\partial}{\partial r} + \frac{\cos \theta \sin \phi}{r} \frac{\partial}{\partial \theta} + \frac{\cos \phi}{r \sin \theta} \frac{\partial}{\partial \phi} \\
\frac{\partial}{\partial x_3} &= \cos \theta \frac{\partial}{\partial r} - \frac{\sin \theta}{r} \frac{\partial}{\partial \theta}
\end{aligned} \tag{3.19}$$

The boundary condition, Eq. (3.10), requires an expression for the unit normal vector to surface which in polar spherical coordinates is:

$$\vec{n} = \sin \theta \cos \phi \vec{e}_1 + \sin \theta \sin \phi \vec{e}_2 + \cos \theta \vec{e}_3 \tag{3.20}$$

The boundary condition of Eq. (3.10) requires the evaluation of the normal component of the linear term of the electric flux density for both the particle and the medium; and thus one may calculate a general expression for $\vec{D}_1(t) \cdot \vec{n}$ from Eq. (3.15) coupled with the transformation equations, Eqs. (3.19) and (3.20); with the result:

$$\begin{aligned}
\vec{D}_1(t) \cdot \vec{n} &= -\underline{\varepsilon}^{(1)} \sum_{i=1}^3 \frac{\partial \psi}{\partial x_i} \vec{e}_i \cdot (\sin \theta \cos \phi \vec{e}_1 + \sin \theta \sin \phi \vec{e}_2 + \cos \theta \vec{e}_3) \\
&= -\underline{\varepsilon}^{(1)} \left(\frac{\partial \psi}{\partial x_1} \sin \theta \cos \phi + \frac{\partial \psi}{\partial x_2} \sin \theta \sin \phi + \frac{\partial \psi}{\partial x_3} \cos \theta \right) \\
&= -\underline{\varepsilon}^{(1)} \frac{\partial \psi}{\partial r}
\end{aligned} \tag{3.21}$$

where azimuthal symmetry has been invoked on the last line. Similarly, one may evaluate the quadratic term required on the particle side of the boundary condition from Eq. (3.18) and Eqs. (3.19) and (3.20):

$$\begin{aligned}
\vec{D}_2(t) \cdot \vec{n} &= \left[\underline{\varepsilon}^{(2)}_{\alpha} \frac{\partial \psi}{\partial x_1} + \underline{\varepsilon}^{(2)}_{\beta} \frac{\partial \psi}{\partial x_2} + \underline{\varepsilon}^{(2)}_{\gamma} \frac{\partial \psi}{\partial x_3} \right] \sum_{i=1}^3 \frac{\partial \psi}{\partial x_i} \vec{e}_i \cdot \\
&\quad (\sin \theta \cos \phi \vec{e}_1 + \sin \theta \sin \phi \vec{e}_2 + \cos \theta \vec{e}_3) \\
&= \left[\underline{\varepsilon}^{(2)}_{\alpha} \frac{\partial \psi}{\partial x_1} + \underline{\varepsilon}^{(2)}_{\beta} \frac{\partial \psi}{\partial x_2} + \underline{\varepsilon}^{(2)}_{\gamma} \frac{\partial \psi}{\partial x_3} \right] \frac{\partial \psi}{\partial r}
\end{aligned}$$

$$\begin{aligned}
&= \left[\left(\underline{\varepsilon}^{(2)}_{\alpha} \cos \phi + \underline{\varepsilon}^{(2)}_{\beta} \sin \phi \right) \sin \theta + \underline{\varepsilon}^{(2)}_{\gamma} \cos \theta \right] \left(\frac{\partial \psi}{\partial r} \right)^2 + \\
&\quad \frac{1}{r} \left[\left(\underline{\varepsilon}^{(2)}_{\alpha} \cos \phi + \underline{\varepsilon}^{(2)}_{\beta} \sin \phi \right) \cos \theta - \underline{\varepsilon}^{(2)}_{\gamma} \sin \theta \right] \left(\frac{\partial \psi}{\partial \theta} \right) \left(\frac{\partial \psi}{\partial r} \right)
\end{aligned} \tag{3.22}$$

The left hand side (particle side) of the boundary condition, Eq. (3.10), may now be determined from Eqs. (3.21) and (3.22):

$$\begin{aligned}
\left(\vec{D}_{1p}(t) + \vec{D}_{2p}(t) \right) \cdot \vec{n} \Big|_{r=R} &= - \underline{\varepsilon}^{(1)} \frac{\partial \psi_p}{\partial r} \Big|_{r=R} + \\
&\quad \left[\left(\underline{\varepsilon}^{(2)}_{\alpha,p} \cos \phi + \underline{\varepsilon}^{(2)}_{\beta,p} \sin \phi \right) \sin \theta + \underline{\varepsilon}^{(2)}_{\gamma,p} \cos \theta \right] \left(\frac{\partial \psi_p}{\partial r} \right)^2 \Big|_{r=R} + \\
&\quad \frac{1}{r} \left[\left(\underline{\varepsilon}^{(2)}_{\alpha,p} \cos \phi + \underline{\varepsilon}^{(2)}_{\beta,p} \sin \phi \right) \cos \theta - \underline{\varepsilon}^{(2)}_{\gamma,p} \sin \theta \right] \left(\frac{\partial \psi_p}{\partial \theta} \right) \left(\frac{\partial \psi_p}{\partial r} \right) \Big|_{r=R}
\end{aligned} \tag{3.23}$$

Substituting the particle potential ψ_p from Eq. (2.26) into Eq. (3.23) gives the much simplified result:

$$\left(\vec{D}_{1p}(t) + \vec{D}_{2p}(t) \right) \cdot \vec{n} \Big|_{r=R} = B_{1,p} \left(B_{1,p} \underline{\varepsilon}^{(2)}_{\gamma,p} - \underline{\varepsilon}^{(1)}_p \right) \cos \theta \tag{3.24}$$

The right hand side (medium side) of Eq. (3.10) is evaluated from Eq. (3.21) with substitution of Eq. (2.27), yielding:

$$\vec{D}_{1m}(t) \cdot \vec{n} \Big|_{r=R} = \underline{\varepsilon}^{(1)}_m \left(\frac{2A_{1,m}}{R^3} + E_0 \right) \cos \theta \tag{3.25}$$

Use is now made of the boundary condition requiring continuity in the electric field potential across the boundary, Eq. (2.28), to eliminate the constant $B_{1,p}$, and then equating Eq. (3.24) to Eq. (3.25) in keeping with the second boundary condition of Eq. (3.10). This results in the following equation, where for the sake of brevity the subscript γ is dropped from the second-order permittivity:

$$\begin{aligned} \underline{\varepsilon}^{(1)}_m \left(\frac{2A_{1,m}}{R^3} + E_0 \right) + \underline{\varepsilon}^{(1)}_p \left(\frac{A_{1,m}}{R^3} - E_0 \right) - \underline{\varepsilon}^{(2)}_p \left(\frac{A_{1,m}}{R^3} - E_0 \right)^2 = \\ \underline{\varepsilon}^{(1)}_m \left(\frac{2A_{1,m}}{R^3} + E_0 \right) - \underline{\varepsilon}^{(1)}_p E_p - \underline{\varepsilon}^{(2)}_p (E_p)^2 = 0 \end{aligned} \quad (3.26)$$

Now this relation clearly declares the resulting extension of the linear model in treating the medium–particle interface in a nonlinear fashion; realizing that when $\underline{\varepsilon}^{(2)}_p$ is set to zero, the standard linear dipolar coefficient results.

This boundary condition is a statement to the fact that the electric flux density on the particle side of the interface must be equal to the electric flux density on the medium side, if no charge is present at the interface. Thus far, the dipolar coefficient $A_{1,m}$ which determines the polarization of the cell, is an unknown quantity and has to be selected in such a way that this balance of the electric flux density is satisfied. It is instructive to write this equation in a form that closely resembles its linear counterpart by defining an *effective* field–dependent permittivity for the particle as follows:

$$\underline{\varepsilon}_{eff,p}(E_p) = \underline{\varepsilon}_{eff,p} \equiv \underline{\varepsilon}^{(1)}_p + \underline{\varepsilon}^{(2)}_p E_p \quad (3.27)$$

$$\underline{\varepsilon}^{(1)}_m \left(\frac{2A_{1,m}}{R^3} + E_0 \right) + \underline{\varepsilon}_{eff,p} \left(\frac{A_{1,m}}{R^3} - E_0 \right) = 0 \quad (3.28)$$

Writing the effective permittivity of the particle in this form emphasizes the fact that the complex permittivity is altered by the action of the field, in contrast to the standard linear permittivity. This, of course, does not preclude a frequency dependence of both $\underline{\varepsilon}^{(1)}_p$ and $\underline{\varepsilon}^{(2)}_p$ and hence $\underline{\varepsilon}_{eff,p}$.

From a physical standpoint, this new quadratic particle field dependence has a profound effect on the properties of the particle. To see this, the situation where there is no external field ($E_0 = 0$) is considered; thus Eq. (3.26) becomes:

$$\frac{A_{1,m}}{R^3} \left(\underline{\varepsilon}^{(1)}_p + 2\underline{\varepsilon}^{(1)}_m - \underline{\varepsilon}^{(2)}_p \frac{A_{1,m}}{R^3} \right) = 0 \quad (3.29)$$

In order to ensure an electric flux density balance, this equation can have two solutions:

$$A_{1,m} = 0 \quad (3.30)$$

$$A_{1,m} = \frac{(\underline{\varepsilon}^{(1)}_p + 2\underline{\varepsilon}^{(1)}_m)R^3}{\underline{\varepsilon}^{(2)}_p} \quad (3.31)$$

If there is no nonlinearity, $\underline{\varepsilon}^{(2)}_p = 0$ (note, this substitution is made to Eq. (3.29)), then the only means available to the system to maintain a flux density balance is via Eq. (3.30). Now if a spontaneous fluctuation should result in $A_{1,m} \neq 0$, thus producing a charge separation or breakdown in electrical symmetry of the particle, then the conditions for the electrical flux density balance are violated and the broken symmetry state will vanish by a fluctuation in the reverse direction. If, however, the nonlinearity is present, $\underline{\varepsilon}^{(2)}_p \neq 0$, then a balance of flux density may be achieved without the dipolar coefficient, $A_{1,m}$, being identically zero, its value being given by Eq. (3.31). It is therefore seen that the presence of a nonlinearity in the system introduces conditions that allow the possibility of the appearance of a permanent dipole (breakdown of electrical symmetry) on the particle by a spontaneous fluctuation process. This type of phenomenon of *spontaneous symmetry breakdown* is known to exist in other branches of physics involving nonlinearities (73).

3.5 Analytical Solutions of Quadratic Equation

Further progress is made upon solving the quadratic equation, Eq. (3.26), which leads to the two roots:

$$A_{1,m}^{\pm} = \frac{R^3}{\underline{\varepsilon}^{(2)}_p} \left[\underline{\varepsilon}^{(1)}_m + \frac{\underline{\varepsilon}^{(1)}_p}{2} + E_0 \underline{\varepsilon}^{(2)}_p \pm \left[(\underline{\varepsilon}^{(1)}_m)^2 + \underline{\varepsilon}^{(1)}_m \underline{\varepsilon}^{(1)}_p + \frac{(\underline{\varepsilon}^{(1)}_p)^2}{4} + 3E_0 \underline{\varepsilon}^{(1)}_m \underline{\varepsilon}^{(2)}_p \right]^{1/2} \right] \quad (3.32)$$

From this expression, the experimentally measurable quantities, which are the real parts of the two Clausius–Mossotti factors, can be obtained from:

$$\operatorname{Re}\{K_e\}_1 = \frac{\operatorname{Re}\{A_{1,m}^-\}}{E_0 R^3}; \quad \operatorname{Re}\{K_e\}_2 = \frac{\operatorname{Re}\{A_{1,m}^+\}}{E_0 R^3} \quad (3.33)$$

Prior to carrying out the calculations envisaged in Eq. (3.33), it is instructive to identify the root in Eq. (3.32) that leads to the standard Clausius–Mossotti factor in the linear analysis (§§2.1.2 and 2.1.3). This is achieved by carrying out a power series expansion in E_0 of both roots in Eq. (3.32):

$$A_{1,m}^- = E_0 R^3 \left(\frac{\underline{\varepsilon}^{(1)}_p - \underline{\varepsilon}^{(1)}_m}{2\underline{\varepsilon}^{(1)}_m + \underline{\varepsilon}^{(1)}_p} \right) + \frac{9E_0^2 R^3 (\underline{\varepsilon}^{(1)}_m)^2 \underline{\varepsilon}^{(2)}_p}{[2\underline{\varepsilon}^{(1)}_m + \underline{\varepsilon}^{(1)}_p]^3} - + \dots \quad (3.34)$$

$$A_{1,m}^+ = \frac{R^3}{\underline{\varepsilon}^{(2)}_p} (2\underline{\varepsilon}^{(1)}_m + \underline{\varepsilon}^{(1)}_p) + E_0 R^3 \left(\frac{\underline{\varepsilon}^{(1)}_p + 5\underline{\varepsilon}^{(1)}_m}{2\underline{\varepsilon}^{(1)}_m + \underline{\varepsilon}^{(1)}_p} \right) - \frac{9E_0^2 R^3 (\underline{\varepsilon}^{(1)}_m)^2 \underline{\varepsilon}^{(2)}_p}{[2\underline{\varepsilon}^{(1)}_m + \underline{\varepsilon}^{(1)}_p]^3} + \dots \quad (3.35)$$

Examination of these two expansions reveals that it is the $A_{1,m}^-$ root that becomes the standard linear Clausius–Mossotti factor when $\underline{\varepsilon}^{(2)}_p = 0$. It is clear that the electric flux density balance equation will lead to the traditional single–valued Clausius–Mossotti factor in the linear analysis, if and only if, $\underline{\varepsilon}^{(2)}_p = 0$, while even infinitesimally small values of this parameter will produce bifurcation to multiple values.

Such a result may at first glance appear strange, but it is a phenomenon that has been observed in other areas of nonlinear dynamics. One of the best known examples is the Andronov–Hopf bifurcation in chemical kinetics (15). In this example, the coupled rate equations describing the concentrations of two chemical species are considered. If the nonlinear second–order terms in the rate equation are ignored, then the equilibrium state of the system consists of a single fixed point with zero concentrations of all chemical species; the analogous situation here being expressed by Eq. (3.30), where a state of zero polarization is predicted. With the inclusion of nonlinearity, a second equilibrium state appears in which the chemical concentrations are no longer vanishing quantities but possess finite values, and this corresponds to Eq. (3.31), where a finite polarization is observed. The Eqs. (3.34) and

(3.35) clearly show the two solutions as power series expansions around these two equilibrium states. It is indeed the appearance of these two states, in the constructed model, that results in the hysteresis in the DEP spectrum, the complete frequency dependence which is to be presented in the next section.

3.6 Extraction of Real Clausius–Mossotti Factors

Having established the point of contact with the traditional theory in a concise manner, the real parts of the two Clausius–Mossotti factors in the second–order theory, described in the previous sections, are derived. It should be remembered that all permittivities considered in this nonlinear model are complex quantities defined by Eq. (3.8), and thus it is convenient to introduce a compact notation as follows:

$$\begin{aligned}
 A_1 &\equiv \varepsilon^{(2)}_p; & A_2 &\equiv -\frac{\sigma^{(2)}_p}{2\omega}; & B_1 &\equiv -\left(2E_0\varepsilon^{(2)}_p + \varepsilon^{(1)}_p + 2\varepsilon^{(1)}_m\right)R^3; \\
 B_2 &\equiv \frac{\left(E_0\sigma^{(2)}_p + \sigma^{(1)}_p + 2\sigma^{(1)}_m\right)R^3}{\omega}; & F_1 &\equiv E_0\left(2E_0\varepsilon^{(2)}_p + \varepsilon^{(1)}_p - \varepsilon^{(1)}_m\right)R^3; \\
 F_2 &\equiv -\frac{E_0\left(E_0\sigma^{(2)}_p + 2\sigma^{(1)}_p - 2\sigma^{(1)}_m\right)R^6}{2\omega}
 \end{aligned} \tag{3.36}$$

In terms of the definitions described in Eq. (3.36), the imaginary part of the quantities under the square root sign in Eq. (3.32) is given by:

$$\eta \equiv 2(A_1F_2 + A_2F_1) - B_1B_2 \tag{3.37}$$

Depending on the sign of η , the real parts of $A_{1,m}^\pm$ can be expressed as follows:

$$\eta < 0: \quad \text{Re}\{A_m^+\} = Z_1 + t_1 - t_2; \quad \text{Re}\{A_m^-\} = Z_1 - t_1 + t_2 \tag{3.38}$$

$$\eta > 0: \quad \text{Re}\{A_m^+\} = Z_1 - t_1 - t_2; \quad \text{Re}\{A_m^-\} = Z_1 + t_1 + t_2 \tag{3.39}$$

Here:

$$Z_1 \equiv -\frac{A_1B_1 + A_2B_2}{2(A_2^2 + A_1^2)}; \quad t_1 \equiv \frac{A_2\sqrt{\mu - \mu'}}{\sqrt{8}(A_2^2 + A_1^2)}; \quad t_2 \equiv \frac{A_1\sqrt{\mu + \mu'}}{\sqrt{8}(A_2^2 + A_1^2)};$$

$$\begin{aligned}\mu^2 &\equiv (B_1^2 + B_2^2)^2 + 8(A_1B_2^2 - 2A_2B_1B_2 - A_1B_1^2)F_1 + 16(A_1^2 + A_2^2)(F_1^2 + F_2^2) \\ &\quad + 8(A_2B_1^2 - 2A_1B_1B_2 - A_2B_2^2)F_2; \\ \mu' &\equiv B_1^2 - B_2^2 - 4A_1F_1 + 4A_2F_2\end{aligned}$$

Thus the experimental quantities $\text{Re}\{K_e\}_1$ and $\text{Re}\{K_e\}_2$ are readily obtained from Eqs. (3.38) and (3.39).

The molecular processes that govern the shape of the polarization curves as a function of the field frequency, from a dynamical point of view, have some common features with the linear case.

(A) It is predominantly ionic motion that is responsible for the polarization of the particle at low frequencies. This can be seen by taking the zero frequency limits of $\text{Re}\{K_e\}_1$ and $\text{Re}\{K_e\}_2$. For $\eta < 0$, the low frequency limits are:

$$\begin{aligned}\lim_{\omega \rightarrow 0} \text{Re}\{K_e\}_{1,2} &= \frac{E_0\sigma^{(2)}_p + \sigma^{(1)}_p + 2\sigma^{(1)}_m}{E_0\sigma^{(2)}_p} +, - \\ &\quad \frac{\sqrt{6E_0\sigma^{(1)}_m\sigma^{(2)}_p + (\sigma^{(1)}_p)^2 + 4\sigma^{(1)}_m\sigma^{(1)}_p + 4(\sigma^{(1)}_m)^2}}{E_0\sigma^{(2)}_p}\end{aligned}\quad (3.40)$$

and for $\eta > 0$, they are:

$$\begin{aligned}\lim_{\omega \rightarrow 0} \text{Re}\{K_e\}_{1,2} &= \frac{E_0\sigma^{(2)}_p + \sigma^{(1)}_p + 2\sigma^{(1)}_m}{E_0\sigma^{(2)}_p} -, + \\ &\quad \frac{\sqrt{6E_0\sigma^{(1)}_m\sigma^{(2)}_p + (\sigma^{(1)}_p)^2 + 4\sigma^{(1)}_m\sigma^{(1)}_p + 4(\sigma^{(1)}_m)^2}}{E_0\sigma^{(2)}_p}\end{aligned}\quad (3.41)$$

(B) At high frequencies, it is the dipolar motion that determines the polarization through the permittivities. Once again, this feature can be ascertained by taking the high-frequency limits of $\text{Re}\{K_e\}_1$ and $\text{Re}\{K_e\}_2$. For $\eta < 0$, the high frequency limits are:

$$\begin{aligned} \lim_{\omega \rightarrow \infty} \operatorname{Re}\{K_e\}_{1,2} &= \frac{E_0 \varepsilon^{(2)}_p + \varepsilon^{(1)}_p + 2\varepsilon^{(1)}_m}{E_0 \varepsilon^{(2)}_p} +, - \\ &\frac{\sqrt{6E_0 \varepsilon^{(1)}_m \varepsilon^{(2)}_p + (\varepsilon^{(1)}_p)^2 + 4\varepsilon^{(1)}_m \varepsilon^{(1)}_p + 4(\varepsilon^{(1)}_m)^2}}{E_0 \varepsilon^{(2)}_p} \end{aligned} \quad (3.42)$$

and for $\eta > 0$, they are:

$$\begin{aligned} \lim_{\omega \rightarrow \infty} \operatorname{Re}\{K_e\}_{1,2} &= \frac{E_0 \varepsilon^{(2)}_p + \varepsilon^{(1)}_p + 2\varepsilon^{(1)}_m}{E_0 \varepsilon^{(2)}_p} -, + \\ &\frac{\sqrt{6E_0 \varepsilon^{(1)}_m \varepsilon^{(2)}_p + (\varepsilon^{(1)}_p)^2 + 4\varepsilon^{(1)}_m \varepsilon^{(1)}_p + 4(\varepsilon^{(1)}_m)^2}}{E_0 \varepsilon^{(2)}_p} \end{aligned} \quad (3.43)$$

At any given moment the particle is characterized by only one of the two Clausius–Mossotti factors (for a given set of parameters η will be either less than zero or greater than zero). Each of these is related by standard equations to the macroscopic dipole moment of the particle (39). Thus, in the nonlinear case, two dipole moments are possible at each frequency and they may be described in terms of the local field. The expressions become particularly simple if it is assumed that to a good approximation the local field is equal to the applied field \vec{E}_0 :

$$\begin{aligned} \vec{\mu}_1 &= 4\pi R^3 \varepsilon^{(1)}_m \operatorname{Re}\{K_e\}_1 \vec{E}_0 \\ \vec{\mu}_2 &= 4\pi R^3 \varepsilon^{(1)}_m \operatorname{Re}\{K_e\}_2 \vec{E}_0 \end{aligned}$$

Corresponding to these dipoles, the energies are given by:

$$\begin{aligned} \mathcal{U}_1 &= -\vec{\mu}_1 \cdot \vec{E}_0 = -4\pi R^3 \varepsilon^{(1)}_m \operatorname{Re}\{K_e\}_1 |\vec{E}_0|^2 \\ \mathcal{U}_2 &= -\vec{\mu}_2 \cdot \vec{E}_0 = -4\pi R^3 \varepsilon^{(1)}_m \operatorname{Re}\{K_e\}_2 |\vec{E}_0|^2 \end{aligned}$$

The probabilities of finding the particle in one of the two Clausius–Mossotti factors are therefore given by:

$$P_1 = \mathcal{N}_1 e^{-\mathcal{U}_1/k_B T} = \mathcal{N}_1 e^{4\pi R^3 \varepsilon^{(1)}_m \operatorname{Re}\{K_e\}_1 |\vec{E}_0|^2 / k_B T} \quad (3.44)$$

$$P_2 = \mathcal{N}_2 e^{-\mathcal{U}_2/k_B T} = \mathcal{N}_2 e^{4\pi R^3 \varepsilon^{(1)}_m \operatorname{Re}\{K_e\}_2 |\vec{E}_0|^2 / k_B T} \quad (3.45)$$

Here, the two constants \mathcal{N}_1 and \mathcal{N}_2 are the normalization constants for the two probability

functions P_1 and P_2 , k_B is Boltzmann's constant, and T is the absolute temperature. From Eqs. (3.44) and (3.45) it can be seen that if both choices ($\text{Re}\{K_e\}_1$ and $\text{Re}\{K_e\}_2$) are available to the particle then it is more likely to be found in the state with the larger value of the Clausius–Mossotti factor. The two dipoles, $\vec{\mu}_1$ and $\vec{\mu}_2$, are macroscopic quantities that characterize the particle as a whole; however, it is important to realize that these are the manifestations of dipoles that are produced as a consequence of the polarization of molecular entities in the particle. If the particle is subjected to an external field in two sweeps in opposite directions (as is done in a typical experiment leading to the DEP spectrum of Fig. 3.1), then during the course of the first sweep, those molecular processes that lead to the larger of the two Clausius–Mossotti factors will come into play predominantly. In addition, if the time required for the relaxation back to their initial conditions is longer than the time between the two sweeps, then the molecular processes leading to the smaller of the two Clausius–Mossotti factors will come into play during the second sweep. The theory predicts that the upper parts of the loops in the DEP spectra will be traced during the initial scan, while the lower parts will appear on reversal of the direction. This prediction is verified by the experiments. Several statements were made earlier in this chapter pointing out that the nonlinear treatment applies to the situation in which the applied field alters the electrical properties of the particle. These statements are to be understood within the context just described, that is within the duration of time during which the molecules have not had the opportunity to relax back to their initial conditions. If this duration is very long, then in effect, the particle has undergone an aging process which is not reversed.

3.7 Numerical Computations and Comparison with Experiment

In order to carry out the numerical computations, experimental values of all the parameters listed in Eq. (3.32) are required. From this list, the electrical properties $\varepsilon^{(1)}_m$, $\sigma^{(1)}_m$, $\varepsilon^{(1)}_p$, and $\sigma^{(1)}_p$ are the standard linear permittivities and conductivities for the medium and particle respectively and are well known, measured quantities being available. The magnitude of the applied field E_o and the particle radius R are also available. At the present time,

however, the second-order electrical permittivity $\varepsilon^{(2)}_p$ and conductivity $\sigma^{(2)}_p$ are not available, since in the present context these quantities have been introduced for the first time. Lacking available values for these parameters, we investigate a range of values and try to obtain bounds that produce dielectrophoretic spectra possessing the qualitative features of the experimentally measured spectra.

As has already been pointed out in §3.2, the low frequency region is not only characterized by multiple Clausius–Mossotti factors, but overlaid on this is also the phenomenon of anomalous dielectrophoresis (introduced in the beginning of this chapter). The traditional linear theory of a concentric shelled sphere (described in Chapter 2), in the absence of this phenomenon, predicts a constant value of -0.5 for the real part of the Clausius–Mossotti factor as the frequency approaches zero for an insulating particle (see Fig. 2.5). Anomalous dielectrophoresis, however, causes a transition to positive values in this frequency domain. It is clear that the observation of multiple Clausius–Mossotti factors will also be colored by this effect. It has not been the intent of this theoretical investigation to focus attention on anomalous dielectrophoresis, but rather to offer explanation into the source of the multiple Clausius–Mossotti factors. Hence it is imperative for the reader to keep in mind that in comparing theory with experiment, the features of anomalous dielectrophoresis appearing in the experimental spectra will not appear in the model. As a consequence of this, it is expected that a typical plot of $\text{Re}\{K_e\}_1$ (since Eq. (3.34) shows that this is the branch that leads to the linear Clausius–Mossotti factor) will display qualitative resemblances to Fig 2.5. The zero frequency limiting value of -0.5 will, however, only be realized for some specific values of $\sigma^{(2)}_p$.

It is seen from the experimental DEP spectrum of Fig. 3.1 that two paths are available to the system as the frequency is changed, and that these two paths meet at the low frequency (below 10 Hz.) and high frequency (above 10^4 Hz.) ends, with a crossing occurring at an intermediate value of about 10^2 Hz.. At frequencies greater than 10^4 Hz., the field is able to penetrate into the cell membrane, and the spectrum is complicated by the appear-

ance of Maxwell–Wagner relaxation effects (see §2.3.2) due to the membrane. Immediately prior to the membrane effects, a double loop is seen in the form of two hysteresis curves. In the model presented here, a shell has not been introduced and thus the applicability is strictly low frequency. The two paths are interpreted to correspond to the two different Clausius–Mossotti factors and as such, it is important that the two roots $A_{1,m}^-$ and $A_{1,m}^+$ become degenerate at frequency values where the curves cross; and approximately degenerate in those regions where they approximate each other.

In order to carry out a numerical investigation into probable values for the unknown second–order parameters, the first–order parameters were initially fixed at some reasonable values that describe a tobacco protoplast immersed in a water based medium. Thus, the following first–order parameters were selected: [1] $\sigma_m^{(1)} = 10^{-4} Sm^{-1}$; [2] since the low frequency region is exclusively influenced by the values of the conductivities, the parameter $\sigma_p^{(1)}$ was allowed to vary from a value of $10^{-9} Sm^{-1}$, corresponding to a pure surface conductance effect (59),(74) to a value of $10^{-4} Sm^{-1}$, where the particle conductivity becomes significant; [3] $\varepsilon_m^{(1)} = 7.083 \times 10^{-10} Fm^{-1}$; [4] $\varepsilon_p^{(1)} = 5.312 \times 10^{-10} Fm^{-1}$; [5] $R = 17.5 \times 10^{-6} m$; and [6] $E_0 = 200 Vm^{-1}$.

The selection of the sign of the second–order permittivity $\varepsilon_p^{(2)}$ was made on the requirement that the root $A_{1,m}^-$ reproduce qualitatively the appearance of the linear Clausius–Mossotti factor in keeping with (3.34). Numerical investigation has shown that this feature is realized for positive values of $\varepsilon_p^{(2)}$ only. Choosing $\varepsilon_p^{(2)} > 0$ implies that $\eta > 0$, and hence the real part of the two Clausius–Mossotti factors (i.e. $\text{Re}\{K_e\}_{1,2}$) must obey Eqs. (3.41) and (3.43). Furthermore, the high frequency limits of the Clausius–Mossotti factors given by Eq. (3.43), coupled with the fact that the two experimentally determined Clausius–Mossotti factors, displayed in Fig. 3.1, approach each other for values of the applied field frequency greater than 10^4Hz. , sets a fairly strong limitation on the numerical values of $\varepsilon_p^{(2)}$. For the typical values of the linear parameters given above, these conditions are reasonably

well realized with $10^{-9} FV^{-1} \leq \varepsilon^{(2)}_p \leq 10^{-7} FV^{-1}$ and in the subsequent calculations this range of values was adopted. The value of $\sigma^{(2)}_p$ determines the low frequency behavior, and a series of values were selected in order to reproduce the experimental observations. The result of these calculations are displayed in Fig. 3.3. Examination of these plots clearly indicates that if the phenomenon of anomalous dielectrophoresis is neglected, then the hysteresis loops observed experimentally are qualitatively represented theoretically.

In all of the above calculations, the implemented electrical properties are the conventional properties, but the nonlinear parameters that are capable of reproducing the experimentally observed DEP spectra with hysteresis are characterized by $\varepsilon^{(2)}_p > 0$ and $\sigma^{(2)}_p < 0$.

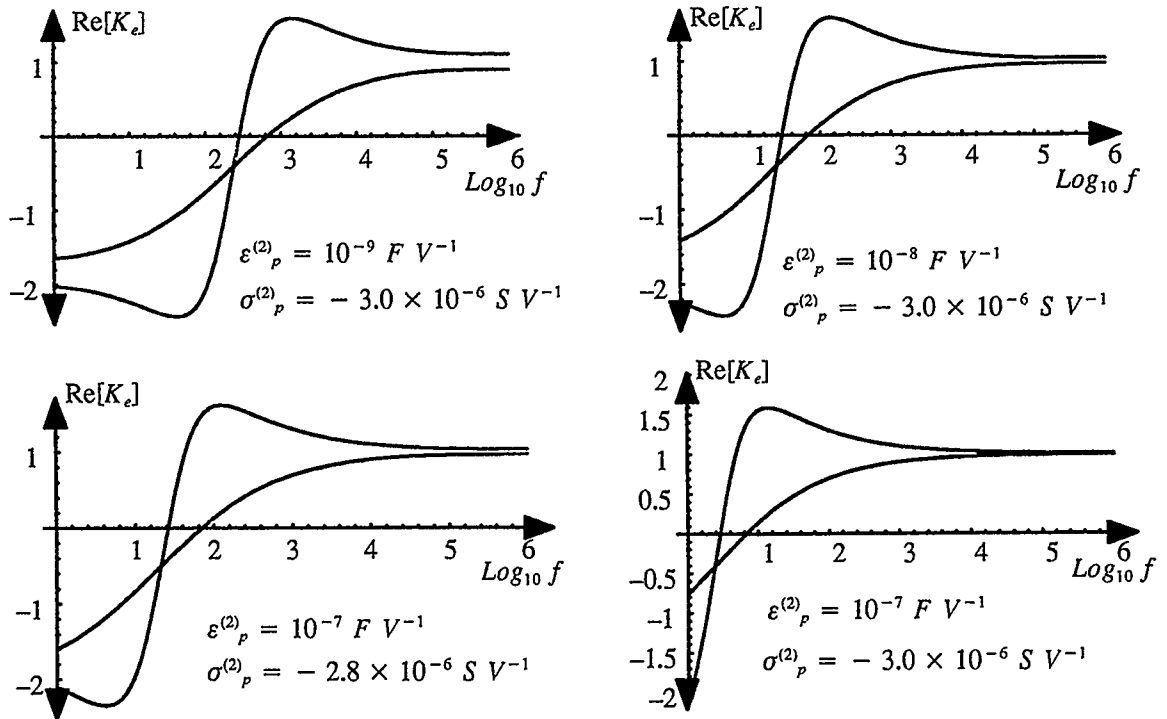


Fig. 3.3 Behavior of the two Clausius–Mossotti factors for different values of the second–order particle parameters.

The implications of this choice of the sign of the second–order parameters on the effective permittivity of the particle may be seen from substitution of the definitions of the complex permittivities (Eq. (3.8)) into Eq. (3.27):

$$\underline{\varepsilon}_{eff,p} = \left(\varepsilon^{(1)}_p + |\varepsilon^{(2)}_p| E_p \right) - \frac{i}{\omega} \left(\sigma^{(1)}_p - \frac{|\sigma^{(2)}_p|}{2} E_p \right) \equiv \varepsilon_{eff,p} - \frac{i}{\omega} \sigma_{eff,p} \quad (3.46)$$

Thus the introduction of the surface nonlinearities results in the real part of the effective particle permittivity being *raised* by a field proportional quantity while the imaginary part is *lowered* by a similar field proportional term. From a physical point of view, increasing the real part of the complex permittivity is equivalent to increasing the density of bound charges, while decreasing the imaginary part appears to an external observer as a decreased conductivity or current, which in turn reflects a decrease in the free charge carrier (ionic) density. All of these are the result of the action of the applied field.

3.8 Conclusions

The traditional cell models and their electrical characters are based on simple static structures. It is well known, however, that cellular components such as the lipid bilayer bear a closer resemblance to ordered fluids rather than to solids, as the transmembrane surface proteins exhibit both lateral and rotational diffusion (72). This diffusional motion is believed to be the result of gradients in the chemical potential but a similar motion could also be induced as a direct consequence of the externally applied field or directly via the double layer polarizations (gradients in the electrical potential). If the time constants associated with such motions are comparable in magnitude to the externally applied field, then it is quite possible that the electrical measurements will be plagued by memory effects leading to a splitting of the Clausius–Mossotti factors, such as that observed in the low frequency regions of the DEP spectra.

The introduction of a nonlinear boundary condition at the cell–medium interface has resulted in multiple Clausius–Mossotti factors which explains the observed hysteresis loops in the DEP spectra. The theory developed here is the simplest possible extension of the linear theory into a nonlinear regime that allows analytical treatments to be performed. It is important to realize that in this analysis no perturbation techniques were carried out which would only have improved the linear results quantitatively without introducing any

new qualitative features such as multiple Clausius–Mossotti factors. In colloidal suspensions where the surface area between the suspended particles and the surrounding medium is very large, the nonlinear interface could play a very major role in determining the physical properties of the suspension.

The hysteresis can be attributed to the motion of the transmembrane proteins under the influence of a local electrical field which produces alterations in the nature of the cell surface. These changes alter the complex permittivity by terms that are linear in the field. In addition, it is imperative to keep in mind the fact that even infinitesimally small values of the proportionality constants that relate the complex permittivity to the local field, will result in a bifurcation of the linear Clausius–Mossotti factor.

Chapter 4: Micromotion

4.1 Introduction

In the initial investigation by Kaler *et al* (9), the experimental observations of low frequency *micromotion* of single DEP levitated plant protoplasts were reported along with the proposal of a simple model equation describing the levitation of a particle with a single-frequency electric field. A number of pertinent physical parameters were varied including: (a) the size of the cell; (b) the frequency of the electric field; (c) the conductivity of the suspending medium; and (d) the cell surface charge. Perhaps the most interesting observation reported by the authors was the fact that the micromotion was not simple harmonic motion at applied electric field frequencies below 20 Hz., but possessed significant higher harmonic components. Their simple modelling of the dynamics could not account or explain the emergence of the additional harmonics seen in the FFT spectra.

A second investigation by Barrie *et al* (10), extended the simple mathematical model, and with the recognition that the micromotion dynamics were nonlinear, studied several additional aspects of the problem. The effects of both the high and low frequency fields in a dual frequency levitator were introduced to the model (the actual experiments were performed using a dual frequency levitation system). In addition, an attempt was made to find the best possible linear approximation to the exact micromotion equation. This revealed that the retention of certain nonautonomous terms, neglected in the initial study (9), were necessary in order to recover the experimentally observed low frequency drop off in the Bode plot (a measure of the linear response of a given system to an excitation). Finally, a careful Fourier expansion was performed on the equation of motion along with a stability analysis, revealing that all modes with frequencies higher than the frequencies of the driving forces were damped out in a linear regime. This led the authors to the conjecture that the higher harmonics may have arisen as a consequence of the nonlinearities resulting from the field inhomogeneities.

The observation of higher harmonics is not unique to the DEP levitation experiments, but has been reported by Gaigalas *et al* (75) in electrophoretic light-scattering experiments with submicron polystyrene latex spheres subject to uniform AC electric fields. The authors observed higher harmonic frequency components below 50 Hz. in aqueous solution. They were, however, unable to discern the physical origins of the nonlinear low frequency electrophoretic response but suggested four possible mechanisms: (a) a hydrodynamic interaction between the particle and the surrounding fluid; (b) a coupling of charge fluctuations in the Helmholtz layer of the particle with the external field; (c) Onsager's theory (18) of the field-induced dissociation of a weak electrolyte; and (d) the theory of Dukhin and co-workers (76) implying the implicit presence of nonlinear terms in the electrophoretic velocity. Since the experimental work of Gaigalas *et al* (75), Robertson (77) estimated the mobility variance by calculating the homodyne correlation function for a general light scattering experiment involving an AC electrophoretic field. His analysis showed that higher harmonics were possible for low field frequencies, but the origins were not disclosed.

This chapter presents the results of a theoretical investigation into physical origins of these higher frequency harmonics in the micromotion of DEP-levitated plant protoplasts. It should be noted that this author has recently published much of the results presented here in the *Journal of Colloid and Interface Science* (78).

4.2 Experimental

Typical experimental FFT spectra, are displayed in Figs. 4.1 and 4.2, of a protoplast excited by a 20 Hz., 1.0 V-rms AC signal, and a 2 Hz., 1.0 V-rms AC signal, respectively. It is appropriate that some details regarding the performed experiments be outlined in this section as the author had opportunity to perform his own experiments. The reader is referred to references: (45), (6), (9), and (79) for complete details. The experimental equipment and measurement technique is described in the next section; and following that, the isolation procedure for the protoplasts.

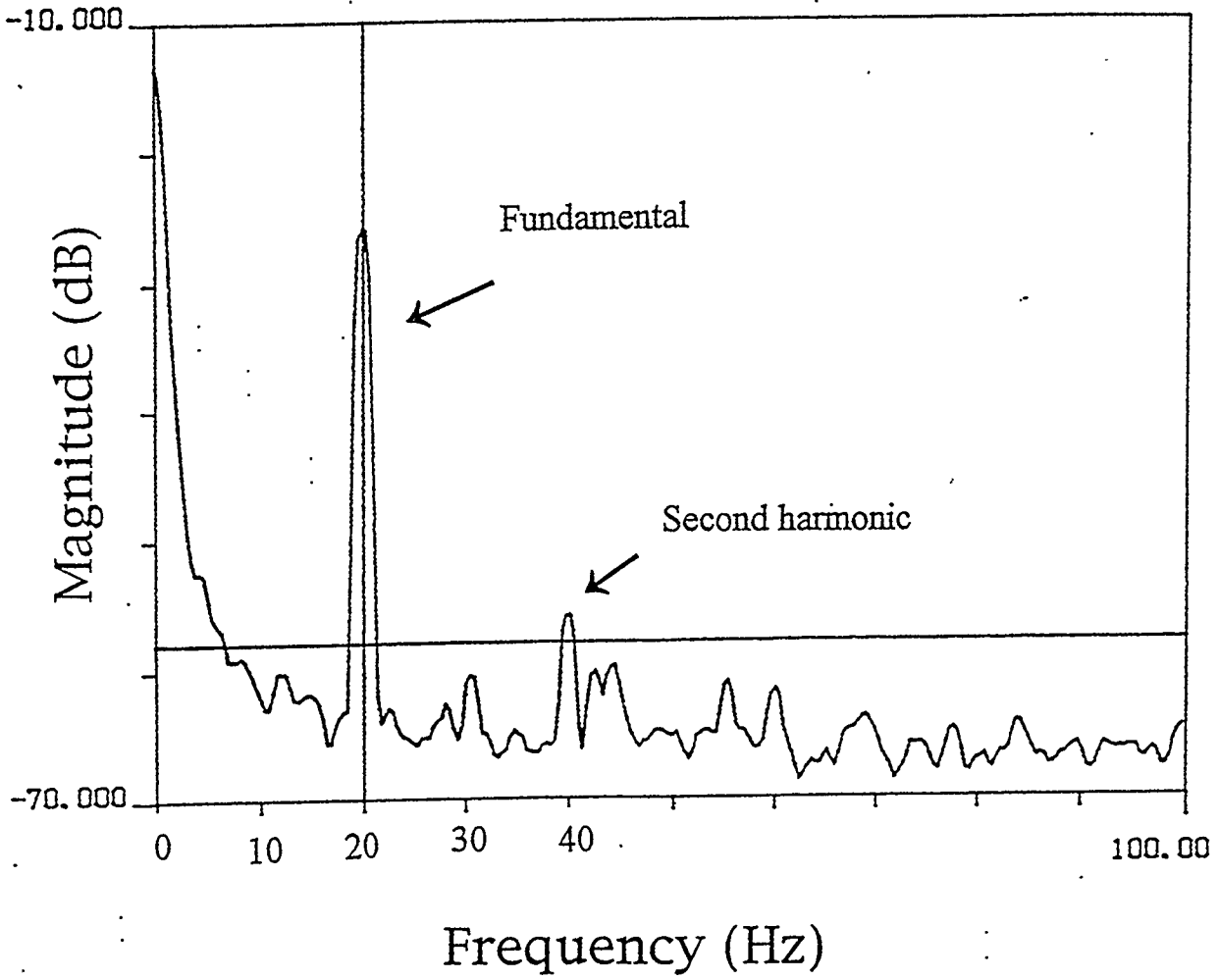


Fig. 4.1 Sample FFT spectrum from the centroid detector obtained for a 45 μm -diameter protoplast excited by a 20 Hz., 1.0 V-rms AC signal (9).

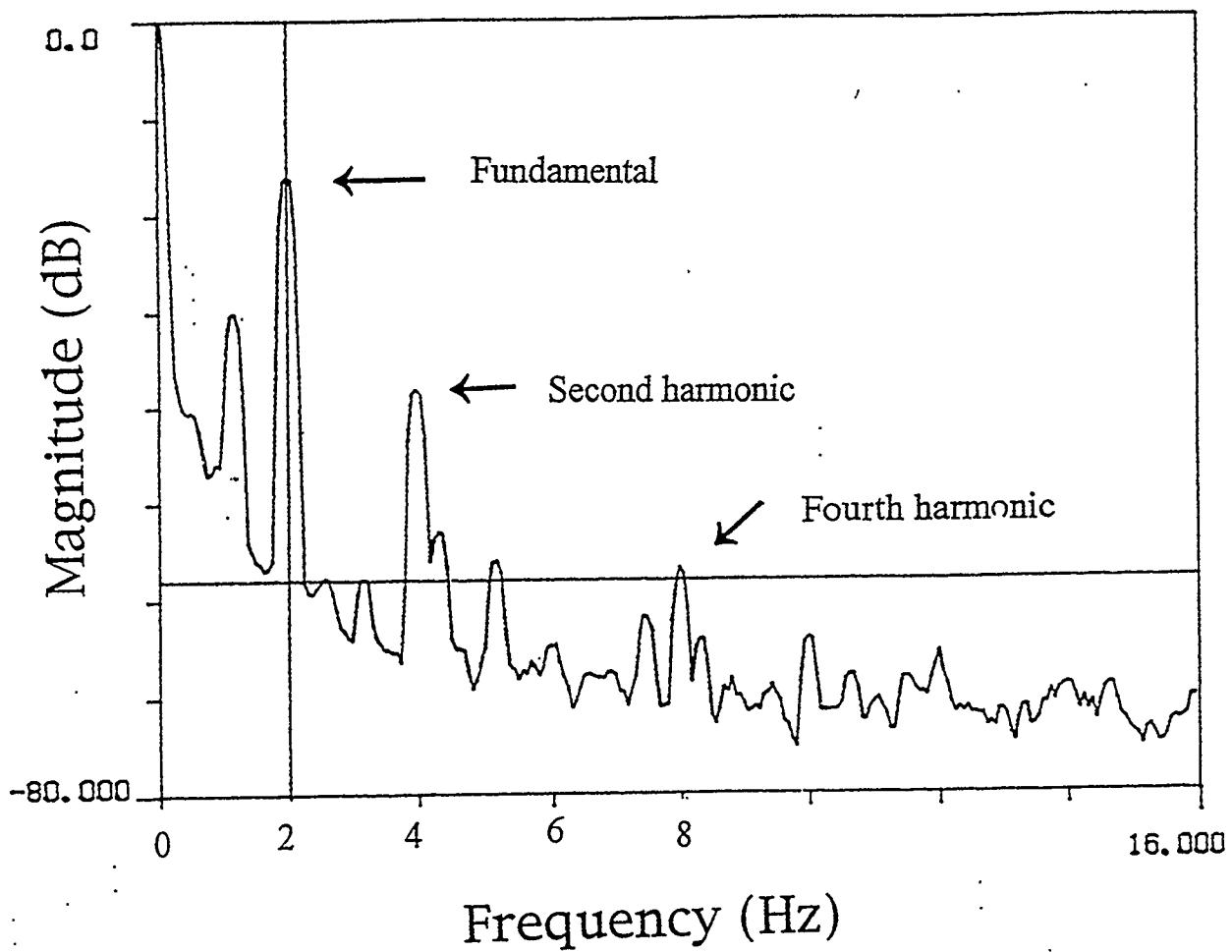


Fig. 4.2 Sample FFT spectrum from the centroid detector obtained for a 45 μm -diameter protoplast excited by a 2 Hz., 1.0 V-rms AC signal (9).

4.2.1 Measurement and Detection of Micromotion

The dual-frequency levitation scheme, described in Chapter 1, was made use of to facilitate the measurement of both the positive and negative DEP spectra of the protoplast cells. The levitator, shown in sectional view in Fig. 4.3, is comprised of gold-plated stainless steel cone-plate electrodes ($z_{\min} = 0.45$ mm and $\theta = 60^\circ$), housed in an acrylic plastic chamber fitted with optical windows to facilitate viewing of levitated cells. The chamber was first loaded with a dilute cell suspension, then sealed and mounted upright on a vertical microscope stage. The optical monitoring was simultaneously performed by two systems: a standard video camera; and a high-resolution, high speed centroid detector.

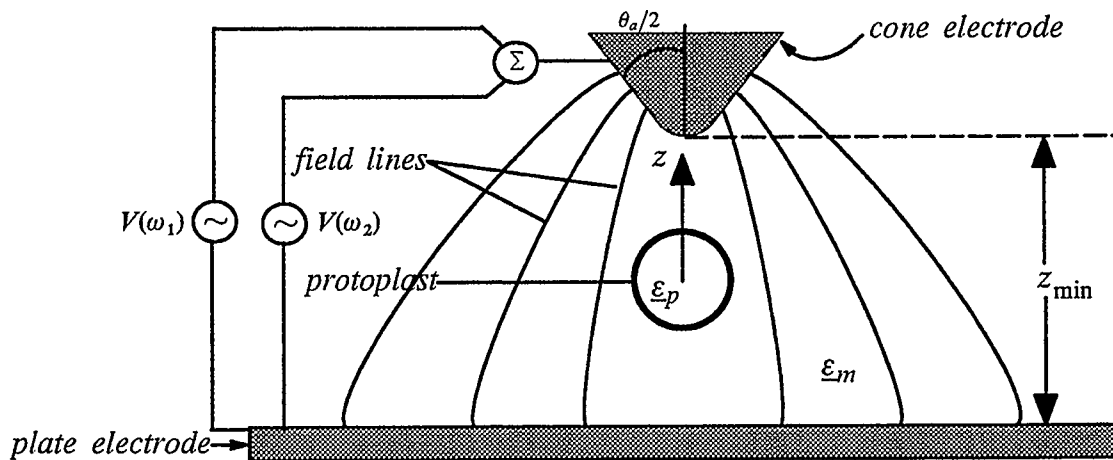


Fig. 4.3 Cross-sectional view of the levitation chamber, showing the axisymmetric electrodes and the dual-frequency excitation scheme used to measure the DEP spectra of a lone protoplast.

In conjunction with the image processing hardware, the video camera monitored the location of the cell, passed information on the position of the cell to the digital feedback control system, and allowed for the visual examination of the characteristics of the levitated cells. The microcomputer-based feedback system employs an adaptive proportional/integral (PI) control algorithm that maintains an individual protoplast at a fixed preset position on the axis. The high frequency voltage $V(\omega_2)$ at fixed frequency ω_2 , is summed with a fixed amplitude, variable frequency signal $V(\omega_1)$ and then applied to the chamber electrodes.

Utilization of a sensitive centroid detector (79), capable of resolving very small cell displacements ($\approx 0.1 \mu\text{m}$), enabled the very close monitoring of the micromotion of the levitated protoplasts. The detector output was fed to a dual-channel spectrum analyzer (HP 5423A) for Fourier analysis to facilitate the processing of both phase and magnitude information. To improve the signal-to-noise ratio of the frequency spectra, at least 10 consecutive sets of data were sampled, transformed, and then averaged.

4.2.2 Protoplast Preparation

Sterile seeds of canola (*Brassica napus* L. cv. Westar) were planted aseptically in sterile Magenta jars (6 seeds/jar) containing 50mL of nutrient medium, developed by Murashige and Skoog (80), of pH of 5.8 and solidified with 0.65% Phytagar® (Gibco BRL). One week after planting the seedlings were thinned to 3/jar. The plants were grown for 3–4 weeks with a 16 hour photo-period (photon fluency rate: $100\text{--}110 \mu\text{mol m}^{-2}\text{s}^{-1}$) at 25 °C, after which the leaves and cotyledons were harvested and used for protoplast isolation.

The leaves (ca. 2g) were cut into pieces about 2 mm long and wide and placed into an enzymatic digestion mixture containing 0.4% Cellulase "Onazuka" RS (Yakult Honsha Co., Ltd., Tokyo), 0.025% Pectolyase Y-23 (Seishin Pharmaceutical Co., Ltd., Tokyo) (45), 1 mg/ml $\text{CaCl}_2 \cdot 2\text{H}_2\text{O}$, and 8% (w/v) sorbitol; pH 5.8 in Petri dishes (about 10 mL of digestion mixture was used per gram of leaves). The leaf pieces were incubated on a gyrotary shaker (ca. 30 rpm) for 12 hours at room temperature. After incubation, the extract was filtered through a 149 μm nylon mesh to remove large debris. The filtrate was then centrifuged at $40 \times g$ to collect the protoplasts. The protoplast pellet was resuspended gently in autoclaved 8% sorbitol (pH 5–6) and then washed 3 times followed by centrifugation ($40 \times g$) and then resuspended. After the final wash in an 8% sorbitol medium of known conductivity and pH, the protoplasts were diluted with 8% sorbitol to a suitable concentration for use in the levitation chamber (the final suspension had a very pale green color), and kept on ice until use. The conductivity and pH of the dilute cell suspension were monitored by a conductivity meter (model #1710 Bio-Rad Laboratory, Richmond, CA) and a pH meter (Accumet, model

#620, Fisher Scientific, Pittsburgh, PA).

4.3 Dynamical Equation of Study

The micromotion of the levitated protoplast at low frequencies may be described by the application of Newton's 2nd law. Derivation of the protoplast dynamics for the various models considered may be found in the first two papers published on the phenomena (9), (10). However, for the purpose of completeness, a complete derivation of the micromotion dynamical equation is presented here.

4.3.1 Derivation

Under dual frequency conditions, the net electric field acting on the levitated particle (protoplast or cell) consists of two components: $E_1(z, t)$ the low frequency electric field; and $E_2(z, t)$ the high frequency electric field; produced by the summation of two AC voltages at distinct frequencies ω_1 and ω_2 . By convention, it is assumed that ω_1 is the test frequency at which all spectra are measured and that $\omega_1 < \omega_2$. Since the phenomenon of dielectrophoresis is basically the response of the particle to the field inhomogeneity, the two fields possess both a spatial and a temporal dependence. In those regions of frequency ω_1 where negative DEP is observed, the potential producing the high frequency component E_2 is automatically adjusted by a feedback controller in order to achieve levitation at some fixed point in the chamber. Mathematically, this implies that the high frequency field must incorporate in its amplitude a factor that would simulate the activities of the feedback controller. Thus the two electric fields will be described by the following expressions:

$$\begin{aligned} E_1(z, t) &= E_{01}(z) \cos(\omega_1 t); & E_2(z, t) &= \mathbb{E}_{02}(z, t) \cos(\omega_2 t) \\ \mathbb{E}_{02}(z, t) \cos(\omega_2 t) &\equiv E_{02}[1 + f(t)] \end{aligned} \quad (4.1)$$

The explicit forms of the two spatially dependent functions (amplitudes) $E_{01}(z)$ and $E_{02}(z)$ will be defined later. The precise form of the feedback-controlled amplitude modulation function $f(t)$ will also be described later.

As alluded to earlier, the dynamics of the cell may be described by Newton's second law; and thus the various forces experienced by the cell will be considered separately.

(1) Because of the surface charge, q , carried by the cell, it experiences electrophoretic forces due to both applied fields:

$$F_{el,1} = qE_{01}(z) \cos(\omega_1 t); \quad F_{el,2} = q\mathcal{E}_{02}(z) \cos(\omega_2 t) \quad (4.2)$$

(2) The induced dipole moment on the cell arising from the two fields results in two dielectrophoretic forces:

$$\begin{aligned} F_{DEP}(\omega_1) &= 2\alpha(\omega_1)E_{01}(z)E'_{01}(z) \cos^2(\omega_1 t) \\ F_{DEP}(\omega_2) &= 2\alpha(\omega_2)\mathcal{E}_{02}(z, t)\mathcal{E}'_{02}(z, t) \cos^2(\omega_2 t) \end{aligned} \quad (4.3)$$

where the prime (') denotes a differentiation with respect to the variable z and the quantities $\alpha(\omega_i)$ are related to the standard linear Clausius–Mossotti factor according to the definition:

$$\alpha(\omega_i) \equiv 2\pi R^3 \varepsilon_m \operatorname{Re}\{\underline{K}_e(\omega_i)\} \quad (4.4)$$

(3) Under the influence of the above forces the protoplast displays periodic motion (micromotion) which is subjected to a viscous damping force arising from the surrounding medium. This force is given by:

$$F_{damping} = b \frac{dz}{dt} \quad (4.5)$$

where b denotes the viscous drag coefficient which may be evaluated from Stoke's equation $b = 6\pi\eta R$ with the parameter η being the medium viscosity.

(4) Both gravity and buoyancy produce a force f_{gb} defined as follows:

$$f_{gb} = -m_b g = -\frac{4}{3}\pi R^3 (\gamma_p - \gamma_m) g \quad (4.6)$$

where m_b is the buoyant mass of the protoplast that depends upon densities γ_p and γ_m of the particle and the medium respectively and upon the radius R of the particle.

With the system forces defined above, the equation of motion can be written from Newton's 2nd law:

$$\begin{aligned}
m_e \frac{d^2 z}{dt^2} + b \frac{dz}{dt} = & q E_{01}(z) \cos(\omega_1 t) + 2\alpha(\omega_1) E_{01}(z) E_{01}'(z) \cos^2(\omega_1 t) + \\
& q \mathbb{S}_{02}(z, t) \cos(\omega_2 t) + 2\alpha(\omega_2) \mathbb{S}_{02}(z, t) \mathbb{S}_{02}'(z, t) \cos^2(\omega_2 t) - m_b g
\end{aligned} \tag{4.7}$$

where m_e is the effective mass of the particle that also depends upon the densities of the particle and medium according to: $m_e = \frac{4}{3}\pi R^3 \left[\gamma_p + \frac{\gamma_m}{2} \right]$. This expression is a result of the additional induced inertia arising from the acceleration of the sphere and fluid, where the fluid contribution is equal to half the mass of the fluid displaced by the sphere.

4.3.2 Approximations

In order to make use of the above derived dynamical equation (Eq. (4.7)), certain assumptions and approximations need to be implemented. If it is assumed that the frequency ω_2 is very high then Eq. (4.7) may be averaged over the period of oscillation $\mathcal{T} \equiv \frac{2\pi}{\omega_2}$ of this field and all time dependent quantities except $\cos(\omega_2 t)$ will be assumed to remain constant during this period. Applying this time average to Eq. (4.7) gives:

$$\begin{aligned}
m_e \frac{d^2 z}{dt^2} + b \frac{dz}{dt} = & q E_{01}(z) \cos(\omega_1 t) + 2\alpha(\omega_1) E_{01}(z) E_{01}'(z) \cos^2(\omega_1 t) + \\
& \langle F_{DEP}(\omega_2) \rangle (z) - m_b g
\end{aligned} \tag{4.8}$$

where :

$$\langle F_{DEP}(\omega_2) \rangle (z) \equiv 2\alpha(\omega_2) \mathbb{S}_{02}(z) \mathbb{S}_{02}'(z) \frac{1}{\mathcal{T}} \int_0^{\mathcal{T}} \cos^2(\omega_2 t) dt = \alpha(\omega_2) \mathbb{S}_{02}(z) \mathbb{S}_{02}'(z)$$

In a typical dielectrophoresis experiment, the particle or protoplast is lifted and maintained at an equilibrium position z_o . As the oscillatory micromotion will occur about the equilibrium position it will be convenient to introduce the following new variable $\delta(t)$ in the dynamical equation:

$$z(t) = z_o + \delta(t) \tag{4.9}$$

Substituting Eq. (4.9) into Eq. (4.8), yields:

$$m_e \frac{d^2\delta}{dt^2} + b \frac{d\delta}{dt} = qE_{01}(z_o + \delta) \cos(\omega_1 t) + 2\alpha(\omega_1)E_{01}(z_o + \delta)E_{01}'(z_o + \delta) \cos^2(\omega_1 t) + \langle F_{DEP}(\omega_2) \rangle (z_o + \delta) - m_b g \quad (4.10)$$

Now Eq. (4.10) is the foundation governing equation that was studied in order to understand the dynamics and characteristics of the micromotion. It is clear from examination of Eq. (4.10) that it is a very complicated nonlinear equation for which closed form analytical solutions are not available. Therefore, approximations were required in order to elucidate the dynamics.

The spatial inhomogeneity of the electric field was modelled through simply expanding the spatial dependent amplitudes of both the high and low frequency fields as Taylor series in z about the point $z = z_o$, and therefore:

$$E_{01}(z_o + \delta) = \lambda_0 + \lambda_1\delta + \lambda_2\delta^2 + \lambda_3\delta^3 + \dots \quad (4.11)$$

$$\text{where : } \lambda_n = \frac{1}{n!} \frac{d^n E_{01}(z_o)}{dz_o^n}$$

$$\text{and : } E_{01}(z_o + \delta)E_{01}'(z_o + \delta) = \gamma_0 + \gamma_1\delta + \gamma_2\delta^2 + \gamma_3\delta^3 + \dots \quad (4.12)$$

$$\text{where : } \gamma_0 = \lambda_0\lambda_1, \quad \gamma_1 = 2\lambda_0\lambda_2 + \lambda_1^2, \quad \gamma_2 = 3\lambda_0\lambda_3 + 3\lambda_1\lambda_2, \text{ etc.}$$

$$E_{02}(z_o + \delta) = \mu_0 + \mu_1\delta + \mu_2\delta^2 + \mu_3\delta^3 + \dots$$

$$\text{where : } \mu_n = \frac{1}{n!} \frac{d^n E_{02}(z_o)}{dz_o^n}$$

$$\text{and with } f(t) = -G\delta(t)$$

$$\langle F_{DEP}(\omega_2) \rangle (z_o + \delta) = 2\alpha(\omega_2) \{ \bar{\gamma}_0 + \bar{\gamma}_1\delta + \bar{\gamma}_2\delta^2 + \bar{\gamma}_3\delta^3 + \dots \} \quad (4.13)$$

where :

$$\bar{\gamma}_0 = \frac{1}{2}\mu_0\mu_1, \quad \bar{\gamma}_1 = \frac{1}{2}(2\mu_0\mu_2 + \mu_1^2 - 2\mu_0\mu_1G), \quad \bar{\gamma}_2 = \frac{1}{2}(3\mu_1\mu_2 + 3\mu_3\mu_0 - 4G\mu_0\mu_2 - 2G\mu_1^2 + G^2\mu_0\mu_1) \text{ etc.}$$

Substitution of Eqs. (4.11), (4.12), and (4.13) into Eq. (4.10) gives the highly nonlinear dy-

namical micromotion equation:

$$m_e \frac{d^2\delta}{dt^2} + b \frac{d\delta}{dt} = q(\lambda_0 + \lambda_1\delta + \lambda_2\delta^2 + \lambda_3\delta^3) \cos(\omega_1 t) + 2\alpha(\omega_1) \cdot \\ (\gamma_0 + \gamma_1\delta + \gamma_2\delta^2 + \gamma_3\delta^3) \cos^2(\omega_1 t) + 2\alpha(\omega_2)(\bar{\gamma}_0 + \bar{\gamma}_1\delta + \bar{\gamma}_2\delta^2 + \bar{\gamma}_3\delta^3) + \dots \quad (4.14)$$

4.3.3 Dimensionless Form

For the purposes of studying the micromotion equation (Eq. (4.14)) numerically, it was cast into the following dimensionless form:

$$\frac{d^2\tilde{\delta}}{d\tilde{t}^2} + \frac{d\tilde{\delta}}{d\tilde{t}} + k\tilde{\delta} + k'\tilde{\delta}^2 + k''\tilde{\delta}^3 = G_0 + \left(G_1 + G_3\tilde{\delta} + G_5\tilde{\delta}^2 + G_7\tilde{\delta}^3 \right) \cos(\tilde{\omega}_1\tilde{t}) + \\ \left(G_2 + G_4\tilde{\delta} + G_6\tilde{\delta}^2 + G_8\tilde{\delta}^3 \right) \cos(2\tilde{\omega}_1\tilde{t}) \quad (4.15)$$

where the variable transformation was accomplished through the following variable definitions:

$$\tilde{\delta} \equiv \frac{\delta}{h}, \quad \tilde{t} \equiv \frac{t}{T_1}, \quad \tilde{\omega}_1 \equiv \omega_1 T_1, \quad T_1 \equiv \frac{m_e}{b}, \quad h \equiv \frac{z_{\min}}{\cos(\frac{\theta_a}{2})} \quad (4.16)$$

z_{\min} denoting the electrode spacing and θ_a the asymptotic angle of the cone electrode; and the following parameter definitions:

$$k \equiv - \left[\alpha'(\tilde{\omega}_1)\gamma_1 + 2\alpha(\omega_2)\bar{\gamma}_1 \right] \frac{T_1^2}{m_e}; \quad k' \equiv - \left[\alpha'(\tilde{\omega}_1)\gamma_2 + 2\alpha(\omega_2)\bar{\gamma}_2 \right] \frac{hT_1^2}{m_e}; \\ k'' \equiv - \left[\alpha'(\tilde{\omega}_1)\gamma_3 + 2\alpha(\omega_2)\bar{\gamma}_3 \right] \frac{h^2T_1^2}{m_e}; \\ G_0 \equiv - \left[\alpha'(\tilde{\omega}_1)\gamma_0 + 2\alpha(\omega_2)\bar{\gamma}_0 - m_b g \right] \frac{T_1^2}{m_e}; \quad G_1 \equiv \frac{\lambda_0 q T_1^2}{hm_e}; \quad G_3 \equiv \frac{\lambda_1 q T_1^2}{m_e}; \\ G_5 \equiv \frac{\lambda_2 q T_1^2 h}{m_e}; \quad G_7 \equiv \frac{\lambda_3 q T_1^2 h^2}{m_e}; \quad G_2 \equiv \frac{\alpha'(\tilde{\omega}_1)\gamma_0 T_1^2}{hm_e}; \quad G_4 \equiv \frac{\alpha'(\tilde{\omega}_1)\gamma_1 T_1^2}{m_e}; \\ G_6 \equiv \frac{\alpha'(\tilde{\omega}_1)\gamma_2 T_1^2 h}{m_e}; \quad G_8 \equiv \frac{\alpha'(\tilde{\omega}_1)\gamma_3 T_1^2 h^2}{m_e} \quad (4.17)$$

$$\text{where : } \alpha'(\tilde{\omega}_1) \equiv \alpha\left(\frac{\tilde{\omega}_1}{T_1}\right) = \alpha(\omega_1)$$

Various forms or truncations of Eq. (4.15) have been examined in the past. The *zero-order model*, (9), is Eq. (4.15) with $k' = k'' = G_0 = G_3 = G_4 = G_5 = G_6 = G_7 = G_8 = 0$; the *first-order model* (10) is the case where $k' = k'' = G_0 = G_5 = G_6 = G_7 = G_8 = 0$; and the *quadratic model* (10), the case where $k' = k'' = G_0 = G_7 = G_8 = 0$. Investigation by the authors into the dynamics of all three of these models showed only simple harmonic motion, i.e. motion containing only a single frequency component (the frequency of the electrophoretic driver ω_1). Because it was the purpose of this investigation to determine the physical origins of the experimentally observed higher harmonics in the very low frequency regime, and believing that they were the result of the inhomogeneity of the electric field, it was decided to study the equation where the nonlinear terms of the left hand side of Eq. (4.15) were retained, and the force constants of the two drivers were assumed to be independent of the displacement. Thus, the nonlinear second order differential equation studied in the initial investigation was:

$$\frac{d^2\tilde{\delta}}{dt^2} + \frac{d\tilde{\delta}}{dt} + k\tilde{\delta} + k'\tilde{\delta}^2 + k''\tilde{\delta}^3 = G_1 \cos(\tilde{\omega}_1\tilde{t}) + G_2 \cos(2\tilde{\omega}_1\tilde{t}) \quad (4.18)$$

4.3.4 Comparison with Duffing Equation

It is not surprising that there exists no analytical solutions of Eq. (4.18), since it is a highly nonlinear nonautonomous differential equation; and thus one is obliged to study the equation numerically. However, prior to seeking for numerical solutions it is useful to make some qualitative observations. Casting Eq. (4.18) into the form of an autonomous vector field:

$$\begin{aligned}
\frac{d\tilde{\delta}_1}{d\tilde{t}} &= \tilde{\delta}_2 \\
\frac{d\tilde{\delta}_2}{d\tilde{t}} &= -k\tilde{\delta}_1 - k'\tilde{\delta}_1^2 - k''\tilde{\delta}_1^3 + G_1 \cos(\tilde{\omega}_1\tilde{\delta}_3) + G_2 \cos(2\tilde{\omega}_1\tilde{\delta}_3) - \tilde{\delta}_2 \\
\frac{d\tilde{\delta}_3}{d\tilde{t}} &= 1
\end{aligned} \tag{4.19}$$

makes it clear that the system is defined on the toroidal phase space $\mathbb{R}^2 \times S^1$ ($S^1 = \mathbb{R}/T$; $T = 2\pi/\tilde{\omega}_1$). It is well known that for a system with such a topology, there exist parameter spaces where the dynamics are nonlinear and even deterministically chaotic. A very well known and studied $\mathbb{R}^2 \times S^1$ system with rich and varied dynamics is the Duffing oscillator (81) of the form (82), (83):

$$\frac{d^2x}{dt^2} + \delta \frac{dx}{dt} - x + x^3 = \gamma \cos(\omega t) \tag{4.20}$$

where the equation models the sinusoidally forced, aerodynamically damped, vibrations of a cantilever beam subjected to a nonuniform magnetic field. This nonlinear system has been studied fairly extensively using both analytical (84), (85) and numerical (86), (87) techniques; and these investigations have revealed regimes in the parameter space where the dynamics are simple (period one motion), more complicated (higher periodicity), and chaotic (motion with essentially an infinite period). Comparison of Eq. (4.18) with Eq. (4.20) shows important qualitative similarities and differences. Although both systems are damped, the Duffing equation allows the flexibility in the sign of the damping (positive or negative) and the magnitude of the damping (the rich dynamics, though, having been observed for $0 < \delta < 1$). The micromotion equation does not contain this flexibility as the transformation to dimensionless form shows that coefficients of the inertial and damping terms are equal. Both of the systems are sinusoidally driven, though Eq. (4.18) is doubly driven; the second driver being at a frequency commensurate with the frequency of the first driver. The internal force terms of the two systems are similar, both containing a cubic term and a linear term. The micro-motion equation, however, also contains a quadratic force contribution,

and in addition possesses 'spring constants' (k , k' , k'') which allow variability in the sign and magnitude of all the internal force terms. Therefore, the significance of all terms are realized in their numerical evaluation.

4.4 Numerical Investigations

Numerical integration of Eq. (4.18) requires the evaluation of the five frequency dependent parameters: k , k' , k'' , G_1 , & G_2 ; and the spatial and temporal scaling factors: h and T_1 , respectively. For the purpose of selecting a set of particle specific parameters needed in the solution of the model equation, the representative experimentally measured Canola protoplast DEP spectrum, shown in Fig. 4.4, was selected. This particular spectrum has the particle specific parameters: $R = 26 \times 10^{-6}m$; $\gamma_p = 1.1 \times 10^3 kgm^{-3}$; and $m_e = 1.2 \times 10^{-10}kg$; the medium specific parameters: $\gamma_m = 1.0 \times 10^3 kgm^{-3}$; $\eta = 1.0 \times 10^{-3} kgm^{-1}s^{-1}$; and $b = 4.9 \times 10^{-7} kgs^{-1}$; and $\epsilon_m = 7.083 \times 10^{-10} Fm^{-1}$; and the experimental system parameters: $\theta_a = 60^\circ$; $z_{min} = 4.25 \times 10^{-4}m$; and $z_0 = 3.25 \times 10^{-4}m$.

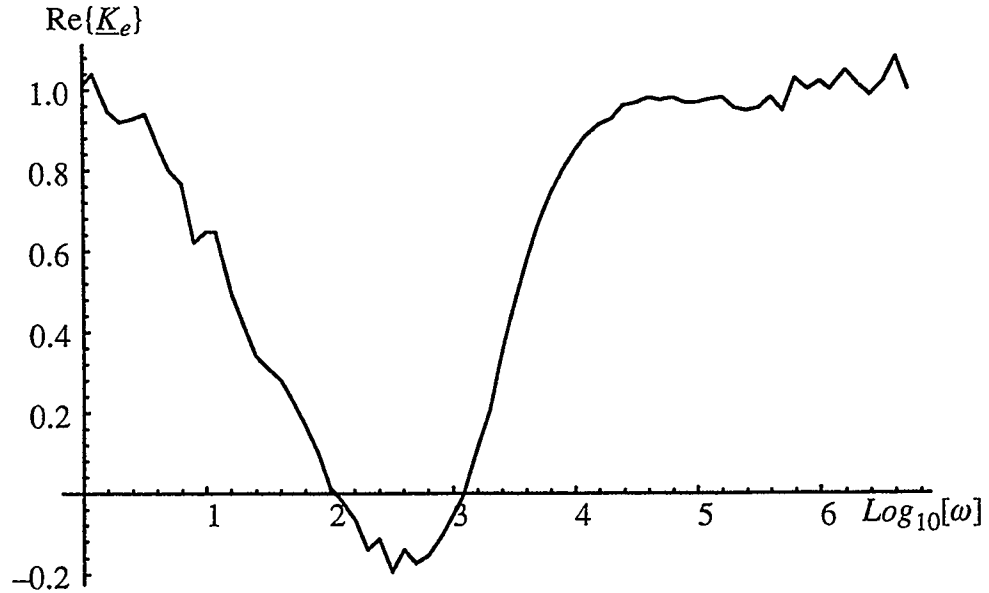


Fig. 4.4 Experimentally measured Canola protoplast DEP spectrum.

As detailed in Eqs. (4.11) – (4.13) and (4.17), the evaluation of the "spring constants"

k , k' , and k'' requires an analytical expression for the induced electric fields (high and low frequency) according to the electrode geometry. The general expression for cone–plate electrode configurations as derived by Jones and Kraybill (44) was adopted for the purposes of these calculations:

$$E_{01,2}(z) = \frac{-2V_{01,2}}{h\left(1 - \left(\frac{z}{h}\right)^2\right) \ln\left[\frac{1 + \cos(\theta_a/2)}{1 - \cos(\theta_a/2)}\right]} \quad (4.21)$$

where $V_{01,2}$ denotes the rms voltage of the low and high frequency fields, respectively. The value of V_{01} was held constant at 1.0 V, while V_{02} fluctuated between approximately 2.0 V and 0.2 V. The evaluation of the force constant of the electrophoretic driver, G_1 , requires, as indicated in Eq. (4.17), an estimate of the surface charge. The "true" unperturbed surface charge of a biological membrane is a difficult physical quantity to measure, largely because the probing alters the charge. Obi *et al* (88) have estimated the surface charge density of barley mesophyll protoplasts by electrophoretic studies to be $-(3.92 \pm 0.05) \times 10^{-3} Cm^{-2}$, and in the extensive review article by Cevc (64) the range of net surface charge density of cell membranes is estimated to lie within the range of $-(0.02 - 0.2) Cm^{-2}$. Since the surface charge on the membrane is not well characterized, the following range for the total surface charge was selected: $-10^{-13}C \leq q \leq -10^{-15}C$.

Previous investigations ((9), (10)) into the dynamics of the micromotion determined that the maximum amplitude, $|\delta|$, in the low frequency (<100 Hz.) region of the spectrum, increased as the driving frequency (ω_1) of the test field was decreased. Therefore, to assess the sensitivity of the model equation to changes in the frequency ω_1 , Eq. (4.18) was numerically integrated using a Runge–Kutta algorithm of the 6th order for the following three test frequencies: 10, 50, and 100 Hz. The calculated frequency dependent and charge dependent parameters for the experimental DEP spectrum of Fig. 4.4 are presented in Table

4.1.

Table 4.1 *Micromotion Equation Parameters*

Frequency	k	k'	k''	G ₂
10	-3.63×10^{-5}	-1.75×10^{-4}	-6.68×10^{-4}	1.8×10^{-6}
50	-3.65×10^{-5}	-1.60×10^{-4}	-5.04×10^{-4}	6.3×10^{-7}
100	-3.66×10^{-5}	-1.53×10^{-4}	-4.21×10^{-4}	3.7×10^{-8}

Charge(C)	G ₁
-10^{-14}	2.69×10^{-5}
-5×10^{-14}	1.35×10^{-4}
-10^{-13}	2.69×10^{-4}

4.4.1 Initial Numerical Results

The results of the numerical integration of Eq. (4.18) with the parameters of Table 4.1 are presented in the form of phase plane portraits in Fig. 4.5, where the initial conditions are kept the same for all calculations and the units of both position and velocity are dimensionless. Displayed in Fig. 4.5 are three sets of portraits computed at distinct frequencies: (a) at 100 Hz.; (b) at 50 Hz.; and (c) at 10 Hz. At each of these three frequencies, separately computed phase plane portraits were generated at distinct estimates for the total surface charge, and labelled (i), (ii), and (iii); where the order is according to increasing surface charge. All portraits labelled (i) were computed from an assumed total surface charge of $q = -10^{-14}$ C; the portraits labelled (ii), $q = -5 \times 10^{-14}$ C; and the portraits labelled (iii), $q = -10^{-15}$ C.

To obtain a measure of the magnitude of the variables plotted in the phase portraits, the Eqs. (4.16) may be used to convert the dimensionless quantities to real measured parameters. For example, an instantaneous point on the phase portrait of Fig. 4.5 of

$\frac{d\bar{\delta}}{d\bar{t}} = 1.2 \times 10^{-5}$ and $\bar{\delta} = 0.001$ corresponds to a realized particle velocity of $2.45 \times 10^{-5} \text{ms}^{-1}$ and a displacement of $0.49 \times 10^{-6} \text{m}$. It is clear from the results that

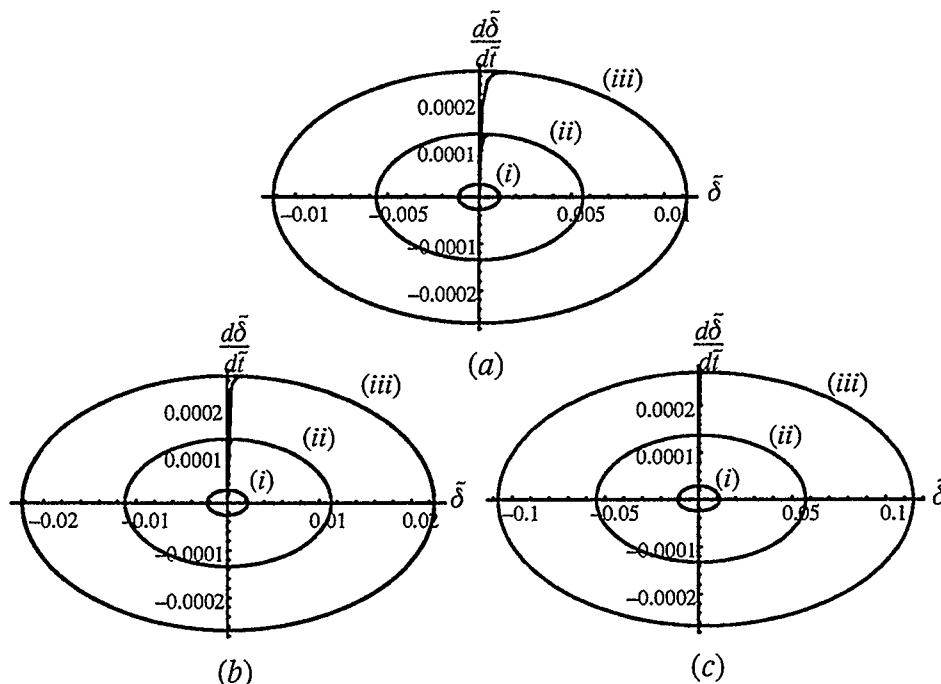


Fig. 4.5 Mathematically generated phase plane portraits.

the micromotion predicted in all parameter spaces investigated, is simple periodic motion; the period being dictated by the low frequency driver and the motion possessing only one frequency component. Comparison of the generated results for the different frequencies correctly predicts the experimentally observed trend that the amplitude of the micromotion is inversely proportional to the driving frequency. In addition, comparison of the maximum amplitude of the motion, at a particular frequency, for different estimates of the surface charge, shows the expected electrophoretic result that charge is directly proportional to amplitude. It is therefore clear that these two agreements with experimental observations provide a means of estimating the surface charge of a given particle through the fitting of numerically generated maximum displacements with experimentally measured maximum displacements. However, the micromotion model as represented in Eq. (4.18) fails to predict any higher harmonic components in the frequency of the oscillations.

When comparison is made of the magnitude of the various parameters it is evident that the "spring" constants are relatively insignificant and that the system is actually

heavily damped. This conclusion may be substantiated by setting the "spring" constants to zero and then numerically solving the resulting differential equation. The phase plane portrait solutions of Eq. (4.18) with $k = k' = k'' = 0$, for the range of surface charge values at a frequency of 50Hz, is plotted in Fig. 4.6.

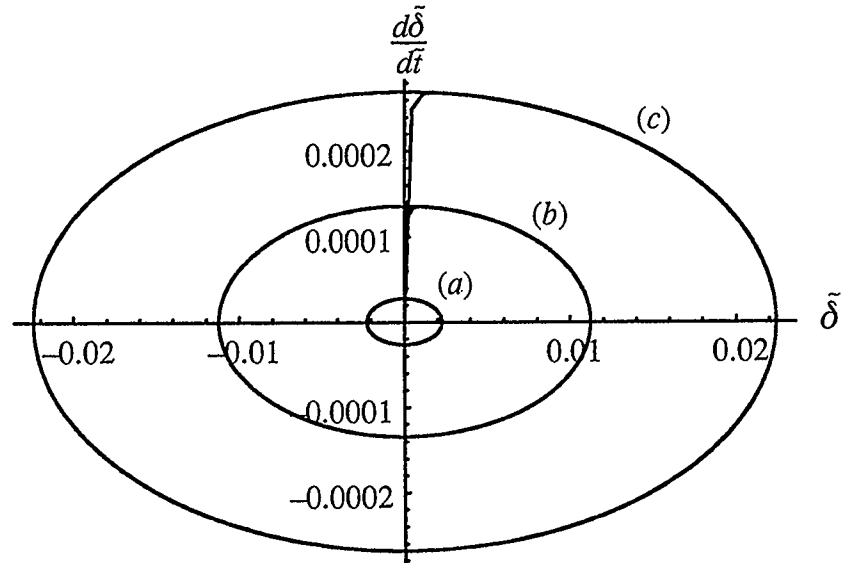


Fig. 4.6 Phase plane portrait solution from Eq. (4.18) with spring constants set to 0.

Comparison of the phase portraits of Fig. 4.6 with those of Fig. 4.5b, reveal that the "spring" constants make no realizable contribution to the dynamics. This, of course, implies that the inhomogeneity of the electric field is not sufficiently nonlinear to cause an observable dielectrophoretic contribution to the particle dynamics. This is not to imply, of course, that the particles equilibrium position is not the result of the field inhomogeneity, but rather that the perturbations or micromotion about the equilibrium position is not effected by the nonlinearity in the electric field. Therefore, from the modelling thus far it can be concluded that the higher harmonics are not the result of the inhomogeneity in the electric field. Furthermore, even the presence of the dielectrophoretic driver, as realized in G_2 , commensurate in frequency with the electrophoretic driver, fails to produce the second harmonic for experimentally realized values. This seems to imply that the experimentally observed second harmonic is not dielectrophoretic in origin.

4.5 Additional Modelling

The attempt to model the micromotion dynamics for the purposes of obtaining insight in the origin of the higher frequency harmonics was unsuccessful through the second order differential equation, Eq. (4.18). Hence, additional modelling was pursued.

4.5.1 Nonlinear Hydrodynamic Interactions

Having ruled out the cause of the higher harmonics being the nonuniformity in the field, attention was turned to the possibility of the nonlinear response being the result of hydrodynamic interactions as suggested by the preliminary analysis of Gaigalas *et al* (75). The existing modelling of viscous drag is incorporated into Eq. (4.18) by means of Stoke's equation, and therefore a straight forward extension to a model with quadratic velocity contributions is through Oseen's formula (89):

$$F = 6\pi\eta R \left[\frac{d\delta}{dt} + \frac{3R\gamma_m}{8\eta} \left(\frac{d\delta}{dt} \right)^2 \right] \quad (4.22)$$

Incorporating Eq. (4.22) into the micromotion (Eq. (4.18)) gives:

$$\frac{d^2\tilde{\delta}}{d\tilde{t}^2} + \frac{d\tilde{\delta}}{d\tilde{t}} + B \left(\frac{d\tilde{\delta}}{d\tilde{t}} \right)^2 + k\tilde{\delta} + k'\tilde{\delta}^2 + k''\tilde{\delta}^3 = G_1 \cos(\tilde{\omega}_1\tilde{t}) + G_2 \cos(2\tilde{\omega}_1\tilde{t}) \quad (4.23)$$

where the parameter B is dimensionless and is defined by: $B \equiv \frac{3hR\gamma_m}{8\eta T_1}$. Evaluation of the parameter B to account for possible effects of convective flow for the experimental parameters given above results in $B = 21.9$. Examination of any of the phase space portraits in Fig. 4.5 indicates that the maximum value of $\frac{d\tilde{\delta}}{d\tilde{t}}$ to be approximately 0.00027. Therefore, it is clear that the parameter B , modelling nonlinear hydrodynamic interactions through Oseen's formula, will make no observable contribution to the micromotion dynamics. Arbitrarily assigning significantly larger numerical values to B causes instability in the oscillations about the equilibrium point.

4.5.2 Field-Dependent Surface Charge Model

Ruling out the significance of hydrodynamic interactions, it seemed logical to pursue the possible electric field induced effects on the cell membrane as a mechanism responsible for inducing the higher frequency harmonics. As was mentioned in the introductory section of this chapter, this possible mechanism was suggested by Gaigalas *et al* based on Onsager's theory. Rather than following the methodology of Onsager, a novel model, based in part on the work of Chiabrera *et al* (90), was constructed to justify the possible field dependence of the surface charge density.

The proposed model assumes that the charge that appears on the surface of a biological cell is the result of the dissociation of weak acids in the protein molecules that lie in the membrane (64), and thus maybe represented in a most elementary fashion as:



and therefore the equilibrium constant maybe simply expressed as:

$$K = \frac{[H^+][A^-]}{[HA]} = \frac{k_1}{k_2} \quad (4.25)$$

where k_1 and k_2 are the kinetic rate constants for the forward and reverse reactions. To determine the effect of the applied electric field on the rate constant k_1 , construction is made of a hypothetical biological cell with surface charge dynamics given by Fig. 4.7. Any cation whose centre lies within the shell of thickness β is considered to be in the bound state HA . The rate constant k_1 is, of course, a unimolecular rate constant and therefore is the inverse of the time required for the centre of the cation to traverse the distance β . This distance β is really a quantum mechanical quantity as it represents the distance where the bond is 'stretched' to the point of 'breaking'. It should not be confused with the Bjerrum length which is a quantity that is governed strictly by electrostatics (91) and concerns ionic association; and thus would be much greater in magnitude than β . Therefore, k_1 may be

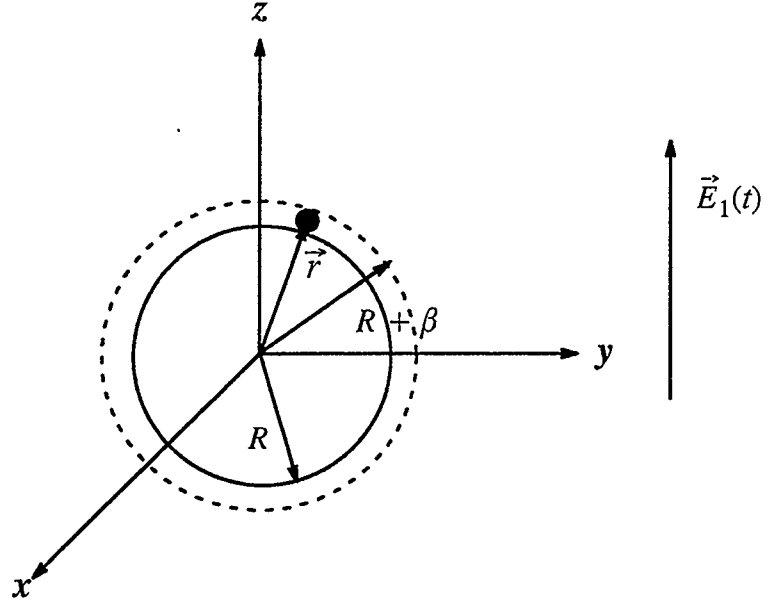


Fig. 4.7 Diagram geometry for electric field frequency dependent surface charge model.

evaluated by determining the traverse time of the cation.

With the assumption that the electric field has a noticeable effect on the surface chemistry, connection is made through transforming the problem into a dynamical one. In order to make progress in this direction, only the radial component of the cation velocity designated v is considered. The location of the cation with respect to the origin of the coordinate frame at the centre of the cell is denoted by the vector \vec{r} . If the mass of the cation is M , then the equation of motion according to Newton's second law is simply:

$$M \frac{dv}{dt} = F \quad (4.26)$$

where F is the sum of the radial components of all the forces that act on the cation. Now the components of the net radial force are: [1] the frictional force:

$$F_f = -\alpha_f v \quad (4.27)$$

where $\alpha_f \equiv$ frictional coefficient; [2] the force due to an external electric field:

$$F_{external} = q_+ E_1 \cos \theta \quad (4.28)$$

where q_+ is the cationic charge; [3] the force due to the induced polarization of the cell;

$$F_{induced} = 2q_+ \operatorname{Re}[K(\omega_1)] R^3 \frac{E_1}{r^3} \cos \theta \quad (4.29)$$

[4] the Coulombic or electrostatic force due to surface charge of the cell:

$$F_{el} = \frac{q_p q_+}{\epsilon_m r^2} = \frac{q_+ p [A^-]}{\epsilon_m r^2} \quad (4.30)$$

where q_p is the charge due to the surface proteins and thus may be related to $[A^-]$ through a constant p ; and [5] a random force due to the solvent denoted as $A'(t)$. Substituting Eqs. (4.27) – (4.30), and incorporating the random force into Eq. (4.26) gives the stochastic or Langevin equation for the dynamics of the cation:

$$M \frac{dv}{dt} = -\alpha_f v + q_+ E_1 \cos \theta + 2q_+ \operatorname{Re}[K(\omega_1)] R^3 \frac{E_1}{r^3} \cos \theta + \frac{q_+ p [A^-]}{\epsilon_m r^2} + A'(t) \quad (4.31)$$

This equation may be written in a more compact form:

$$\frac{dv}{dt} + a_0 v = a_1 \cos \omega_1 t + a_2 [A^-] + A(t) \quad (4.32)$$

where: $a_0 \equiv \frac{\alpha_f}{M}$, $a_1 \equiv \frac{q_+ E_1 \cos \theta}{M} \left[1 + \frac{2 \operatorname{Re}[K(\omega_1)] R^3}{r^3} \right] = b \cos \theta$, $a_2 \equiv \frac{q_+ p}{\epsilon_m r^2}$, and

$A(t) \equiv \frac{A'(t)}{M}$. Now Eq. (4.32) was written in this form to explicitly show the time dependence of the various terms; thus the constants a_0 , a_1 , and a_2 are assumed to be independent of t . In reality, however, the variable r depends upon t ; however, r may be treated as a constant over this extremely short distance β (essentially the H–A bond distance), in which the value of r does not change appreciably. In addition, it has been assumed that the Clausius–Mossotti factor remains essentially constant within β .

In order to make progress with Eq. (4.32) the stochastic force, $A(t)$, is initially neglected and thus the corresponding dynamical equation in the radial velocity variable $v_0(t)$ that is wholly deterministic is:

$$\frac{dv_0}{dt} + a_0 v = a_1 \cos \omega_1 t + a_2 [A^-] \quad (4.33)$$

which upon integrating with the initial condition $v_0(t = 0) = 0$, gives:

$$v_0(t) = \frac{a_1(\omega_1 \sin \omega_1 t + a_0 \cos \omega_1 t)}{\omega_1^2 + a_0^2} + \frac{a_2[A^-]}{a_0} + \frac{(a_2\omega_1^2[A^-] + a_0^2(a_2[A^-] + a_1))e^{-a_0 t}}{a_0(\omega_1^2 + a_0^2)} \quad (4.34)$$

Thus, the cation velocity may be considered to have two components:

$$v(t) = v_0(t) + v_R(t) \quad (4.35)$$

where $v_R(t)$ is the random force velocity contribution. The corresponding displacement $r(t)$ can be evaluated by integrating Eq. (4.35) over t :

$$\begin{aligned} r(t) &= \int_0^t v(t') dt' = \int_0^t v_0(t') dt' + \int_0^t v_R(t') dt' \\ &= \frac{a_1(a_0 \sin \omega_1 t - \omega_1 \cos \omega_1 t)}{\omega_1(\omega_1^2 + a_0^2)} + \frac{a_2[A^-](a_0 t - 1)}{a_0^2} + \\ &\quad \frac{(a_2[A^-]\omega_1^2 + a_0^2(a_2[A^-] + a_1))e^{-a_0 t}}{a_0^2(\omega_1^2 + a_0^2)} + \int_0^t v_R(t') dt' \end{aligned} \quad (4.36)$$

If the system is assumed to be heavily damped then the second last term may be dropped:

$$\begin{aligned} r(t) &= \frac{a_1(a_0 \sin \omega_1 t - \omega_1 \cos \omega_1 t)}{\omega_1(\omega_1^2 + a_0^2)} + \frac{a_2[A^-](a_0 t - 1)}{a_0^2} + \int_0^t v_R(t') dt' \\ &= T_1 + T_2 + T_3 \end{aligned} \quad (4.37)$$

Taking the ensemble average of the square of Eq. (4.37) gives:

$$\begin{aligned} \langle r^2(t) \rangle &= \langle T_1^2 \rangle + \langle T_2^2 \rangle + \langle T_3^2 \rangle + 2 \langle T_1 T_2 \rangle + 2 \langle T_1 T_3 \rangle + \\ &\quad 2 \langle T_2 T_3 \rangle \\ &= T_1^2 + T_2^2 + \langle T_3^2 \rangle + 2T_1 T_2 \end{aligned} \quad (4.38)$$

where the averaging of a purely stochastic term with a purely deterministic term is taken to be 0, and the ensemble average of the product of any two deterministic terms is simply the

product of the two terms. Now the ensemble averaging performed in Eq. (4.38) are thermal averages but due to the angular dependence (θ), an angular average must also be performed.

Thus Eq. (4.38) becomes:

$$\langle \langle r^2(t) \rangle \rangle_{ang} = \langle T_1^2 \rangle_{ang} + \langle T_2^2 \rangle_{ang} + \langle \langle T_3^2 \rangle \rangle_{ang} + 2 \langle T_1 T_2 \rangle_{ang} \quad (4.39)$$

where the angular average is defined to be:

$$\langle Q \rangle_{ang} = \frac{\int_0^{2\pi} d\phi \int_0^\pi d\theta \sin \theta Q(\theta, \phi)}{\int_0^{2\pi} d\phi \int_0^\pi d\theta \sin \theta} = \frac{1}{4\pi} \int_0^{2\pi} d\phi \int_0^\pi d\theta \sin \theta Q(\theta, \phi) \quad (4.40)$$

Applying the definition of Eq. (4.40) to Eq. (4.39) gives:

$$\langle r^2(t) \rangle = \frac{1}{3} \frac{b^2(a_0 \sin \omega_1 t - \omega_1 \cos \omega_1 t)^2}{\omega_1^2(\omega_1^2 + a_0^2)^2} + \frac{a_2^2[A^-]^2(a_0 t - 1)^2}{a_0^4} + \int_0^t dt' \int_0^t dt'' \langle v_R(t') v_R(t'') \rangle_{th} \quad (4.41)$$

With introduction of a diffusion coefficient for the cation, the third term of Eq. (4.41) may be set to:

$$\int_0^t dt' \int_0^t dt'' \langle v_R(t') v_R(t'') \rangle_{th} = 6Dt \quad (4.42)$$

and therefore Eq. (4.41) becomes:

$$\langle r^2(t) \rangle = \frac{1}{3} \frac{b^2(a_0 \sin \omega_1 t - \omega_1 \cos \omega_1 t)^2}{\omega_1^2(\omega_1^2 + a_0^2)^2} + \frac{a_2^2[A^-]^2(a_0 t - 1)^2}{a_0^4} + 6Dt \quad (4.43)$$

Now if the time dependent radial distance, $r(t = t_1)$, be set equal to β , the thickness of the

region over which the activated complex must pass before allowing the cation to escape, then the time t_1 will be the reciprocal of the rate constant for the forward reaction of the dissociation of the surface protein (Eq. (4.24)). Furthermore, if it is assumed that ω_1 is very small (the low frequency region) then the oscillating functions are the result of the oscillations in the applied electric field which possesses a large period, and hence the time variation of these oscillating functions will be much slower than the cationic motion. Thus the dynamics of the cation may be decoupled from the oscillation of the electric field by selectively substituting for t_1 . With these substitutions and assumptions, Eq. (4.43) becomes:

$$\beta^2 \equiv \frac{1}{3} \frac{b^2 (a_0 \sin \omega_1 t - \omega_1 \cos \omega_1 t)^2}{\omega_1^2 (\omega_1^2 + a_0^2)^2} + \frac{a_2^2 [A^-]^2 \left(\frac{a_0}{k_1} - 1 \right)^2}{a_0^4} + \frac{6D}{k_1} \quad (4.44)$$

Before solving for k_1 in Eq. (4.44), the following compact notation is introduced:

$$\begin{aligned} x_1 &\equiv \frac{a_0 b}{\sqrt{3} \omega_1 (\omega_1 + a_0)} & x_2 &\equiv \frac{-\omega_1 b}{\sqrt{3} \omega_1 (\omega_1 + a_0)} & x_3 &\equiv \frac{a_2^2}{a_0^4} \\ \phi &\equiv \tan^{-1} \left(\frac{-a_0}{\omega_1} \right) & u &\equiv \cos(\omega_1 t + \phi) \end{aligned} \quad (4.45)$$

and thus with these definitions Eq. (4.44) may concisely be written:

$$\beta^2 = u^2 + [A^-]^2 x_3 \left(\frac{a_0}{k_1} - 1 \right)^2 + \frac{6D}{k_1} \quad (4.46)$$

Solving for k_1 in Eq. (4.25) and substituting the result into Eq. (4.46) gives:

$$\beta^2 = u^2 + x_3 (C_1 a_0 - [A^-])^2 + \frac{6DC_1}{[A^-]} \quad (4.47)$$

where $C_1 \equiv \frac{[HA]}{[H^+]k_2}$. Solving for $[A^-]$ in Eq. (4.47) gives a real root of the form:

$$[A^-] = \frac{1}{3} \left(2a_0 C_1 - \frac{\sqrt[3]{2} C_5}{C_2} + \frac{C_2}{\sqrt[3]{2} x_3} \right) \quad (4.48)$$

where:

$$\begin{aligned}
C_2 &\equiv \sqrt[3]{C_3 + C_4} & C_3 &\equiv \sqrt{C_4^2 + 4x_3 C_5} & C_5 &\equiv 3(u^2 - \beta^2) - a_0 x_3^2 C_1^2 \\
C_4 &\equiv 18x_3 C_6 (u^2 - \beta^2 + a_0 C_1 C_6) + 16C_6^3 - 162x_3^2 C_1 D & C_6 &\equiv a_0 C_1 x_3
\end{aligned}$$

As was alluded to previously, the surface charge of the particle, q , is directly related to the concentration of the anions, $[A^-]$. Therefore, the result derived above (Eq. (4.48)) shows that the surface charge is a nonlinear function of the electric field frequency. To see this, Eq. (4.48) may be expanded as a Taylor series in u ; the exact details which are omitted here because of their messiness and the fact that the details offer nothing to the final result. However, computation of the power series in u from Eq. (4.48) reveals, not surprisingly, that only the odd powers in $\cos(\omega_1 t)$ are non-zero. Therefore, the Taylor expansion of the corresponding surface charge may be written in the general form:

$$\begin{aligned}
q &= q_p = q_0 + q_1 u + q_3 u^3 + \dots \\
&= q_0 + q'_1 \cos(\omega_1 t) + q'_3 \cos^3(\omega_1 t) + \dots
\end{aligned} \tag{4.49}$$

From this 'remodelling' of the surface, the external force constant, G_1 , in the micromotion equation will become a function of the low frequency electric field according to:

$$G_1 = G_{10} + G_{11} \cos(\bar{\omega}_1 \bar{t}) + G_{13} \cos^3(\bar{\omega}_1 \bar{t}) + \dots \tag{4.50}$$

and therefore the electrophoretic driver becomes:

$$\begin{aligned}
G_1 \cos(\bar{\omega}_1 \bar{t}) &= G_{10} \cos(\bar{\omega}_1 \bar{t}) + G_{11} \cos^2(\bar{\omega}_1 \bar{t}) + G_{12} \cos^4(\bar{\omega}_1 \bar{t}) + \dots \\
&= G_{10} \cos(\bar{\omega}_1 \bar{t}) + G'_{11} \cos(2\bar{\omega}_1 \bar{t}) + G'_{12} \cos(4\bar{\omega}_1 \bar{t}) + \dots
\end{aligned} \tag{4.51}$$

4.6 Final Numerical Results

The previous numerical results, §4.4.1, have shown that the "spring" constants k , k' , and k'' make no contribution to the micro motion dynamics. In addition the significance of nonlinear hydrodynamic interactions through Oseen's formula have been ruled out. Therefore, with incorporation of the electric field frequency dependent surface charge modelling the micromotion equation becomes:

$$\frac{d^2\tilde{\delta}}{d\tilde{t}^2} + \frac{d\tilde{\delta}}{d\tilde{t}} = G_{10} \cos(\tilde{\omega}_1 \tilde{t}) + G'_{11} \cos(2\tilde{\omega}_1 \tilde{t}) + G'_{12} \cos(4\tilde{\omega}_1 \tilde{t}) + \cdots + G_2 \cos(2\tilde{\omega}_1 \tilde{t}) \quad (4.52)$$

Unlike for Eq. (4.18), analytic solutions exist for the various truncations of Eq. (4.52). Considering only electrophoretic force constants to G'_{11} , Eq. (4.52) may be integrated to give the solution:

$$\tilde{\delta}(\tilde{t}) = \frac{G_{10}}{1 + \tilde{\omega}_1^2} [1 + \sin(\tilde{\omega}_1 \tilde{t}) - \cos(\tilde{\omega}_1 \tilde{t})] + \frac{G'_{11} + G_2}{1 + 4\tilde{\omega}_1^2} \left[1 + \frac{1}{2} \sin(2\tilde{\omega}_1 \tilde{t}) - \cos(2\tilde{\omega}_1 \tilde{t}) \right] \quad (4.53)$$

where the requirement that the displacement remain finite has been invoked along with the initial condition that $\tilde{\delta}(\tilde{t} = 0) = 0$. As was alluded to previously, the surface charge model has introduced parameters into the force constant (G_{10} , G'_{11} , G'_{12} , etc.) of the electrophoretic driver to which little or no experimental information exists as to the estimation of their magnitude. Thus, one is obliged to estimate the value of these parameters through fitting to the experimentally obtained spectral data. For the purpose here of modelling the higher harmonics observed in the FFT spectra, selection for testing of Eq. (4.52) and thereby the frequency dependent surface charge model, an electric field frequency of 20 Hz. and a surface charge of -10^{-14} C were chosen. The numerical value of G_{10} was selected to correspond to the previously calculated magnitude of G_1 (see Table 1), and then the value of G'_{11} was estimated to be equal to the value of G_{10} . As no additional harmonics were observed at an electric field frequency of 20 Hz., the higher components G'_{12} , G'_{13} , etc. have been set to zero. The phase plane portrait solution of Eq. (4.52), for the stated parameters, is presented in Fig. 4.8. In addition, a Fourier transform of the numerical solution is displayed in Fig. 4.9. Examination of the phase portrait indicates, not surprisingly, that the introduction of a "second electrophoretic driver", G'_{11} , has increased the maximum displacements slightly and changed the overall character of the oscillations from simple harmonic motion to motion possessing an additional frequency component with the same periodicity.

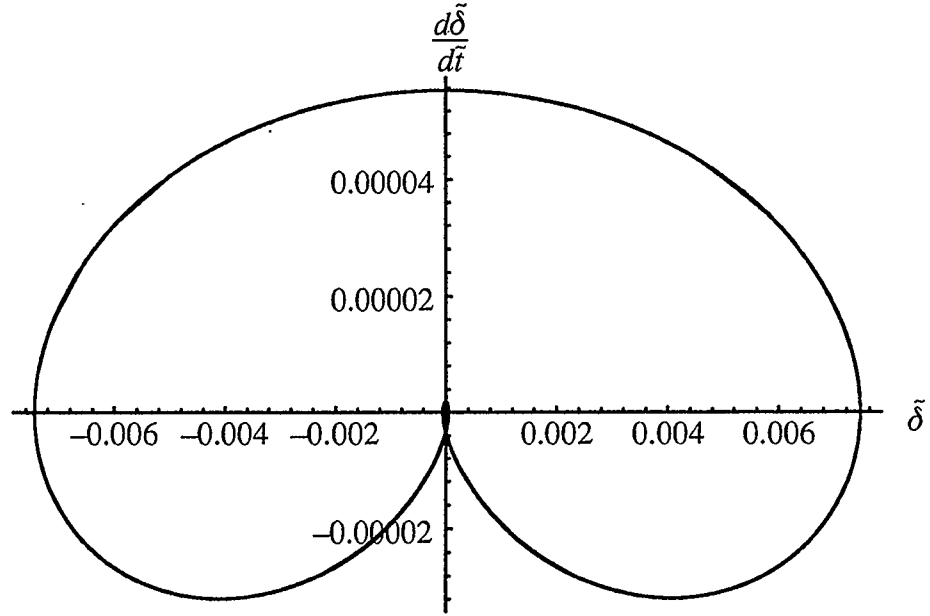


Fig. 4.8 Phase plane portrait from numerical solution of Eq. (4.52) @ 20 Hz.; with $G'_{11} = G_{10} = 2.69 \times 10^{-5}$.

The Fourier transform clearly shows the appearance of a significant second harmonic similar to that observed experimentally (compare to Fig. 4.1). This numerical result is clearly substantiated by examination of the analytical solution of Eq. (4.53) where the Fourier coefficients can virtually be seen by simple inspection.

By including higher components in the electrophoretic driver, i.e. G'_{12} , G'_{13} , etc., it is clear that additional harmonics would appear and that these harmonics would be even multiples of the driver frequency (i.e. $4\bar{\omega}_1$, $6\bar{\omega}_1$, etc.) consistent with experimental observations in the very low frequency region (< 10 Hz.). To prove this Eq. (4.53) was solved at 10 Hz. with $G'_{12} = 1/2 \times G'_{11}$ and $G'_{11} = G_{10} = 2.69 \times 10^{-5}$. The Fourier transform of the solution is displayed in Fig. 4.10.

4.7 Conclusions

Various extensions of the originally proposed micromotion equation have been carefully studied with the purpose of determining the physical origins of the observed higher harmonics in the low frequency region of the DEP spectrum. The original conjecture,

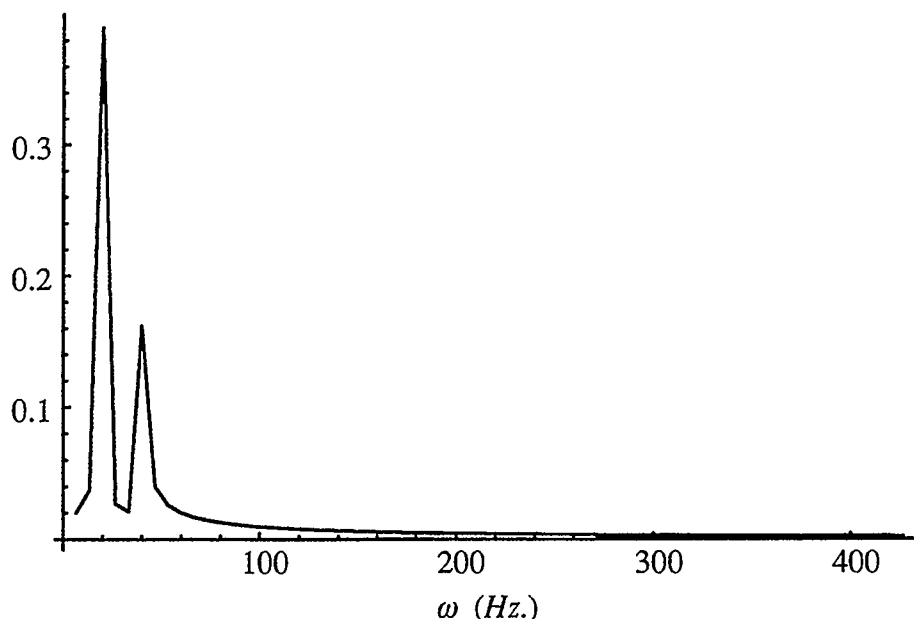


Fig. 4.9 Fourier transform of the displacement for the numerical solution displayed in Fig. 4.8.

reported previously (10), that these higher harmonics were probably the result of the intrinsic dielectrophoretic response resulting from the external inhomogeneous electric field, has been proven incorrect and that even the second harmonic at the frequency of the dielectrophoretic force can not be obtained from the field inhomogeneities. Furthermore, if the motion was primarily dielectrophoretic in origin the dominant frequency would be twice the applied frequency; both the experiment and the model indicate that the dominant frequency is the electric field frequency. The proposal, by others (75), that the higher harmonics could be the result of a nonlinear hydrodynamic interaction between the particle and the surrounding medium, if modelled through Oseen's formula has been shown to be insignificant in the particle dynamics. Having exhausted these plausible explanations as the source of this nonlinear response, an investigation was launched into the possible electric field frequency effects on the surface charge of the particle; a phenomena originally suggested by Onsager (18). The implementation of the derived electric field frequency dependent surface charge model into the micromotion equation, has resulted in good agreement with experimental observations of this nonlinear response; attesting to this being the source of the phenomena. The modelling predicts the higher harmonics to be only even multiples of the fundamental

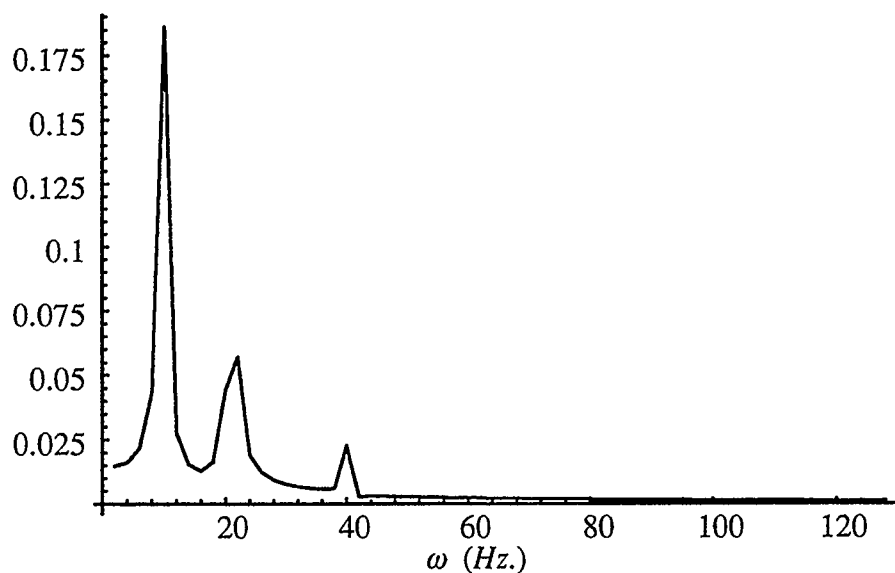


Fig. 4.10 Fourier transform of the displacement from the solution of Eq. (4.53) @ 10 Hz., with $G'_{12} = 1/2 \times G'_{11}$ and $G'_{11} = G_{10} = 2.69 \times 10^{-5}$.

frequency; similar to experimental observations. Numerically generated phase portraits provide a means of estimating the surface charge through comparison of predicted maximum displacement in oscillation to that seen in experiments. Thus strong evidence has been provided to show that the dissociation constant of the carboxylic groups within the membrane, and thereby the surface charge, is effected by the application of an external AC electric field.

Chapter 5: The Melnikov Method

5.1 Introduction

The micromotion equation derived initially (i.e. Eq. (4.18)) in the investigation of the nonlinear dynamics displayed by a levitated protoplast in the low frequency domain (< 20 Hz.), was compared in § 4.3.4 with the well studied Duffing oscillator (81) – (87). This insightful comparison was made because the two systems are topologically equivalent; i.e. the dynamics of both systems occur on an $\mathbb{R}^2 \times S^1$ toroidal phase space. It was also stated that for certain regions in the parameter space, the dynamics of such systems may be exceedingly complex; that is, highly nonlinear and possibly even deterministically chaotic. During the initial study of the micromotion dynamics, attempts were made to analytically determine regimes where the dynamics became nonlinear. This was deemed important because of the experimental observation that the onset of nonlinear dynamics in the micromotion of a levitated protoplast occurred only as the frequency of the applied electric field was reduced below 50 Hz.

An analytical method for analyzing the dynamics or motion near separatrices was originally developed by Melnikov (92) and applied to the study of perturbed dynamical systems by Morosov (93), (94), McLaughlin (95), and Holmes (84), (96). As both Morosov and Holmes have studied Duffing's equation using this technique, the Melnikov method was deemed suitable for application to the micromotion system.

In this chapter the results of applying the Melnikov method to determine conditions where the dynamics of the micromotion equation become chaotic, is presented. Prior to deriving and applying the Melnikov method to the micromotion system, a number of fundamental definitions are presented, followed by a derivation of the method. The reader is referred to Wiggins (97) for additional details.

5.2 Definitions

The study of nonlinear dynamics involves a number of important ideas, con-

cepts, definitions, and jargon; the fundamentals as required in the Melnikov method, of which, are presented in this section.

5.2.1 The Vector Field

The form of the *vector field* or *ordinary differential equation* derived for the purposes of studying the micromotion dynamics has already been presented, Eq. (4.19). In general, a nonautonomous vector field describing a dynamical system may be expressed in the following form:

$$\dot{x} = f(x, t; \mu) \quad (5.1)$$

where the overdot means " $\frac{d}{dt}$ ". For the $\mathbb{R}^2 \times S^1$ systems considered here: $x \in U \subset \mathbb{R}^2$; $t \in S^1 = \mathbb{R}^1/T$; and $\mu \in V \subset \mathbb{R}^p$. In addition, T is the period (fixed) of the vector field, U and V are open sets in \mathbb{R}^2 and \mathbb{R}^p respectively, and μ the parameters. In the representation given in Eq. (5.1), one notes the explicit time-dependence of the vector field (hence, *nonautonomous*) and the parameter dependence of the system.

5.2.2 Phase Space

The space of dependent variables of the vector field is called the *phase space*.

5.2.3 Initial Condition(s)

With $x(t)$ denoting a solution of Eq. (5.1), an *initial condition* for the system is denoted:

$$x(t_0) = x_0 \quad (5.2)$$

where t_0 is some initial time chosen to begin observation of the system, and x_0 the vector field at this time.

5.2.4 Solution(s)

The *solution* of the vector field may be represented as follows:

$$x(t, t_0, x_0; \mu)$$

where the explicit dependence of the solution on both the initial time, t_0 , and the vector field at the initial time is implied. The solution is often referred to as a *trajectory* or *phase curve*

through the point \mathbf{x}_0 at $t = t_0$.

5.2.5 Integral Curve

The graph of $\mathbf{x}(t, t_0, \mathbf{x}_0)$ over t is referred to as an *integral curve*. More precisely, graph $\mathbf{x}(t, t_0, \mathbf{x}_0) = \{(\mathbf{x}, t) \in \mathbb{R}^2 \times S^1 \mid \mathbf{x} = \mathbf{x}(t, t_0, \mathbf{x}_0), t \in I\}$ where I is the time interval of existence.

5.2.6 Orbit

If \mathbf{x}_0 is a point in the phase space of Eq. (5.1), then the *orbit through \mathbf{x}_0* , denoted $O(\mathbf{x}_0)$, is the set of points in phase space that lie on a trajectory passing through \mathbf{x}_0 . More precisely, for $\mathbf{x}_0 \in U \subset \mathbb{R}^2$, the orbit through \mathbf{x}_0 is given by $O(\mathbf{x}_0) = \{\mathbf{x} \in \mathbb{R}^2 \mid \mathbf{x} = \mathbf{x}(t, t_0, \mathbf{x}_0), t \in I\}$.

5.2.6.1 Homoclinic Orbit

An orbit that connects a hyperbolic fixed point (see §5.2.11.1) unto itself. It should be noted that a *homoclinic orbit* is sometimes called a *separatrix* because it is the boundary between two distinctly different types of motion.

5.2.6.2 Heteroclinic Orbit

An orbit that connects two distinct hyperbolic fixed points (see §5.2.11.1).

5.2.7 Manifold

The concept of a manifold in its full generality is vast and deep. For the purposes here, a *manifold*, roughly speaking, is a set (or more specifically, a solution set of the vector field) which locally has the structure of Euclidean space; and thus for the vector field defined in Eq. (5.1), the manifold is either a linear vector subspace of \mathbb{R}^2 or a surface embedded in \mathbb{R}^2 which can be locally represented as a graph (justified by the implicit function theorem).

5.2.8 Equilibrium Solution

Consider the *autonomous* vector field:

$$\dot{x} = f(x); \quad x \in \mathbb{R}^2 \quad (5.3)$$

An *equilibrium solution* of the autonomous vector field is a point $\bar{x} \in \mathbb{R}^2$ such that $f(\bar{x}) = 0$; thus \bar{x} is a solution which does not change in time. Other terms used synonymously with equilibrium solution are: *fixed point, stationary point, rest point, singularity, critical point, or steady state*.

5.2.9 Stability (of the fixed point)

Once a solution of Eq. (5.3) has been found, the *stability* of the solution is determined. Roughly speaking, the solution $\bar{x}(t)$ is *stable* if solutions starting "close" to $\bar{x}(t)$ at a given time remain close to $\bar{x}(t)$ for all later times. Formally, the stability of a solution is classified as *Liapunov stable* or *asymptotically stable* according to the following definitions: (a) $\bar{x}(t)$ is said to be *Liapunov stable* if, given $\varepsilon > 0$, there exists a $\delta = \delta(\varepsilon) > 0$ such that, for any other solution, $y(t)$, of Eq. (5.3) satisfying $|\bar{x}(t_0) - y(t_0)| < \delta$, then $|\bar{x}(t) - y(t)| < \varepsilon$ for $t > t_0$, $t_0 \in \mathbb{R}$; (b) $\bar{x}(t)$ is said to be *asymptotically stable* if it is Liapunov stable and if there exists a constant $b > 0$ such that, if $|\bar{x}(t_0) - y(t_0)| < b$, then $\lim_{t \rightarrow \infty} |\bar{x}(t) - y(t)| = 0$.

5.2.10 Determination of Stability: Linearization

The stability of a solution $\bar{x}(t)$ is determined through understanding the nature of solutions near $\bar{x}(t)$. Let

$$x = \bar{x}(t) + y \quad (5.4)$$

Substitution of Eq. (5.4) into Eq. (5.3) gives:

$$\dot{x} = \dot{\bar{x}}(t) + \dot{y} = f(\bar{x}(t) + y) \quad (5.5)$$

Taylor expanding $f(\bar{x}(t) + y)$ about the point $\bar{x}(t)$ yields:

$$f(\bar{x}(t) + y) = f(\bar{x}(t)) + Df(\bar{x}(t)) \cdot y + O(|y|^2) \quad (5.6)$$

where Df is the derivative of f (essentially a 2 by 2 Jacobian). Substitution of Eq. (5.6) into Eq. (5.5) gives after straight forward manipulation:

$$\dot{\mathbf{y}} = Df(\bar{\mathbf{x}}(t)) \cdot \mathbf{y} \quad (5.7)$$

where the higher order terms have been neglected under the requirement that \mathbf{y} is small. Thus, Eq. (5.7) implies that the question of the stability of $\bar{\mathbf{x}}(t)$ involves the determination of the stability of $\dot{\mathbf{y}}$. It should also be clear from Eq. (5.7) that the system of $\dot{\mathbf{y}}$ is a linear system, whereas the system of Eq. (5.3) was not necessarily linear. If $\bar{\mathbf{x}}(t)$ is an equilibrium solution, i.e., $\bar{\mathbf{x}}(t) = \bar{\mathbf{x}}$, then $Df(\bar{\mathbf{x}}(t)) = Df(\bar{\mathbf{x}})$ is a matrix with constant entries, and thus the solution of Eq. (5.7) through some point $\mathbf{y}_0 \in \mathbb{R}^2$ of $t = 0$ can immediately be written as:

$$\mathbf{y}(t) = e^{Df(\bar{\mathbf{x}})t} \mathbf{y}_0 \quad (5.8)$$

Therefore, the stability of the solution, $\bar{\mathbf{x}}(t) = \bar{\mathbf{x}}$, of the autonomous vector field, Eq. (5.3), may be determined by evaluating the eigenvalues of $Df(\bar{\mathbf{x}})$ (obtained from the corresponding secular equation). It should be clear from the definition of asymptotic stability in §5.2.9, that if all of the eigenvalues of $Df(\bar{\mathbf{x}})$ have negative real parts, then the equilibrium solution is asymptotically stable.

5.2.11 Stability Classification

The stability of a fixed point is classified under the linear approximation described above (§5.2.10) according to the nature of the eigenvalues of the associated linearization.

5.2.11.1 Hyperbolic

An equilibrium solution, $\bar{\mathbf{x}}$, of a vector field is called a *hyperbolic fixed point* if none of the eigenvalues of $Df(\bar{\mathbf{x}})$ have zero real part.

5.2.11.2 Saddle Point

A hyperbolic fixed point of a vector field is called a *saddle* if some, but not all, of the eigenvalues of the associated linearization have real parts greater than zero and the rest of the eigenvalues have real parts less than zero.

5.2.11.3 Stable Node (Sink)

A hyperbolic fixed point where all of the eigenvalues of the associated linearization have negative real parts is referred to as a *stable node* or *sink*.

5.2.11.4 Unstable Node (Source)

An *unstable node* or *source* is a hyperbolic fixed point where all of the eigenvalues of the associated linearization have positive real parts.

5.2.11.5 Center or Elliptic Point

A nonhyperbolic fixed point where the eigenvalues of the associated linearization are purely imaginary and nonzero is termed a *center* or *elliptic point*.

5.2.12.1 Stable Manifold

A *stable manifold* is a manifold that under the flow (evolution) of the vector field tends toward an equilibrium solution.

5.2.12.2 Unstable Manifold

An *unstable manifold* is a manifold that under the flow (evolution) of the vector field moves away from an equilibrium solution.

5.3 Derivation of the Melnikov Method

The following derivation of the Melnikov method is only an outline, and does not contain the rigor or details that would satisfy the mathematician. For the complete details of the derivation, the reader is referred to the article of Greenspan and Holmes (85), and the texts of: Guckenheimer and Holmes (98); Arrowsmith and Place (99); Wiggins (97), (100); and Lichtenberg and Lieberman (101).

The purpose of the Melnikov method is to analytically determine the parametric conditions required in a near integrable system (i.e. systems that are Hamiltonian – see Eq. (5.12) for the explicit mathematical definition), where the stable and unstable manifolds of an unstable periodic orbit near a separatrix, intersect transversely. These transverse intersections, for the perturbed vector field, imply that the motion near the separatrix is exceedingly complicated having embedded orbits of arbitrarily large period, the dynamics of

which are equivalent to the Smale horseshoe map (102). These intersections of the stable and unstable manifolds result in what is referred to as a *homoclinic tangle* which implies local deterministic chaos. For this reason, this particular method has been referred to as the *homoclinic Melnikov method* (the original theory of Melnikov (92) was much more general).

5.3.1 Perturbed Vector Field

The general class of systems that the homoclinic Melnikov method will be applied to is:

$$\dot{x} = f(x) + \varepsilon g(x, t, \varepsilon; \mu) \quad (5.9)$$

which for the $\mathbb{R}^2 \times S^1$ vector field considered here, may be written as an autonomous three-dimensional system in expanded form:

$$\begin{aligned} \dot{x}_1 &= f_1(x_1, x_2) + \varepsilon g_1(x_1, x_2, \phi, \varepsilon) \\ \dot{x}_2 &= f_2(x_1, x_2) + \varepsilon g_2(x_1, x_2, \phi, \varepsilon) \\ \dot{\phi} &= \omega \end{aligned} \quad (x_1, x_2, \phi) \in \mathbb{R}^2 \times S^1 \quad (5.10)$$

where the parameter dependence is assumed but not explicitly written, and the frequency of this periodically forced system is ω . It should be evident after comparing Eq. (5.10) to the initial representation of a nonautonomous vector, Eq. (5.1), that written in this form, a *perturbation*, of the order of ε , to the system has been implied. The *unperturbed* system is therefore, the system where $\varepsilon = 0$; i.e.:

$$\begin{aligned} \dot{x}_1 &= f_1(x_1, x_2) \\ \dot{x}_2 &= f_2(x_1, x_2) \end{aligned} \quad (5.11)$$

Now the unperturbed system is taken to be integrable or Hamiltonian (that is, conservative), and therefore Eq. (5.11) may be written:

$$\begin{aligned} \dot{x}_1 &= \frac{\partial H}{\partial x_2}(x_1, x_2) \\ \dot{x}_2 &= -\frac{\partial H}{\partial x_1}(x_1, x_2) \end{aligned} \quad (5.12)$$

where H is the Hamiltonian for the unperturbed system.

It is also assumed that for $\varepsilon = 0$, the perturbed vector field of Eq. (5.10) pos-

sesses a homoclinic orbit $q^0(t)$, to a hyperbolic saddle point p_0 . Therefore, from the above definitions this implies:

$$\lim_{t \rightarrow \pm \infty} q^0(t) = p_0 \quad (5.13)$$

It will also be necessary to define a *Poincaré map* $P_\varepsilon^{t_0}: \Sigma^{t_0} \rightarrow \Sigma^{t_0}$, where $\Sigma^{t_0} = \{(x, t) \mid t = t_0 \in [0, T]\} \subset \mathbb{R}^2 \times S^1$ is the global cross section at time t_0 for the suspended (i.e. a "snap shot over the period") autonomous flow of Eq. (5.10).

The derivation is based on two fundamental perturbation results stated in the form of Lemmas (97).

Lemma 1: *Under the above assumptions, for sufficiently small ε , the system of Eq. (5.10) has a unique hyperbolic periodic orbit $\gamma_\varepsilon^0(t) = p_0 + O(\varepsilon)$. Correspondingly, the Poincaré map $P_\varepsilon^{t_0}$ has a unique hyperbolic saddle point $p_\varepsilon^{t_0} = p_0 + O(\varepsilon)$.*

Lemma 2: *The local stable and unstable manifolds $W_{loc}^s(\gamma_\varepsilon)$, $W_{loc}^u(\gamma_\varepsilon)$ of the perturbed periodic orbit are C^r -close to those of the unperturbed periodic orbit $p_0 \times S^1$. Moreover, orbits $q_\varepsilon^s(t, t_0)$, $q_\varepsilon^u(t, t_0)$ lying in $W_{loc}^s(\gamma_\varepsilon)$, $W_{loc}^u(\gamma_\varepsilon)$ and based on Σ^{t_0} can be expressed as follows, with uniform validity in the indicated time intervals:*

$$\begin{aligned} q_\varepsilon^s(t, t_0) &= q^0(t - t_0) + \varepsilon q_1^s(t, t_0) + O(\varepsilon^2), & t \in [t_0, \infty); \\ q_\varepsilon^u(t, t_0) &= q^0(t - t_0) + \varepsilon q_1^u(t, t_0) + O(\varepsilon^2), & t \in (-\infty, t_0]. \end{aligned} \quad (5.14)$$

This implies that solutions lying in the stable manifold are uniformly approximated, for $t \geq 0$, by the solution $q_1^s(t, t_0)$ of the first variational equation (i.e. the time derivative of Eq. (5.14)):

$$\dot{q}_1^s(t, t_0) = Df(q^0(t - t_0))q_1^s(t, t_0) + g(q^0(t - t_0), t) \quad (5.15)$$

and implies similarly for $q_1^u(t, t_0)$ with $t \leq t_0$:

$$\dot{q}_1^u(t, t_0) = Df(q^0(t - t_0))q_1^u(t, t_0) + g(q^0(t - t_0), t) \quad (5.16)$$

5.3.2 Computation of the Separation Distance of the Stable and Unstable Manifolds

As outlined at the onset of this derivation, the Melnikov method provides a means of determining the conditions where the stable and unstable manifolds intersect transversely. Thus, the next step is to derive an expression for the *separation distance* of the manifolds $W^u(\mathbf{p}'_\varepsilon)$ and $W^s(\mathbf{p}'_\varepsilon)$.

The time-dependent distance function is defined:

$$\Delta_\varepsilon(t, t_0) \stackrel{\text{def}}{=} \mathbf{f}(\mathbf{q}^0(t - t_0)) \wedge [\mathbf{q}^u(t, t_0) - \mathbf{q}^s(t, t_0)] \quad (5.17)$$

and the individual distance functions for the unstable and stable manifolds:

$$\Delta_\varepsilon^{u,s}(t, t_0) \stackrel{\text{def}}{=} \mathbf{f}(\mathbf{q}^0(t - t_0)) \wedge \varepsilon \mathbf{q}_1^{u,s}(t, t_0) \quad (5.18)$$

where in Eqs. (5.17) and (5.18) the wedge product is defined by $\mathbf{a} \wedge \mathbf{b} \stackrel{\text{def}}{=} a_1 b_2 - a_2 b_1$ ($\mathbf{a}, \mathbf{b} \in \mathbb{R}^2$; possessing Cartesian coordinates (a_1, a_2) and (b_1, b_2) , respectively). Therefore, in combining Eqs. (5.17) and (5.18), the time-dependent distance function may be expressed:

$$\Delta_\varepsilon(t, t_0) = \Delta_\varepsilon^u(t, t_0) - \Delta_\varepsilon^s(t, t_0) + O(\varepsilon^2) \quad (5.19)$$

The differential equations for $\Delta_\varepsilon^s(t, t_0)$ and $\Delta_\varepsilon^u(t, t_0)$ are obtained from differentiating Eq. (5.18):

$$\begin{aligned} \dot{\Delta}_\varepsilon^s(t, t_0) &= \varepsilon \left[D\mathbf{f}(\mathbf{q}^0(t - t_0)) \dot{\mathbf{q}}^0(t - t_0) \wedge \mathbf{q}_1^s(t, t_0) + \mathbf{f}(\mathbf{q}^0(t - t_0)) \wedge \dot{\mathbf{q}}_1^s(t, t_0) \right] \\ \dot{\Delta}_\varepsilon^u(t, t_0) &= \varepsilon \left[D\mathbf{f}(\mathbf{q}^0(t - t_0)) \dot{\mathbf{q}}^0(t - t_0) \wedge \mathbf{q}_1^u(t, t_0) + \mathbf{f}(\mathbf{q}^0(t - t_0)) \wedge \dot{\mathbf{q}}_1^u(t, t_0) \right] \end{aligned} \quad (5.20)$$

It should be clear from Eq. (5.10) and the definition of $\mathbf{q}^0(t)$ that $\dot{\mathbf{q}}^0(t - t_0) = \mathbf{f}(\dot{\mathbf{q}}^0(t - t_0))$ and therefore with this identity, and the first variational equations, Eqs. (5.15) and (5.16), Eq. (5.20) becomes:

$$\begin{aligned} \dot{\Delta}_\varepsilon^s &= \varepsilon \left[D\mathbf{f}(\mathbf{q}^0) \mathbf{f}(\mathbf{q}^0) \wedge \mathbf{q}_1^s + \mathbf{f}(\mathbf{q}^0) \wedge (D\mathbf{f}(\mathbf{q}^0) \mathbf{q}_1^s + \mathbf{g}(\mathbf{q}^0, t)) \right] \\ &= \varepsilon \left[\text{trace} D\mathbf{f}(\mathbf{q}^0) \Delta_\varepsilon^s + \mathbf{f}(\mathbf{q}^0) \wedge \mathbf{g}(\mathbf{q}^0, t) \right] \end{aligned} \quad (5.21)$$

$$\begin{aligned}
\dot{\Delta}_\varepsilon^u &= \varepsilon \left[Df(\mathbf{q}^0) f(\mathbf{q}^0) \wedge \mathbf{q}_1^u + f(\mathbf{q}^0) \wedge (Df(\mathbf{q}^0) \mathbf{q}_1^u + \mathbf{g}(\mathbf{q}^0, t)) \right] \\
&= \varepsilon \left[\text{trace} Df(\mathbf{q}^0) \Delta_\varepsilon^u + f(\mathbf{q}^0) \wedge \mathbf{g}(\mathbf{q}^0, t) \right]
\end{aligned} \tag{5.22}$$

Because the unperturbed system is Hamiltonian (see Eq. (5.12)), the Eqs. (5.21) and (5.22) are simplified through the consequent identity: $\text{trace} Df \equiv 0$. Integrating Eq. (5.21) from t_0 to ∞ gives the desired expression for $\Delta_\varepsilon^s(t_0, t_0)$:

$$\Delta_\varepsilon^s(t_0, t_0) = -\varepsilon \int_{t_0}^{\infty} f(\mathbf{q}^0(t - t_0)) \wedge \mathbf{g}(\mathbf{q}^0(t - t_0), t) dt \tag{5.23}$$

where use has been made of the fact that $\Delta_\varepsilon^s(\infty, t_0) = 0$ because $\lim_{t \rightarrow \infty} f(\mathbf{q}^0(t - t_0)) = 0$.

Similarly, integrating Eq. (5.22) from $-\infty$ to t_0 gives for $\Delta_\varepsilon^u(t_0, t_0)$:

$$\Delta_\varepsilon^u(t_0, t_0) = \varepsilon \int_{-\infty}^{t_0} f(\mathbf{q}^0(t - t_0)) \wedge \mathbf{g}(\mathbf{q}^0(t - t_0), t) dt \tag{5.24}$$

Through use of Eq. (5.19), Eqs. (5.23) and (5.24) may be combined to give an expression for the time-dependent distance function at t_0 :

$$\Delta_\varepsilon(t_0, t_0) = \varepsilon \int_{-\infty}^{\infty} f(\mathbf{q}^0(t - t_0)) \wedge \mathbf{g}(\mathbf{q}^0(t - t_0), t) dt \tag{5.25}$$

The separation of the manifolds $W^u(\mathbf{p}_\varepsilon^{t_0})$ and $W^s(\mathbf{p}_\varepsilon^{t_0})$ on the section Σ^{t_0} at the point $\mathbf{q}^0(0)$ is defined as:

$$d(t_0) \stackrel{\text{def}}{=} \mathbf{q}_\varepsilon^u(t_0) - \mathbf{q}_\varepsilon^s(t_0) \tag{5.26}$$

where $\mathbf{q}_\varepsilon^u(t_0) \stackrel{\text{def}}{=} \mathbf{q}_\varepsilon^u(t_0, t_0)$, $\mathbf{q}_\varepsilon^s(t_0) \stackrel{\text{def}}{=} \mathbf{q}_\varepsilon^s(t_0, t_0)$ are the unique points on $W^u(\mathbf{p}_\varepsilon^{t_0})$, $W^s(\mathbf{p}_\varepsilon^{t_0})$ "closest" to $\mathbf{p}_\varepsilon^{t_0}$ and lying on the normal:

$$\mathbf{f}^\perp(\mathbf{q}^0(0)) = \left(-f_2(\mathbf{q}^0(0)), f_1(\mathbf{q}^0(0)) \right)^T \tag{5.27}$$

to Γ^0 ($\Gamma^0 = \{\mathbf{q}^0(t) \mid t \in \mathbb{R}\} \cup \{\mathbf{p}_0\}$) at $\mathbf{q}^0(0)$. The C^r closeness of the manifolds to Γ^0 , and

Lemma 2, then imply that:

$$d(t_0) = \varepsilon \frac{f(\mathbf{q}^0(0)) \wedge [q_1^u(t_0) - q_1^s(t_0)]}{|f(\mathbf{q}^0(0))|} + O(\varepsilon^2) \quad (5.28)$$

where $f(\mathbf{q}^0(0)) \wedge [q_1^u(t_0) - q_1^s(t_0)]$ is the projection of $q_1^u(t_0) - q_1^s(t_0)$ onto $f^\perp(\mathbf{q}^0(0))$.

5.3.3 Melnikov Function

Finally, the *Melnikov function* is defined as:

$$M(t_0) = \int_{-\infty}^{\infty} f(\mathbf{q}^0(t - t_0)) \wedge \mathbf{g}(\mathbf{q}^0(t - t_0), t) dt \quad (5.29)$$

and therefore from Eqs. (5.25) and (5.28), the separation of the manifolds $W^u(\mathbf{p}_\varepsilon^{t_0})$, $W^s(\mathbf{p}_\varepsilon^{t_0})$ may be expressed in terms of the Melnikov function as:

$$d(t_0) = \frac{\varepsilon M(t_0)}{|f(\mathbf{q}^0(0))|} + O(\varepsilon^2) \quad (5.30)$$

5.3.4 Final Remarks

Since $|f(\mathbf{q}^0(0))| = O(1)$, $M(t_0)$ provides a good measure of the separation of the manifolds at $\mathbf{q}^0(0)$ on Σ^{t_0} . From Eq. (5.27) it should be fairly clear that the vector $f^\perp(\mathbf{q}^0(0))$ and its base point $\mathbf{q}^0(0)$ are fixed on the section Σ^{t_0} and that, as t^0 varies, Σ^{t_0} sweeps around $\mathbb{R}^2 \times S^1$. Therefore, if $M(t_0)$ oscillates about zero with maxima and minima independent of ε , then from Eqs. (5.26) – (5.28), $q_\varepsilon^u(t_0)$ and $q_\varepsilon^s(t_0)$ must change their orientation with respect to $f^\perp(\mathbf{q}^0(0))$ as t^0 varies. It is thus required, that $M(t_0)$ be independent of ε to ensure that ε can be chosen sufficiently small so that the $O(\varepsilon^2)$ error in Eq. (5.30) is dominated by the term $\frac{\varepsilon M(t_0)}{|f(\mathbf{q}^0(0))|}$. This leads to the fundamental theorem of the Melnikov method:

Theorem: If $M(t_0)$ has simple zeros ($dM(t_0)/dt_0 \neq 0$) and is independent of ε , then, for $\varepsilon > 0$ sufficiently small, $W^u(\mathbf{p}_\varepsilon^{t_0})$ and $W^s(\mathbf{p}_\varepsilon^{t_0})$ intersect transversely. If $M(t_0)$ remains away from zero then $W^u(\mathbf{p}_\varepsilon^{t_0}) \cap W^s(\mathbf{p}_\varepsilon^{t_0}) = \emptyset$.

5.4 Application of Melnikov's Method

Having presented a number of pertinent definitions and concepts followed by a derivation of the Melnikov method, the reader is hopefully in a frame of mind to appreciate and understand the application of the method to the micromotion system. The Melnikov method was applied to the vector field described by the nonlinear differential equation of Eq. (4.18):

$$\frac{d^2\tilde{\delta}}{d\tilde{t}^2} + \frac{d\tilde{\delta}}{d\tilde{t}} + k\tilde{\delta} + k'\tilde{\delta}^2 + k''\tilde{\delta}^3 = G_1 \cos(\tilde{\omega}_1\tilde{t}) + G_2 \cos(2\tilde{\omega}_1\tilde{t}) \quad (5.31)$$

In keeping with the notation dictated in the previous sections of this chapter, Eq. (5.31) is rewritten in the following form:

$$\ddot{x} + \delta\dot{x} + ax + bx^2 + cx^3 = \gamma \cos(\omega t) + \zeta \cos(2\omega t) \quad (5.32)$$

where comparison of the two equations makes clear the variable transformation; and where, undoubtedly the astute reader notices, that the variable δ has been arbitrarily inserted as a means of "measuring" the contribution of the dissipative term \dot{x} . As a means of studying the significance of the quadratic and cubic "spring" constants, and to keep the analytical treatment which follows solvable, Eq. (5.32) is split up into the following two "study" equations:

$$\ddot{x} + \delta\dot{x} + ax + bx^2 = \gamma \cos(\omega t) + \zeta \cos(2\omega t) \quad (5.33)$$

$$\ddot{x} + \delta\dot{x} - ax + cx^3 = \gamma \cos(\omega t) + \zeta \cos(2\omega t) \quad (5.34)$$

To indicate explicitly the integrable part and the perturbation part, these equations are written:

$$\ddot{x} + ax + bx^2 = \varepsilon(-\delta\dot{x} + \gamma \cos(\omega t) + \zeta \cos(2\omega t)) \quad (5.35)$$

$$\ddot{x} - ax + cx^3 = \varepsilon(-\delta\dot{x} + \gamma \cos(\omega t) + \zeta \cos(2\omega t)) \quad (5.36)$$

These differential equations are nonautonomous and are transformed into autonomous sys-

tems after the form of Eq. (5.10). For the first system of Eq. (5.35), the transformation gives:

$$\begin{aligned}\dot{x}_1 &= x_2 \\ \dot{x}_2 &= -ax_1 - bx_1^2 + \varepsilon(-\delta x_2 + \gamma \cos \phi + \zeta \cos 2\phi) \\ \dot{\phi} &= \omega\end{aligned}\quad (5.37)$$

and for the second system of Eq. (5.36):

$$\begin{aligned}\dot{x}_1 &= x_2 \\ \dot{x}_2 &= ax_1 - cx_1^3 + \varepsilon(-\delta x_2 + \gamma \cos \phi + \zeta \cos 2\phi) \\ \dot{\phi} &= \omega\end{aligned}\quad (5.38)$$

Examination of Eqs. (5.37) and (5.38) indicates that the Hamiltonian systems (i.e. $\varepsilon = 0$) are different but the perturbation to the integrable systems are identical.

In order to evaluate the Melnikov function (Eq. (5.29)) the homoclinic orbit of the unperturbed systems, $\mathbf{q}^0(t - t_0)$ must be evaluated. Prior to determining an analytical expression for this homoclinic orbit, it is worth noting that the change of variables $t \rightarrow t + t_0$ makes evaluation of the Melnikov integral a little more straight forward. With this variable transformation, Eq. (5.29) becomes:

$$M(t_0) = \int_{-\infty}^{\infty} \mathbf{f}(\mathbf{q}^0(t)) \wedge \mathbf{g}(\mathbf{q}^0(t), t + t_0) dt \quad (5.39)$$

and hence $\mathbf{q}^0(t)$ must be determined.

From this point on, the two systems are examined separately; Eq. (5.37) being examined first. The unperturbed system is:

$$\begin{aligned}\dot{x}_1 &= x_2 \\ \dot{x}_2 &= -ax_1 - bx_1^2\end{aligned}\quad (5.40)$$

or after the vector notation of Eq.(5.3):

$$\dot{\mathbf{x}} = \mathbf{f}(\mathbf{x}) = \begin{pmatrix} x_2 \\ -ax_1 - bx_1^2 \end{pmatrix} \quad (5.41)$$

From Eq. (5.12) the Hamiltonian for this system is therefore:

$$H = \frac{1}{2}x_2^2 + \frac{a}{2}x_1^2 + \frac{b}{3}x_1^3 \quad (5.42)$$

The equilibrium solutions are obtained from:

$$f(\bar{x}) = \begin{pmatrix} 0 \\ 0 \end{pmatrix} = \begin{pmatrix} x_2 \\ -ax_1 - bx_1^2 \end{pmatrix} \quad (5.43)$$

and thus the two fixed points are: $\bar{x}_1 = (0, 0)$ and $\bar{x}_2 = (-\frac{a}{b}, 0)$. Classification of the stability of these two points by linearization requires the evaluation of the Jacobian:

$$Df = \begin{pmatrix} \frac{\partial f_1}{\partial x_1} & \frac{\partial f_1}{\partial x_2} \\ \frac{\partial f_2}{\partial x_1} & \frac{\partial f_2}{\partial x_2} \end{pmatrix} \quad (5.44)$$

which for this system, at the two fixed point solutions, gives:

$$Df(\bar{x}_1) = \begin{pmatrix} 0 & 1 \\ -a - 2bx_1 & 0 \end{pmatrix} \quad Df(\bar{x}_2) = \begin{pmatrix} 0 & 1 \\ -a & 0 \end{pmatrix} \quad (5.45)$$

The eigenvalues of the corresponding secular equations are: (a) for \bar{x}_1 : $\lambda = \pm i\sqrt{a}$; and (b) for \bar{x}_2 : $\lambda = \pm \sqrt{a}$. Therefore, these two fixed points are classified as a center and a hyperbolic saddle point, respectively. This infers that the homoclinic orbit $q^0(t)$ will include the fixed point \bar{x}_2 . Now to determine the equation for the homoclinic orbit, $q^0(t)$, use is made of the equation for the constant energy of the unperturbed system (i.e. the Hamiltonian). Substitution of the hyperbolic saddle point solution into Eq. (5.42), results in the Hamiltonian with a value of $\frac{a^3}{6b^2}$; which when substituted back into Eq. (5.42) and upon rearranging for x_2 , gives:

$$x_2 = \pm \left(\frac{a^3}{3b^2} - ax_1^2 - \frac{2}{3}bx_1^3 \right)^{1/2} \quad (5.46)$$

By means of Eq. (5.40), Eq. (5.46) may be transformed into the first order differential equation:

$$\frac{dx_1}{dt} = \pm \left(\frac{a^3}{3b^2} - ax_1^2 - \frac{2}{3}bx_1^3 \right)^{1/2} \quad (5.47)$$

which upon selection of the positive root and integrated, gives:

$$x_1^+(t) = \frac{a}{2b} \left[1 - 3 \tanh^2 \left[\frac{\sqrt{a}}{2} (-t - \sqrt{3} C_1) \right] \right] \quad (5.48)$$

Choosing the integration constant C_1 to be zero, gives for $x_1^+(t)$ on the homoclinic orbit:

$$x_1^+(t) = \frac{a}{2b} \left[1 - 3 \tanh^2 \left(\frac{\sqrt{a}}{2} t \right) \right] \quad (5.49)$$

Thus the homoclinic orbit, $\mathbf{q}_+^0(t)$, involving the saddle point $\bar{x}_2 = (-\frac{a}{b}, 0)$ and the point $(\frac{a}{2b}, 0)$ is:

$$\mathbf{q}_+^0(t) = \frac{a}{2b} \left(1 - 3 \tanh^2 \left(\frac{\sqrt{a}}{2} t \right), -3\sqrt{a} \tanh \left(\frac{\sqrt{a}}{2} t \right) \operatorname{sech}^2 \left(\frac{\sqrt{a}}{2} t \right) \right)^T \quad (5.50)$$

Evaluation of the Melnikov integral, Eq. (5.39), requires computation of a wedge product of the Hamiltonian part of the system with the perturbation part of the system (i.e. $\mathbf{f} \wedge \mathbf{g}$); the components of which may be identified from Eq. (5.37) when written in the form:

$$\begin{pmatrix} \dot{x}_1 \\ \dot{x}_2 \end{pmatrix} = \mathbf{f}(\mathbf{x}) + \varepsilon \mathbf{g}(\mathbf{x}) = \begin{pmatrix} x_2 \\ -ax_1 - bx_1^2 \end{pmatrix} + \begin{pmatrix} 0 \\ \gamma \cos(\omega t) + \zeta \cos(2\omega t) - \delta x_2 \end{pmatrix} \quad (5.51)$$

The wedge product $\mathbf{f}(\mathbf{x}) \wedge \mathbf{g}(\mathbf{x}, t)$, is therefore:

$$\begin{aligned} \mathbf{f}(\mathbf{x}) \wedge \mathbf{g}(\mathbf{x}, t) &= x_2(\gamma \cos \omega t + \zeta \cos 2\omega t - \delta x_2) - 0(-ax_1 - bx_1^2) \\ &= x_2(\gamma \cos \omega t + \zeta \cos 2\omega t - \delta x_2) \end{aligned} \quad (5.52)$$

Thus, the wedge product for the homoclinic orbit in Eq. (5.39) is:

$$\begin{aligned} \mathbf{f}(\mathbf{q}_+^0(t)) \wedge \mathbf{g}(\mathbf{q}_+^0(t), t') &= -\frac{3}{2b} a^{3/2} \tanh \left(\frac{\sqrt{a}}{2} t \right) \operatorname{sech}^2 \left(\frac{\sqrt{a}}{2} t \right) (\gamma \cos \omega t' + \zeta \cos 2\omega t') - \\ &\quad \delta \frac{9}{4b^2} a^3 \tanh^2 \left(\frac{\sqrt{a}}{2} t \right) \operatorname{sech}^4 \left(\frac{\sqrt{a}}{2} t \right) \end{aligned} \quad (5.53)$$

where $t' = t + t_0$. The Melnikov integral for this first "study" equation, therefore, involves the computation of three integrals:

$$\begin{aligned}
 M(t_0) = & -\frac{3\sqrt{a^3}}{2b}\gamma \int_{-\infty}^{\infty} \tanh\left(\frac{\sqrt{a}}{2}t\right) \operatorname{sech}^2\left(\frac{\sqrt{a}}{2}t\right) \cos(\omega(t + t_0))dt - \\
 & \frac{3\sqrt{a^3}}{2b}\xi \int_{-\infty}^{\infty} \tanh\left(\frac{\sqrt{a}}{2}t\right) \operatorname{sech}^2\left(\frac{\sqrt{a}}{2}t\right) \cos(2\omega(t + t_0))dt - \\
 & \frac{9a^3}{4b^2}\delta \int_{-\infty}^{\infty} \tanh^2\left(\frac{\sqrt{a}}{2}t\right) \operatorname{sech}^4\left(\frac{\sqrt{a}}{2}t\right) dt \quad (5.54)
 \end{aligned}$$

Prior to evaluating these integrals, return is made to the second "study" system (i.e. Eq. (5.38)).

A similar analysis when performed on the second system reveals for the unperturbed system:

$$\begin{aligned}
 \dot{x}_1 &= x_2 \\
 \dot{x}_2 &= ax_1 - cx_1^3 \quad (5.55)
 \end{aligned}$$

a Hamiltonian:

$$H = \frac{1}{2}x_2^2 - \frac{a}{2}x_1^2 + \frac{c}{4}x_1^4 \quad (5.56)$$

The equilibrium solutions for this system are: $\bar{x}_1 = (0, 0)$, $\bar{x}_2 = (\sqrt{\frac{a}{c}}, 0)$ and $\bar{x}_3 = (-\sqrt{\frac{a}{c}}, 0)$. Stability analysis using linearization shows that the first root is a hyperbolic saddle point and the latter two are elliptic fixed points. The value of the Hamiltonian for the desired homoclinic orbit (i.e. for \bar{x}_1) is, of course 0; and therefore the analytical form of $q^0(t)$ is obtained by solving the differential equation:

$$\frac{dx_1}{dt} = \pm x_1 \left(a - \frac{c}{2}x_1^2 \right)^{1/2} \quad (5.57)$$

Selection of the positive root results in the homoclinic orbit, $q_+^0(t)$, with coordinates:

$$\mathbf{q}_+^0(t) = \sqrt{\frac{2a}{c}} (\operatorname{sech}(\sqrt{a}t), -\sqrt{a} \operatorname{sech}(\sqrt{a}t) \tanh(\sqrt{a}t))^T \quad (5.58)$$

The wedge product $\mathbf{f}(\mathbf{x}) \wedge \mathbf{g}(\mathbf{x}, t)$, is the same as before, i.e.:

$$\mathbf{f}(\mathbf{x}) \wedge \mathbf{g}(\mathbf{x}, t) = x_2(\gamma \cos \omega t + \xi \cos 2\omega t - \delta x_2) \quad (5.59)$$

Thus, the wedge product for the homoclinic orbit in Eq. (5.39) is:

$$\begin{aligned} \mathbf{f}(\mathbf{q}_+^0(t)) \wedge \mathbf{g}(\mathbf{q}_+^0(t), t) &= -a \sqrt{\frac{2}{c}} \operatorname{sech}(\sqrt{a}t) \tanh(\sqrt{a}t) (\gamma \cos \omega t + \xi \cos 2\omega t) - \\ &\quad \delta \frac{2}{c} a^2 \tanh^2(\sqrt{a}t) \operatorname{sech}^2(\sqrt{a}t) \end{aligned} \quad (5.60)$$

Thus, the Melnikov integral for this second "study" equation involves the evaluation of the following three integrals:

$$\begin{aligned} M(t_0) &= -\gamma a \sqrt{\frac{2}{c}} \int_{-\infty}^{\infty} \operatorname{sech}(\sqrt{a}t) \tanh(\sqrt{a}t) \cos(\omega(t + t_0)) dt - \\ &\quad \xi a \sqrt{\frac{2}{c}} \int_{-\infty}^{\infty} \operatorname{sech}(\sqrt{a}t) \tanh(\sqrt{a}t) \cos(2\omega(t + t_0)) dt - \\ &\quad \frac{2a^2}{c} \delta \int_{-\infty}^{\infty} \tanh^2(\sqrt{a}t) \operatorname{sech}^2(\sqrt{a}t) dt \end{aligned} \quad (5.61)$$

Examination of the Melnikov integrals for the two systems (i.e. Eqs. (5.54) and (5.61)) shows that all the integrals are quite similar in form involving various powers of sech and tanh. At the onset of the evaluation of these integrals it is beneficial to convert the argument of the hyperbolic functions into simply t . Therefore, for Eq. (5.54) the variable transformation $\frac{\sqrt{a}}{2}t \Rightarrow t_1 \Rightarrow t$ is made, resulting in the Melnikov integral:

$$M(t_0) = -\frac{3a}{b}\gamma \int_{-\infty}^{\infty} \tanh(t) \operatorname{sech}^2(t) \cos\left(\omega\left(\frac{2}{\sqrt{a}}t + t_0\right)\right) dt -$$

$$\begin{aligned} & \frac{3a}{b} \zeta \int_{-\infty}^{\infty} \tanh(t) \operatorname{sech}^2(t) \cos\left(2\omega\left(\frac{2}{\sqrt{a}}t + t_0\right)\right) dt - \\ & \frac{9a^{5/2}}{2b^2} \delta \int_{-\infty}^{\infty} \tanh^2(t) \operatorname{sech}^4(t) dt \end{aligned} \quad (5.62)$$

$$= m_1 + m_2 + m_3$$

Following this variable change, the cosine functions in the first two integrals are expanded according to:

$$\begin{aligned} \cos\left(\omega\left(\frac{2}{\sqrt{a}}t + t_0\right)\right) &= \cos\frac{2\omega}{\sqrt{a}}t \cos\omega t_0 - \sin\frac{2\omega}{\sqrt{a}}t \sin\omega t_0 \\ \cos\left(2\omega\left(\frac{2}{\sqrt{a}}t + t_0\right)\right) &= \cos\frac{4\omega}{\sqrt{a}}t \cos 2\omega t_0 - \sin\frac{4\omega}{\sqrt{a}}t \sin 2\omega t_0 \end{aligned}$$

and thus, because of the symmetry of the integration, the first two integrals m_1 , m_2 become:

$$\begin{aligned} m_1 &= \frac{3a}{b} \gamma \sin(\omega t_0) \int_{-\infty}^{\infty} \tanh t \operatorname{sech}^2 t \sin\left(\frac{2\omega}{\sqrt{a}}t\right) dt \\ m_2 &= \frac{3a}{b} \zeta \sin(\omega t_0) \int_{-\infty}^{\infty} \tanh t \operatorname{sech}^2 t \sin\left(\frac{4\omega}{\sqrt{a}}t\right) dt \end{aligned} \quad (5.63)$$

Now of these three integrals, m_3 is the most easily evaluated through a standard integral formula giving:

$$\begin{aligned} m_3 &= \frac{9a^{5/2}}{2b^2} \delta \int_{-\infty}^{\infty} \tanh^2 t \operatorname{sech}^4 t dt = \frac{9a^{5/2}}{b^2} \delta \int_0^{\infty} \tanh^2 t \operatorname{sech}^4 t dt \\ &= \frac{9a^{5/2}}{b^2} \delta \left(\frac{\operatorname{sech}^5 t}{120} (-20 \sinh t + 5 \sinh 3t + \sinh 5t) \right) \Big|_0^{\infty} \\ &= \frac{9a^{5/2}}{b^2} \delta \left(\frac{2}{15} - 0 \right) \\ &= \frac{6a^{5/2}}{5b^2} \delta \end{aligned} \quad (5.64)$$

The first two integrals (i.e. m_1 , m_2) require somewhat more ingenuity to evaluate. As they are very similar (the only difference being the argument of the sine function), only the details will be shown for m_1 .

The procedure in evaluating m_1 begins by recalling:

$$\tanh t \operatorname{sech}^2 t \, dt = -\frac{1}{2} \frac{d}{dt} (\operatorname{sech}^2 t)$$

and therefore, m_1 may be written:

$$m_1 = -\frac{3a}{2b} \gamma \sin(\omega t_0) \int_{-\infty}^{\infty} \frac{d}{dt} (\operatorname{sech}^2 t) \sin\left(\frac{2\omega}{\sqrt{a}} t\right) dt \quad (5.65)$$

This integral may be integrated by parts with the result:

$$\begin{aligned} m_1 &= \frac{3\sqrt{a}}{b} \omega \gamma \sin(\omega t_0) \int_{-\infty}^{\infty} \operatorname{sech}^2 t \cos\left(\frac{2\omega}{\sqrt{a}} t\right) dt \\ &= \frac{3\sqrt{a}}{b} \omega \gamma \sin(\omega t_0) \int_{-\infty}^{\infty} \frac{\cosh\left(\frac{2\omega i}{\sqrt{a}} t\right)}{\cosh^2 t} dt \end{aligned} \quad (5.66)$$

Progress with the integral appearing in Eq. (5.66) requires the application of *the method of residues*. Consider the integral around the rectangle C in the complex plane: $\oint_C \frac{e^{2\omega'iz}}{\cosh^2 z} dz$

diagramed in Fig. 5.1; where after conventional notation $z = x + yi$, and $\omega' \equiv \frac{\omega}{\sqrt{a}}$.

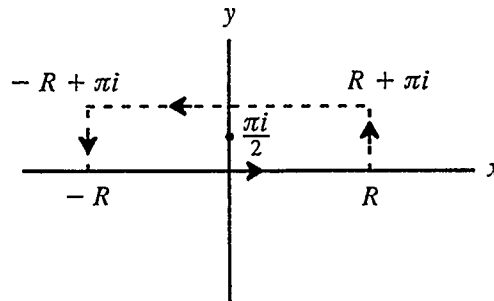


Fig. 5.1 Integration contour diagram.

The poles of $\frac{e^{2\omega'iz}}{\cosh^2 z}$ occur where $\cosh^2 z = 0$, that is, where $z = \left(n + \frac{1}{2}\right)\pi i$; $n = 0, \pm 1, \pm 2, \dots$. The only pole totally enclosed by C is $\frac{\pi i}{2}$ (see Fig. 5.1). Therefore the residue, a_{-1} , of $\frac{e^{2\omega'iz}}{\cosh^2 z}$ at $z = \frac{\pi i}{2}$ is:

$$\begin{aligned} a_{-1} &= \lim_{z \rightarrow \frac{\pi i}{2}} \frac{1}{(2-1)!} \frac{d}{dz} \left\{ \left(z - \frac{\pi i}{2}\right)^2 \frac{e^{2\omega'iz}}{\cosh^2 z} \right\} \\ &= \lim_{z \rightarrow \frac{\pi i}{2}} \frac{1}{2} (2z - \pi i) \operatorname{sech}^2 z e^{2\omega'iz} (2 + \pi\omega' + 2\omega'iz + \pi i \tanh z - 2z \tanh z) \\ &= -\frac{2\omega'i}{e^{\pi\omega'}} \end{aligned}$$

Therefore, by the *Residue Theorem*:

$$\oint_C \frac{e^{2\omega'iz}}{\cosh^2 z} dz = 2\pi i \left(-\frac{2\omega'i}{e^{\pi\omega'}} \right) = \frac{4\pi\omega'}{e^{\pi\omega'}} \quad (5.67)$$

Now the integral around the rectangle C may be broken up as follows:

$$\begin{aligned} \oint_C \frac{e^{2\omega'iz}}{\cosh^2 z} dz &= \int_{-R}^R \frac{e^{2\omega'ix}}{\cosh^2 x} dx + \int_0^\pi \frac{e^{2\omega'i(R+iy)}}{\cosh^2(R+iy)} idy + \\ &\quad \int_R^{-R} \frac{e^{2\omega'i(x+\pi i)}}{\cosh^2(x+\pi i)} dx + \int_\pi^0 \frac{e^{2\omega'i(-R+iy)}}{\cosh^2(-R+iy)} idy \end{aligned} \quad (5.68)$$

In evaluation of the second integral in Eq. (5.68), consider the following arguments:

$$\begin{aligned} |e^{2\omega'i(R+iy)}| &= |e^{2\omega'iR} e^{-2\omega'y}| \leq e^{-2\omega'y} \\ |\cosh(R+iy)| &= \left| \frac{e^{R+iy} + e^{-R-iy}}{2} \right| \geq \frac{1}{2} \{ |e^{R+iy}| - |e^{-R-iy}| \} = \frac{1}{2} (e^R - e^{-R}) \geq \frac{1}{4} e^R \\ \therefore \int_0^\pi \frac{e^{2\omega'i(R+iy)}}{\cosh^2(R+iy)} idy &\leq \int_0^\pi \frac{e^{-2\omega'y}}{\frac{1}{4} e^R} dy = \frac{4}{e^R} \left(-\frac{1}{2\omega'} e^{-2\omega'y} \Big|_0^\pi \right) \end{aligned}$$

Hence, it should be clear from the above arguments that for the entire complex plane (i.e.

when $R \rightarrow \infty$), the second and fourth integrals are simply:

$$\lim_{R \rightarrow \infty} \left[\int_0^{\pi} \frac{e^{2\omega' i(R+iy)}}{\cosh^2(R+iy)} idy \right] = \lim_{R \rightarrow \infty} \left[\int_{\pi}^0 \frac{e^{2\omega' i(-R+iy)}}{\cosh^2(-R+iy)} idy \right] = 0 \quad (5.69)$$

Therefore, from Eq. (5.69), the integral around an infinitely large rectangle (Eq. (5.68)) simplifies to:

$$\oint_{C_{\infty}} \frac{e^{2\omega' iz}}{\cosh^2 z} dz = \lim_{R \rightarrow \infty} \left[\int_{-R}^R \frac{e^{2\omega' ix}}{\cosh^2 x} dx + \int_R^{-R} \frac{e^{2\omega' i(x+\pi i)}}{\cosh^2(x+\pi i)} dx \right] \quad (5.70)$$

Realizing $\cosh(x+\pi i) = -\cosh x$, and hence $\cosh^2(x+\pi i) = \cosh^2 x$; Eq. (5.70) becomes:

$$\begin{aligned} \oint_{C_{\infty}} \frac{e^{2\omega' iz}}{\cosh^2 z} dz &= \lim_{R \rightarrow \infty} \left[\int_{-R}^R \frac{e^{2\omega' ix}}{\cosh^2 x} dx + e^{-2\omega' \pi} \int_R^{-R} \frac{e^{2\omega' ix}}{\cosh^2 x} dx \right] \\ &= \lim_{R \rightarrow \infty} \left[\int_{-R}^R \frac{e^{2\omega' ix}}{\cosh^2 x} dx - e^{-2\omega' \pi} \int_R^{-R} \frac{e^{2\omega' ix}}{\cosh^2 x} dx \right] \\ &= (1 - e^{-2\omega' \pi}) \int_{-\infty}^{\infty} \frac{e^{2\omega' ix}}{\cosh^2 x} dx \end{aligned} \quad (5.71)$$

Substituting the result obtained from the residue theorem (Eq. (5.67)), Eq. (5.71) becomes:

$$\frac{4\pi\omega'}{e^{\pi\omega'}} = (1 - e^{-2\omega' \pi}) \int_{-\infty}^{\infty} \frac{e^{2\omega' ix}}{\cosh^2 x} dx \quad (5.72)$$

which upon rearrangement gives:

$$\begin{aligned} \int_{-\infty}^{\infty} \frac{e^{2\omega' ix}}{\cosh^2 x} dx &= \frac{\frac{4\pi\omega'}{e^{\pi\omega'}}}{(1 - e^{-2\omega' \pi})} \\ &= \frac{2\pi\omega'}{\sinh \pi\omega'} \end{aligned} \quad (5.73)$$

It may be concluded, therefore, that the method of residues has been used to derive a result

for an integral very similar to the integral appearing in the expression for m_1 (Eq. (5.66)). All that remains is manipulation of the left hand side of Eq. (5.73) to make connect with the desired integral in m_1 . This may be achieved as follows:

$$\begin{aligned}
\int_{-\infty}^{\infty} \frac{e^{2\omega'ix}}{\cosh^2 x} dx &= \int_{-\infty}^0 \frac{e^{2\omega'ix}}{\cosh^2 x} dx + \int_0^{\infty} \frac{e^{2\omega'ix}}{\cosh^2 x} dx \\
&= - \int_{\infty}^0 \frac{e^{-2\omega'ix}}{\cosh^2 x} dx + \int_0^{\infty} \frac{e^{2\omega'ix}}{\cosh^2 x} dx \\
&= \int_0^{\infty} \frac{e^{-2\omega'ix}}{\cosh^2 x} dx + \int_0^{\infty} \frac{e^{2\omega'ix}}{\cosh^2 x} dx \\
&= 2 \int_0^{\infty} \frac{\cos(2\omega'x)}{\cosh^2 x} dx = 2 \int_0^{\infty} \frac{\cosh(2\omega'ix)}{\cosh^2 x} dx \\
&= \int_{-\infty}^{\infty} \frac{\cosh\left(\frac{2\omega i}{\sqrt{a}}x\right)}{\cosh^2 x} dx
\end{aligned} \tag{5.74}$$

Therefore, from Eqs. (5.73) and (5.74), the value of m_1 is:

$$m_1 = \frac{6\pi\omega^2\gamma \sin(\omega t_0)}{b \sinh\left(\frac{\pi\omega}{\sqrt{a}}\right)} \tag{5.75}$$

and that of m_2 is:

$$m_2 = \frac{24\pi\omega^2\zeta \sin(2\omega t_0)}{b \sinh\left(\frac{2\pi\omega}{\sqrt{a}}\right)} \tag{5.76}$$

Combining the results of Eqs. (5.64), (5.75), and (5.76) gives the following expression for the Melnikov integral for the first "study" system (Eq. (5.37)):

$$M(t_0) = \frac{6\pi\omega^2\gamma \sin(\omega t_0)}{b \sinh\left(\frac{\pi\omega}{\sqrt{a}}\right)} + \frac{24\pi\omega^2\zeta \sin(2\omega t_0)}{b \sinh\left(\frac{2\pi\omega}{\sqrt{a}}\right)} - \frac{6a^{5/2}}{5b^2} \delta \tag{5.77}$$

A similar methodology including the application of the method of residues is used to evalu-

ate the Melnikov integral (Eq. (5.61)) for the second system (Eq. (5.38)); with the final result being:

$$M(t_0) = \pi\omega \sqrt{\frac{2}{c}}\gamma \sin(\omega t_0) \operatorname{sech}\left(\frac{\pi\omega}{2\sqrt{a}}\right) + 2\pi\omega \sqrt{\frac{2}{c}}\xi \sin(2\omega t_0) \operatorname{sech}\left(\frac{\pi\omega}{\sqrt{a}}\right) - \frac{4\sqrt{a^3}}{3c}\delta \quad (5.78)$$

5.5 Discussion of Results

Although both of the derived expressions (Eqs. (5.77) and (5.78)) for the Melnikov function are quite complicated in appearance (i.e. they involve several parameters), conditions in the parameter space may be chosen so that $M(t_0) = 0$, $dM(t_0)/dt_0 \neq 0$; these being the requirements for local deterministic chaos (see Theorem in §5.3.4). Hence, the critical parameters upon which nonlinear dynamics may depend are: a , b or c , γ , δ , and ω ; all of which may be determined or estimated. The implemented change of variables (see Eq. (5.31)) from the original micromotion system to the "study" systems along with the approximate magnitude of the parameters (see Table 4.1) is presented here in Table 5.1 for purposes of the discussion following.

Table 5.1 *Variable Transformation*

<i>Melnikov Parameter</i>	<i>Micromotion Parameter</i>	<i>Magnitude</i>
a	k	10^{-5}
b	k'	10^{-4}
c	k''	5×10^{-4}
γ	G_1	10^{-5} to 10^{-4}
ξ	G_2	10^{-8} to 10^{-6}
δ	—	1
ω	$\tilde{\omega}_1$	10^{-2}

Examination of the magnitude of the first 5 parameters clearly indicates that all are at least 4 orders of magnitude smaller than the "damping" coefficient (δ). This, of course, implies as previously indicated (§4.4.1), that the system is very highly damped. The significance of this strong damping to the results of the Melnikov method is that the *per-*

turbation to the integrable system (i.e. the combination of the two drivers – electrophoretic and dielectrophoretic – and the damping) *is not small*. This is seen clearly by rewriting the micromotion equation in the approximate form:

$$\frac{d^2\tilde{\delta}}{d\tilde{t}^2} + k\tilde{\delta} + k'\tilde{\delta}^2 + k''\tilde{\delta}^3 = 10^{-5}\left(\cos(\tilde{\omega}_1\tilde{t}) + 10^{-2}\cos(2\tilde{\omega}_1\tilde{t}) - 10^5\frac{d\tilde{\delta}}{d\tilde{t}}\right) \quad (5.79)$$

where ε has been arbitrarily given the value of 10^{-5} . Now the first two terms on the left hand side of Eq. (5.79) are obviously small (of the order of ε), but the last term is not. This parameter analysis indicates that the micromotion system with the experimental parameters of the sorbitol suspended protoplasts *is not near-integrable*; and therefore the Melnikov method is not applicable. This system is not near-integrable because it is far from being a conservative system. It is the significant damping of the micromotion caused by the interaction of the protoplast with the suspension medium that results in a perturbation that is far from small.

Chapter 6: Concluding Remarks

6.1 Connection

The theoretical investigations (Chapters 3 and 4) into the two distinct anomalous responses of DEP levitated plant protoplasts subjected to inhomogeneous electric fields, although treated and analyzed separately, are nevertheless connected. The two phenomena were observed under essentially identical experimental conditions with the same apparatus. The studies were performed on same type of particles (canola and tobacco protoplasts), and the phenomena observed within a similar region of the DEP spectrum (< 50 Hz.). More importantly, both observations are nonlinear; where specifically: the nonlinear response occurs at the particle/medium interface as a result of the applied electric field. The hysteresis is attributed to an electric field dependent permittivity at the interface, and the higher harmonics in the micromotion attributed to an electric field dependent ionization constant at the interface. The fact that these observations occurred at only low field frequencies is not too surprising, as it is only under these conditions that the cellular components have sufficient time to respond to the electric field. It should also be realized that both phenomena indicate that the electric field profoundly changes the character or nature of the dielectrophoretic measurement; not simply a relative or proportional alteration.

6.2 Future Research

As with any research effort, there always remains more to be explored and additional investigations that will possibly add additional understanding or strengthen existing understanding. Such is certainly the case with this work. The following three suggestions are offered as possible areas of future research.

1. As mentioned earlier in this dissertation, the scale of these experimental measurements may be classified as "mesoscopic". On this scale, precise understanding of the underlying physical processes and mechanisms causing the observable behavior of the levitated protoplast, is somewhat elusive. Thus, measurement on a "microscopic scale" needs to be per-

formed. The intent of these measurements would be to elucidate the actual mechanism (presumably polarization related) that is responsible for either the hysteresis or nonlinear micromotion. Having concluded that these phenomena are the result of the action of the electric field on the protoplast/medium interface, suggests that the measurements should focus on the determining the field functionality of the permittivity of the cell membrane as a result of the possible flux of membrane proteins and lipids.

2. Although the Melnikov method could not be successfully implemented to the micromotion system because of the heavy damping of the motion, through providing conditions where the particle is levitated in a medium with a very small frictional drag coefficient, it would be applicable. The requirements of a near-integrable system may be met by the use of air as the medium. Under these conditions, the Melnikov method might be used as a means of determining conditions under which the micromotion may become deterministically chaotic.

3. The conclusion that the higher harmonics in the micromotion are the result of electric field induced alteration in the dissociation constants of surface proteins, is not really measured. To the knowledge of this author, the specific measurement of the effects of electric fields on the dissociation constant of weak acids has not been made. In the early work of Onsager (18), experimental estimates of a two-fold relative increase in the dissociation constant of benzene occurred under applied electric field strengths of approximately an order of magnitude greater than used in these DEP studies. Further work needs to be done in measuring the effects of electric fields of similar magnitude (≈ 5 kV/m) on the dissociation constants of weak acids.

References

1. Pethig, R.; Kell, D.B. *Phys. Med. Biol.*, **1987**, *32*, 933.
2. Foster, K.R.; Schwan, H.P. *Critical Reviews in Biomedical Engineering*, **1989**, *17*, 25.
3. a) Pohl, H.A.; Crane, J.S. *Biophys. J.*, **1971**, *11*, 711. b) Pohl, H.A. in *Methods of Cell Separation*; Catsimpoolas, N., Ed.; Plenum Press: New York, 1978; vol 1; pp. 67–169.
4. a) Becker, F.F.; Wang, X.-B.; Huang, Y.; Pethig, R.; Vykoukal, J.; Gascoyne, P.R.C. *J. Phys. D: Appl. Phys.*, **1994**, *27*, 2659. b) Gascoyne, P.R.C.; Noshari, J.; Becker, F.F.; Pethig, R. *IEEE Trans. Ind. Appl.*, **1994**, *30*, 829. c) Becker, F.F.; Wang, X.-B.; Huang, Y.; Pethig, R.; Vykoukal, J.; Gascoyne, P.R.C. *Proc. Natl. Acad. Sci. USA*, **1995**, *92*, 860.
5. Mason, B.D.; Townsely, P.M. *Can. J. Microbiol.*, **1971**, *17*, 879.
6. Kaler, K.V.I.S.; Xie, J-P.; Jones, T.B.; Paul, R. *Biophys. J.*, **1992**, *63*, 58.
7. Paul, R.; Kaler, K.V.I.S.; Jones, T.B. *J. Phys. Chem.*, **1993**, *97*, 4745.
8. Barrie, G.B. *Anomalous Dielectrophoresis and the Theory of Micro-motion*; M.Sc. Thesis, The University of Calgary, 1993.
9. Kaler, K.V.I.S.; Jones, T.B.; Paul, R. *J. Colloid Interface Sci.*, **1995**, *175*, 108.
10. Barrie, G.; Paul, R.; Kaler, K.V.I.S.; Jones, T.B. *J. Colloid Interface Sci.*, **1995**, *175*, 97.
11. Burt, J.P.H.; Pethig, R.; Gascoyne, P.R.C.; Becker, F.F. *Biochim. Biophys. Acta*, **1990**, *1034*, 93.
12. Gascoyne, P.R.C.; Pethig, R.; Burt, J.P.H.; Becker, F.F. *Biochim. Biophys. Acta*, **1993**, *1149*, 119.
13. Pethig, R.; Huang, Y.; Wang, X.-B.; Burt, J.P.H. *J. Phys. D: Appl. Phys.*, **1992**, *24*, 881.
14. Arnold, W.M.; Schwan, H.P.; Zimmermann, U. *J. Phys. Chem.*, **1987**, *91*, 5093.
15. Jackson, E. A. *Perspectives of Nonlinear Dynamics*; Cambridge University Press: New York, 1991; p. 6.

16. Debye, P. *Polar Molecules*; Dover: New York, 1929.
17. a) Wien, M. *Phys. Z.*, **1928**, 29, 751. b) Wien, M. *Phys.Z.*, **1931**, 32, 545.
18. a) Onsager, L. *J. Chem. Phys.*, **1934**, 2, 599. b) Onsager, L. *J. Am. Chem. Soc.*, **1936**, 58, 1486.
19. Bass, L. *Trans. Faraday Soc.*, **1968**, 64, 2153.
20. Takashima, S. *Electrical Properties of Biopolymers and Membranes*; IOP: Worcester, 1989.
21. a) Piekara, A.; Kielich, S. *Acta Phys. Pol.*, **1958**, 18, 109. b) Piekara, A.; Kielich, S. *J. Chem. Phys.*, **1958**, 29, 1297.
22. a) Malecki, J. *Acta Phys. Pol.*, **1962**, 21, 13. b) Malecki, J. *J. Chem. Phys.*, **1965**, 43, 1351.
23. Böettcher, C.J. E.; Bordewijk, P. *Theory of Electric Polarisation*, 2nd edn.; Elsevier: Amsterdam, 1973; vol. 1.
24. Block, H.; Hayes, E.F. *Trans. Faraday Soc.*, **1970**, 66, 2512.
25. Gregson, M.; Jones, G.P.; Davies, M. *Trans. Faraday Soc.*, **1971**, 67, 1630.
26. Jones, P. *Biophys, Chem.*, **1979**, 9, 91.
27. a) Schwan, H.P. *Adv. Biol. Med. Phys.*, **1957**, 5, 147. b) Schwan, H.P. *Phys. Tech. Biol. Res.*, **1963**, 6, 323. c) Hanai, T.; Asami, K.; Koizumi, N. *Bull. Inst. Chem. Res. Kyoto Univ.*, **1979**, 57, 297.
28. Starzak, M.E. *The Physical Chemistry of Membranes*; Academic Press: Orlando, 1977; pp. 164–170.
29. Maxwell, J.C. *A Treatise on Electricity and Magnetism*; Dover: New York, 1891; vol. 1.
30. a) Fricke, H. *J. Phys. Chem.*, **1955**, 59, 168. b) Bordi, F.; Cametti, C.; di Biaso, A. *Bio-electrochem. Bioenerg.*, **1989**, 22, 135.
31. a) Sakmann, B.; Neher, E. *Single Channel Recording*; Plenum Publishing Corp.: New York, 1983. b) Takashima, S.; Asami, K.; Takahashi, T. *Biophys. J.*, **1988**, 54, 995.

32. a) Arnold, W.M.; Schwan, H.P.; Zimmermann, U. *Z. Naturforsch.*, **1982**, *37*, 908. b) Arnold, W.M.; Zimmermann, U. *J. Electrostatics*, **1988**, *21*, 151.
33. a) Lovelace, R.V.E.; Stout, D.G.; Steponkus, P.I. *J. Membrane Biol.*, **1984**, *82*, 157. b) Fuhr, G; Hageborn, R.; Goring, H. *Plant and Cell Physiol.*, **1985**, *26*, 1527. c) Fuhr, G.; Glaser, R.; Hageborn, R. *Biophys. J.*, **1986**, *49*, 395.
34. Sauer, F.A.; Schlögl, R.W. in *Interactions between electromagnetic fields and cells*; Chiabrera, A.; Nicolini, C.; Schwan, H.P., Eds.; Plenum: New York, 1985; pp.203–251.
35. Sheng, Y. *Electrorotation Studies on Protoplasts*; M.Sc. Thesis, The University of Calgary, 1994.
36. Nagata, T.; Melchers, G. *Planta*, **1978**, *142*, 235.
37. Obi, I.; Ichikawa, T.; Kakutani, T.; Senda, M. *Plant Cell Physiol.*, **1989**, *30*, 129.
38. Tulp, A.; Timmerman, A.; Barnhoorn, M.G. *Anal. Biochem.*, **1982**, *124*, 432.
39. Pohl, H.A. *Dielectrophoresis: The behavior of neutral matter in nonuniform electric fields*; Cambridge University Press: Cambridge, 1978.
40. a) Pohl, H.A.; Hawk, I. *Science*, **1966**, *152*, 647. b) Pohl, H.A.; Kaler, K.V.I.S.; Pollock, K. *J. Biol. Phys.*, **1981**, *9*, 67. c) Kaler, K.V.I.S.; Pohl, H.A. *IEEE Trans. Ind. Appl.*, **1983**, *IA-19(6)*, 1089. d) Adamson, R.J.; Kaler, K.V.I.S. *IEEE Trans. Ind. Appl.*, **1988**, *IA-24(1)*, 93. e) Kaler, K.V.I.S.; Fritz Jr., O.G.; Adamson, R.J. *J. Electrostatics*, **1988**, *21*, 193. f) Price, J.A.R.; Burt, J.P.H.; Pethig, R. *Biochim. Biophys. Acta*, **1988**, *964*, 221. g) Marsalek, P.; Zielinski, J.J. *Bioelectrochem. Bioenerg.*, **1989**, *22*, 289.
41. a) Jones, T.B.; Kallio, G.A. *J. Electrostatics*, **1979**, *6*, 207. b) Jones, T.B.; Loomans, L.W. *J. Electrostatics*, **1983**, *14*, 269.
42. Jones, T.B.; Bliss, G.W. *J. Appl. Phys.*, **1977**, *48*, 1412.
43. Holmes, L.M. *J. Appl. Phys.*, **1978**, *49*, 3102.
44. Jones, T.B.; Kraybill, J.P. *J. Appl. Phys.*, **1986**, *60*, 1247.
45. Kaler, K.V.I.S.; Jones, T.B. *Biophys. J.*, **1990**, *57*, 173.

46. Xie, J. *Measurement of Electrical Properties of Biological Cells using a Dielectrophoretic Levitation System*; M.Sc. Thesis, The University of Calgary, 1991.
47. Stratton, J.A. *Electromagnetic Theory*; McGraw-Hill: New York, 1941; Chaps. 1–3.
48. Jones, T.B. *Electromechanics of Particles*; Cambridge University Press: Cambridge, 1995.
49. Sauer, F.A. in *Coherent Excitations in Biological Systems*; Frohlich, H.; Kremer, F., Eds.; Springer-Verlag: Berlin, 1983; pp. 134–144.
50. Pohl, H.A. *J. Appl. Phys.*, **1951**, *22*, 869.
51. Sauer, F.A. in *Interactions between electromagnetic fields and cells*; Chiabrera, A.; Nicolini, C.; Schwan, H.P., Eds.; Plenum: New York, 1985; pp.181–202.
52. Giner, V.; Sancho, M.; Martinez, G. *Am. J. Phys.*, **1995**, *63*, 749.
53. Pauly, H.; Schwan, H.P. *Z. Naturforsch.*, **1959**, *14b*, 125.
54. a) Dekker, A.J. *Solid State Physics*; Macmillan: London, 1962. b) Kittel, C. *Elementary Solid State Physics*; John Wiley & Sons: New York, 1973.
55. Dukhin, S.S.; Shilov, V.N. *Dielectric Phenomena and the Double Layer in Disperse Systems*; John Wiley & Sons: New York, 1974.
56. Schwan, H.P.; Schwarz, G.; Maczuk, J.; Pauly, H. *J. Phys. Chem.*, **1962**, *66*, 2626.
57. Einolf, C.W.; Carstensen, E.L. *Biophys. J.*, **1973**, *13*, 8.
58. Mandel, M. *Ann. N. Y. Acad. Sci.*, **1977**, *303*, 74.
59. Schwarz, G. *J. Phys. Chem.*, **1962**, *66*, 2636.
60. Schurr, J.M. *J. Phys. Chem.*, **1964**, *68*, 2407.
61. a) Fixman, M. *J. Chem. Phys.*, **1980**, *72*, 5177. b) Fixman, M. *J. Chem. Phys.*, **1983**, *78*, 1483.
62. a) Chew, W.C.; Sen, P.N. *J. Chem. Phys.*, **1982**, *77*, 2042. b) Chew, W.C.; Sen, P.N. *J. Chem. Phys.*, **1982**, *77*, 4683. c) Chew, W.C. *J. Chem. Phys.*, **1984**, *81*, 4541.
63. a) Grosse, C.; Foster, K.R. *J. Phys. Chem.*, **1987**, *91*, 3073. b) Grosse, C. *J. Phys. Chem.*, **1988**, *92*, 3905.

64. Cevc, G. *Biochim. Biophys. Acta*, **1990**, *1031*, 311.
65. Paddison, S.J.; Paul, R.; Kaler, K.V.I.S. *Bioelectrochem. Bioenerg.*, **1995**, *38*, 321.
66. Kaler, K.V.I.S. private communication.
67. Scaife, B.K.P. *Principles of Dielectrics*; Clarendon Press: Oxford, 1989.
68. Ames, W.F. *Nonlinear Partial Differential Equations in Engineering*; Academic Press: New York, 1965; Section 6.2.
69. Butcher, P.N.; Cotter, D. *The Elements of Nonlinear Optics*; Cambridge University Press: New York, 1990.
70. Bordi, F.; Cametti, C. *Bioelectrochem. Bioenerg.*, **1989**, *22*, 135.
71. Beck, J.S. *Biomembranes Fundamentals in Relation to Human Biology*; Hemisphere Publishing Corporation: Washington, 1980.
72. Kell, D.B.; Harris, C.M. *Eur. Biophys. J.*, **1985**, *12*, 181.
73. Haken, H. *Synergetics, An Introduction*; Springer: Berlin, 1983.
74. Åkesson, T.; Jönsson, B. *J. Phys. Chem.*, **1985**, *89*, 2401.
75. Gaigalas, A.K.; Woo, S.; Hubbard, J.B. *J. Colloid Interface Sci.*, **1990**, *136*, 213.
76. Dukhin, S.S.; Mishchuls, N.A.; Rukobratskii, N.I. *Kolloidn. Zh.*, **1988**, *50(1)*, 17 [Russian].
77. Robertson, B. *J. Chem. Phys.*, **1991**, *95*, 3873.
78. Paddison, S.J.; Paul, R.; Kaler, K.V.I.S. *J. Colloid Interface Sci.*, **1996**, in press.
79. Gonnason, W.R.; Haslett, J.W.; Trofimenkoff, F.N. *IEEE Trans. Instrum. and Meas.*, **1990**, *39*, 658.
80. Murashige, T.; Skoog, F. *Physiologia Plantarum*, **1962**, *15*, 473.
81. Duffing, G., *Erzwungene Schwingen bei Veränderlichen Eigenfrequenz*; F. Vieweg u. Sohn, Braunschweig; 1918.
82. Moon, F.C.; Holmes, P.J. *J. Sound Vib.*, **1979**, *65*, 285.
83. Moon, F.C.; Holmes, P.J. *J. Sound Vib.*, **1980**, *69*, 339.
84. Holmes, P.J. *Phil. Trans. Roy. Soc. A*, **1979**, *292*, 419.

85. Greenspan, B.D.; Holmes, P.J. in *Nonlinear Dynamics and Turbulence*; Barenblatt, G.; Ioss, G.; Joseph D.D., Eds.; Pitman: London, 1982; pp. 172–214.
86. Ueda, Y. in *New Approaches to Nonlinear Problems in Dynamics*; Holmes, P.J., Ed.; SIAM Publications: Philadelphia, 1980.
87. Ueda, Y. *Annals of the New York Academy of Science*, **1980**, 357, 422.
88. Obi, I.; Ichikawa, Y.; Nonaka, R.; Kakutani, T.; Senda, M. *Plant Cell Physiol.*, **1989**, 30, 759.
89. Landau, L.D.; Lifshitz, E.M. *Fluid Mechanics*; Pergamon Press: Oxford, 1982; Section 20.
90. Chiabrera, A.; Grattarola, M.; Viviani, R. *Bioelectromagnetics*; **1984**, 5, 173.
91. Harned, H.S.; Owen, B.B. *The Physical Chemistry of Electrolytic Solutions*; Reinhold Publishing Corporation: New York, 1958; Chap. 3.
92. Melnikov, V.K. *Trans. Moscow Math. Soc.*, **1963**, 12, 1.
93. Morosov, A.D. *USSR Comput. Math. Phys.*, **1973**, 13, 45.
94. Morosov, A.D. *J. Differential Equations*, **1976**, 12, 164.
95. McLaughlin, J.B. *Phys. Rev.*, **1979**, A20, 2114.
96. Holmes, P.J. *SIAM J. Appl. Math.*, **1980**, 38, 65.
97. Wiggins, S. *Introduction to Applied Nonlinear Dynamical Systems and Chaos*; Springer–Verlag: New York, 1990.
98. Guckenheimer, J.; Holmes, P. *Nonlinear Oscillations, Dynamical Systems, and Bifurcations of Vector Fields*; Springer–Verlag: New York, 1983; pp. 184–226.
99. Arrowsmith, D.K.; Place, C.M. *An Introduction to Dynamical Systems*; Cambridge University Press: Cambridge, 1990; pp. 170–180.
100. Wiggins, S. *Global Bifurcations and Chaos: Analytical Methods*; Springer–Verlag: New York, 1988; Chap. 4.
101. Lichtenberg, A.J.; Lieberman, M.A. *Regular and Chaotic Dynamics*; Springer–Verlag: New York, 1992; pp. 560–569.

102. Smale, S. *Bull. Amer. Math. Soc.*, **1967**, 73, 747.

Appendix

As the dielectrophoretic (DEP) force is fundamental to the theoretical work of this dissertation, a rigorous derivation from first principles explicitly showing all assumptions and approximations is presented here. Although the DEP force was first derived for a lossless particle and medium, more recently it has been extended to include a particle with dielectric losses.

The DEP force was first derived for lossy particles by Friedrich Sauer in his article: "Interaction–Forces between Microscopic Particles in an External Electromagnetic Field" (49). His derivation is fairly complicated and many of the details are not explicitly shown and therefore this appendix will clearly declare these details.

We begin by defining two fundamental electromagnetic entities: (a) the electromagnetic field energy density:

$$u_e \equiv \frac{1}{2} \left(\vec{E}^T \cdot \vec{D} + \vec{H}^T \cdot \vec{B} \right) \quad (A.1)$$

and (b) the electromagnetic momentum density:

$$\vec{p}_e \equiv \frac{1}{c^2} \left(\vec{E} \times \vec{H} \right) \quad (A.2)$$

where a superscript T indicates the transpose of the vector (and thus a row vector) and \vec{E} , \vec{D} , \vec{H} , and \vec{B} denote, in accordance with the standard electrodynamic convention, the electric field intensity, the electric field displacement, the magnetic field intensity, and the magnetic induction, respectively. The balance equation or general conservation equation for either of these quantities will possess the general form:

$$\frac{\partial A}{\partial t} = - \text{divergence (Flow of A)} + (\text{Production of A}) .$$

And thus for the electromagnetic field energy density, the time derivative of Eq. (A.1) is:

$$\frac{\partial u_e}{\partial t} = \frac{1}{2} \left[\frac{\partial \vec{E}^T}{\partial t} \cdot \vec{D} + \vec{E}^T \cdot \frac{\partial \vec{D}}{\partial t} + \frac{\partial \vec{H}^T}{\partial t} \cdot \vec{B} + \vec{H}^T \cdot \frac{\partial \vec{B}}{\partial t} \right] \quad (A.3)$$

We recall the fundamental classical equations that govern all electromagnetic phenomena, the Maxwell equations:

$$\begin{aligned}\vec{\nabla} \times \vec{H} &= \vec{J} + \frac{\partial \vec{D}}{\partial t} & \vec{\nabla} \times \vec{E} &= -\frac{\partial \vec{B}}{\partial t} \\ \vec{\nabla}^T \cdot \vec{D} &= \rho & \vec{\nabla}^T \cdot \vec{B} &= 0\end{aligned}\quad (\text{A.4})$$

where \vec{J} denotes the current density and ρ denotes the charge density.

Use of the Maxwell equations in Eq. (A.3) gives for the time change of the field energy density:

$$\frac{\partial u_e}{\partial t} = \frac{1}{2} \left(\vec{D}^T \cdot \frac{\partial \vec{E}}{\partial t} + \vec{E}^T \cdot (\vec{\nabla} \times \vec{H}) - \vec{E}^T \cdot \vec{J} + \vec{B}^T \cdot \frac{\partial \vec{H}}{\partial t} - \vec{H}^T \cdot (\vec{\nabla} \times \vec{E}) \right) \quad (\text{A.5})$$

Now in general for any two vectors \vec{a} and \vec{b} :

$$\vec{\nabla}^T \cdot (\vec{a} \times \vec{b}) = \vec{b}^T \cdot (\vec{\nabla} \times \vec{a}) - \vec{a}^T \cdot (\vec{\nabla} \times \vec{b})$$

and therefore application of this vector identity to Eq. (A.5) gives:

$$\frac{\partial u_e}{\partial t} = \frac{1}{2} \left(\vec{D}^T \cdot \frac{\partial \vec{E}}{\partial t} - \vec{\nabla}^T \cdot (\vec{E} \times \vec{H}) + \vec{B}^T \cdot \frac{\partial \vec{H}}{\partial t} - \vec{E}^T \cdot \vec{J} \right) \quad (\text{A.6})$$

Now we have seen from Maxwell's equations that:

$$\begin{aligned}\vec{E}^T \cdot \frac{\partial \vec{D}}{\partial t} + \vec{H}^T \cdot \frac{\partial \vec{B}}{\partial t} &= -\vec{\nabla}^T \cdot (\vec{E} \times \vec{H}) - \vec{E}^T \cdot \vec{J} \\ \text{and } \therefore \frac{1}{2} \left(-\vec{\nabla}^T \cdot (\vec{E} \times \vec{H}) - \vec{E}^T \cdot \vec{J} - \vec{E}^T \cdot \frac{\partial \vec{D}}{\partial t} - \vec{H}^T \cdot \frac{\partial \vec{B}}{\partial t} \right) &= 0\end{aligned}\quad (\text{A.7})$$

Adding the left hand side of Eq. (A.7) to the right hand side of Eq. (A.6) gives:

$$\frac{\partial u_e}{\partial t} = -\vec{\nabla}^T \cdot (\vec{E} \times \vec{H}) + \frac{1}{2} \left(\vec{D}^T \cdot \frac{\partial \vec{E}}{\partial t} - \vec{E}^T \cdot \frac{\partial \vec{D}}{\partial t} + \vec{B}^T \cdot \frac{\partial \vec{H}}{\partial t} - \vec{H}^T \cdot \frac{\partial \vec{B}}{\partial t} \right) - \vec{E}^T \cdot \vec{J} \quad (\text{A.8})$$

It is clear from comparison of the above outlined general statement of a balance equation and Eq. (A.8), that Eq. (A.8) is not in generality a conservation law. The deviation from the continuity equation for the electromagnetic energy density is realized in the dissipated power term:

$$Q_{pw} = \vec{E}^T \cdot \vec{J} - \frac{1}{2} \left(\vec{D}^T \cdot \frac{\partial \vec{E}}{\partial t} - \vec{E}^T \cdot \frac{\partial \vec{D}}{\partial t} + \vec{B}^T \cdot \frac{\partial \vec{H}}{\partial t} - \vec{H}^T \cdot \frac{\partial \vec{B}}{\partial t} \right) \quad (A.9)$$

a term which expresses the dielectric losses in the media. For periodic fields we have:

$$\begin{aligned} \vec{E} &= \vec{E}(\vec{r}, t) = \text{Re} \left\{ \vec{E}_o(\vec{r}) e^{-i\omega t} \right\} \\ \vec{D} &= \vec{D}(\vec{r}, t) = \text{Re} \left\{ \vec{D}_o(\vec{r}) e^{-i\omega t} \right\} \\ \vec{H} &= \vec{H}(\vec{r}, t) = \text{Re} \left\{ \vec{H}_o(\vec{r}) e^{-i\omega t} \right\} \\ \vec{B} &= \vec{B}(\vec{r}, t) = \text{Re} \left\{ \vec{B}_o(\vec{r}) e^{-i\omega t} \right\} \\ \vec{J} &= \vec{J}(\vec{r}, t) = \text{Re} \left\{ \vec{J}_o(\vec{r}) e^{-i\omega t} \right\} \end{aligned} \quad (A.10)$$

and therefore the expression for the dissipated power becomes:

$$Q_{pw} = \text{Re} \vec{E}^T \cdot \text{Re} \vec{J} - \frac{1}{2} \left(\text{Re} \vec{D}^T \cdot \text{Re} \frac{\partial \vec{E}}{\partial t} - \text{Re} \vec{E}^T \cdot \text{Re} \frac{\partial \vec{D}}{\partial t} + \text{Re} \vec{B}^T \cdot \text{Re} \frac{\partial \vec{H}}{\partial t} \right) + \frac{1}{2} \left(\text{Re} \vec{H}^T \cdot \text{Re} \frac{\partial \vec{B}}{\partial t} \right) \quad (A.11)$$

Now the time average of Eq. (A.11) is:

$$\bar{Q}_{pw} = \overline{\text{Re} \vec{E}^T \cdot \text{Re} \vec{J}} - \frac{1}{2} \left(\overline{\text{Re} \vec{D}^T \cdot \text{Re} \frac{\partial \vec{E}}{\partial t}} - \overline{\text{Re} \vec{E}^T \cdot \text{Re} \frac{\partial \vec{D}}{\partial t}} + \overline{\text{Re} \vec{B}^T \cdot \text{Re} \frac{\partial \vec{H}}{\partial t}} \right) + \frac{1}{2} \left(\overline{\text{Re} \vec{H}^T \cdot \text{Re} \frac{\partial \vec{B}}{\partial t}} \right) \quad (A.12)$$

which upon application of the Cycle Average Theorem gives:

$$\begin{aligned} \bar{Q}_{pw} &= \frac{1}{2} \text{Re} \left\{ \vec{E}^T \cdot \vec{J}^* \right\} - \frac{1}{2} \left[\frac{1}{2} \text{Re} \left\{ \vec{D}^T \cdot \frac{\partial \vec{E}^*}{\partial t} \right\} - \frac{1}{2} \text{Re} \left\{ \vec{E}^T \cdot \frac{\partial \vec{D}^*}{\partial t} \right\} \right] - \\ &\quad \frac{1}{2} \left[\frac{1}{2} \text{Re} \left\{ \vec{B}^T \cdot \frac{\partial \vec{H}^*}{\partial t} \right\} - \frac{1}{2} \text{Re} \left\{ \vec{H}^T \cdot \frac{\partial \vec{B}^*}{\partial t} \right\} \right] \end{aligned} \quad (A.13)$$

where the * denotes the complex conjugated quantity. If the following linear relationships are assumed:

$$\begin{aligned}
\vec{D} &= \underline{\varepsilon} \vec{E} \\
\vec{B} &= \underline{\mu} \vec{H} \\
\vec{J} &= \underline{\sigma} \vec{E}
\end{aligned} \tag{A.14}$$

where: $\underline{\varepsilon}$ is the complex electric permittivity, i.e. $\underline{\varepsilon} = \varepsilon' + i\varepsilon''$; $\underline{\mu}$ is the complex magnetic permeability, i.e. $\underline{\mu} = \mu' + i\mu''$; and $\underline{\sigma}$ is the complex conductivity, i.e. $\underline{\sigma} = \sigma' + i\sigma''$; then the time average of the dissipated power over the period of the oscillating fields of frequency ω becomes:

$$\begin{aligned}
\overline{Q}_{pw} &= \frac{1}{2} \operatorname{Re} \left\{ \vec{E}^T \cdot \underline{\sigma}^* \vec{E}^* \right\} - \frac{1}{4} \left(\operatorname{Re} \left\{ \underline{\varepsilon} \vec{E}^T \cdot i\omega \vec{E}^* - \vec{E}^T \cdot i\omega \underline{\varepsilon}^* \vec{E}^* \right\} \right) - \\
&\quad \frac{1}{4} \left(\operatorname{Re} \left\{ \underline{\mu} \vec{H}^T \cdot i\omega \vec{H}^* - \vec{H}^T \cdot i\omega \underline{\mu}^* \vec{H}^* \right\} \right) \\
&= \frac{1}{2} \operatorname{Re} \left\{ \underline{\sigma}^* |\vec{E}_o|^2 \right\} - \frac{1}{4} \left(\operatorname{Re} \left\{ i\omega (\underline{\varepsilon} - \underline{\varepsilon}^*) |\vec{E}_o|^2 \right\} \right) - \frac{1}{4} \left(\operatorname{Re} \left\{ i\omega (\underline{\mu} - \underline{\mu}^*) |\vec{H}_o|^2 \right\} \right) \\
&= \frac{1}{2} \sigma'' |\vec{E}_o|^2 - \frac{1}{4} \left(\operatorname{Re} \left\{ -2\omega \varepsilon'' |\vec{E}_o|^2 \right\} \right) - \frac{1}{4} \left(\operatorname{Re} \left\{ -2\omega \mu'' |\vec{H}_o|^2 \right\} \right) \\
&\quad \text{and } \therefore \overline{Q}_{pw} = \frac{1}{2} (\sigma'' + \omega \varepsilon'') |\vec{E}_o|^2 + \frac{1}{2} \omega \mu'' |\vec{H}_o|^2 \tag{A.15}
\end{aligned}$$

It is clear from Eq. (A.15) that for dissipative particles and media where: $\sigma' \neq 0$, $\varepsilon'' \neq 0$, and $\mu'' \neq 0$, that \overline{Q}_{pw} will not be equal to zero and therefore a force calculation using the law of the conservation of electromagnetic energy density will lead to meaningless results. We therefore turn to the electromagnetic momentum balance equation to derive an expression for the body force. From the definition of the electromagnetic momentum density and the use of Maxwell's equations it can be shown for the local time change of \vec{p}_e :

$$\frac{\partial \vec{p}_e}{\partial t} = \left(\underline{\underline{\Pi}} \cdot \vec{\nabla} \right) - \vec{f}_e; \quad \text{where we define: } \left(\underline{\underline{\Pi}} \cdot \vec{\nabla} \right)_i = \sum_{k=1}^3 \frac{\partial \Pi_{ik}}{\partial x_k} \tag{A.16}$$

and $\underline{\underline{\Pi}}$ is the Maxwell stress tensor and \vec{f}_e the electromagnetic body force. We choose $\underline{\underline{\Pi}}$ to

be a symmetric tensor of the form:

$$\underline{\underline{\Pi}} = \frac{1}{2} \left(\vec{E}\vec{D}^T + \vec{D}\vec{E}^T + \vec{H}\vec{B}^T + \vec{B}\vec{H}^T - \left(\vec{D}^T \cdot \vec{E} + \vec{B}^T \cdot \vec{H} \right) \underline{\underline{U}} \right) \quad (\text{A.17})$$

where the product $\vec{a}\vec{b}^T$ is the dyadic product of the two vector \vec{a} and \vec{b} , i.e.:

$$\vec{a}\vec{b}^T = \begin{pmatrix} a_1 \\ a_2 \\ a_3 \end{pmatrix} (b_1, b_2, b_3) = \begin{bmatrix} a_1b_1 & a_1b_2 & a_1b_3 \\ a_2b_1 & a_2b_2 & a_2b_3 \\ a_3b_1 & a_3b_2 & a_3b_3 \end{bmatrix}$$

and $\underline{\underline{U}}$ the unit tensor whose elements are δ_{ik} . Now from the definition of the *ith* component of the product $(\underline{\underline{\Pi}} \cdot \vec{\nabla})$ in Eq. (A.16) and from our choice of a symmetric Maxwell stress tensor, it is clear after some very straight forward manipulation that:

$$\begin{aligned} (\underline{\underline{\Pi}} \cdot \vec{\nabla}) &= \frac{1}{2} \left[\left(\vec{D}^T \cdot \vec{\nabla} \right) \vec{E} + \vec{E} \left(\vec{\nabla}^T \cdot \vec{D} \right) + \left(\vec{E}^T \cdot \vec{\nabla} \right) \vec{D} + \vec{D} \left(\vec{\nabla}^T \cdot \vec{E} \right) \right] + \\ &\frac{1}{2} \left[\left(\vec{B}^T \cdot \vec{\nabla} \right) \vec{H} + \vec{H} \left(\vec{\nabla}^T \cdot \vec{B} \right) + \left(\vec{H}^T \cdot \vec{\nabla} \right) \vec{B} + \vec{B} \left(\vec{\nabla}^T \cdot \vec{H} \right) - \vec{\nabla} \left(\vec{D}^T \cdot \vec{E} + \vec{B}^T \cdot \vec{H} \right) \right] \end{aligned} \quad (\text{A.18})$$

The last term in Eq. (A.18) may be expanded by use of the following vector identity:

$$\vec{\nabla}(\vec{a}^T \cdot \vec{b}) = \left(\vec{\nabla}^T \cdot \vec{a} \right) \vec{b} + \left(\vec{\nabla}^T \cdot \vec{b} \right) \vec{a} + \vec{a} \times \left(\vec{\nabla} \times \vec{b} \right) + \vec{b} \times \left(\vec{\nabla} \times \vec{a} \right)$$

Thus:

$$\begin{aligned} \vec{\nabla} \left(\vec{D}^T \cdot \vec{E} + \vec{B}^T \cdot \vec{H} \right) &= \left(\vec{\nabla}^T \cdot \vec{D} \right) \vec{E} + \left(\vec{\nabla}^T \cdot \vec{E} \right) \vec{D} + \vec{D} \times \left(\vec{\nabla} \times \vec{E} \right) + \vec{E} \times \left(\vec{\nabla} \times \vec{D} \right) \\ &+ \left(\vec{\nabla}^T \cdot \vec{B} \right) \vec{H} + \left(\vec{\nabla}^T \cdot \vec{H} \right) \vec{B} + \vec{B} \times \left(\vec{\nabla} \times \vec{H} \right) + \vec{H} \times \left(\vec{\nabla} \times \vec{B} \right) \end{aligned} \quad (\text{A.19})$$

Substitution of Eq. (A.19) into Eq. (A.18) gives:

$$\begin{aligned} (\underline{\underline{\Pi}} \cdot \vec{\nabla}) = & \frac{1}{2} \left[\left(\vec{D}^T \cdot \vec{\nabla} \right) \vec{E} + \left(\vec{E}^T \cdot \vec{\nabla} \right) \vec{D} + \left(\vec{B}^T \cdot \vec{\nabla} \right) \vec{H} + \left(\vec{H}^T \cdot \vec{\nabla} \right) \vec{B} \right] - \\ & \frac{1}{2} \left[\vec{D} \times \left(\vec{\nabla} \times \vec{E} \right) + \vec{E} \times \left(\vec{\nabla} \times \vec{D} \right) + \vec{B} \times \left(\vec{\nabla} \times \vec{H} \right) + \vec{H} \times \left(\vec{\nabla} \times \vec{B} \right) \right] \end{aligned} \quad (\text{A.20})$$

From Maxwell's equations we know:

$$\left(\vec{D}^T \cdot \vec{\nabla} \right) \vec{E} = \rho \vec{E} \quad \text{and} \quad \therefore \quad \frac{1}{2} \left(\vec{D}^T \cdot \vec{\nabla} \right) \vec{E} = \rho \vec{E} - \frac{1}{2} \left(\vec{D}^T \cdot \vec{\nabla} \right) \vec{E} \quad (\text{A.21})$$

$$\left(\vec{B}^T \cdot \vec{\nabla} \right) \vec{H} = 0 \quad (\text{A.22})$$

$$\vec{B} \times \left(\vec{\nabla} \times \vec{H} \right) = \vec{B} \times \vec{J} + \vec{B} \times \frac{\partial \vec{D}}{\partial t} = -\vec{J} \times \vec{B} - \frac{\partial \vec{D}}{\partial t} \times \vec{B}$$

$$\vec{D} \times \left(\vec{\nabla} \times \vec{E} \right) = -\vec{D} \times \frac{\partial \vec{B}}{\partial t}$$

$$\text{and} \quad \therefore \quad \vec{B} \times \left(\vec{\nabla} \times \vec{H} \right) + \vec{D} \times \left(\vec{\nabla} \times \vec{E} \right) + \vec{J} \times \vec{B} + \frac{\partial}{\partial t} \left(\vec{D} \times \vec{B} \right) = 0 \quad (\text{A.23})$$

and therefore with application of Eqs. (A.21) – (A.23), Eq. (A.20) becomes:

$$\begin{aligned} (\underline{\underline{\Pi}} \cdot \vec{\nabla}) = & \frac{1}{2} \left[\left(\vec{\nabla}^T \cdot \vec{E} \right) \vec{D} - \left(\vec{\nabla}^T \cdot \vec{D} \right) \vec{E} + \vec{D} \times \left(\vec{\nabla} \times \vec{E} \right) - \vec{E} \times \left(\vec{\nabla} \times \vec{D} \right) \right] + \rho \vec{E} + \\ & \frac{1}{2} \left[\left(\vec{\nabla}^T \cdot \vec{H} \right) \vec{B} + \vec{B} \times \left(\vec{\nabla} \times \vec{H} \right) - \vec{H} \times \left(\vec{\nabla} \times \vec{B} \right) \right] + \vec{J} \times \vec{B} + \frac{\partial}{\partial t} \left(\vec{D} \times \vec{B} \right) \end{aligned} \quad (\text{A.24})$$

From the continuity equation in the electromagnetic momentum density, Eq. (A.16), the definition of the electromagnetic momentum density, Eq. (A.2), and the derived result of Eq.

(A.24), we have for the body force:

$$\begin{aligned} \vec{f}_e = & \frac{1}{2} \left[\left(\vec{\nabla}^T \cdot \vec{E} \right) \vec{D} - \left(\vec{\nabla}^T \cdot \vec{D} \right) \vec{E} + \vec{D} \times \left(\vec{\nabla} \times \vec{E} \right) - \vec{E} \times \left(\vec{\nabla} \times \vec{D} \right) \right] + \\ & \frac{1}{2} \left[\left(\vec{\nabla}^T \cdot \vec{H} \right) \vec{B} + \vec{B} \times \left(\vec{\nabla} \times \vec{H} \right) - \vec{H} \times \left(\vec{\nabla} \times \vec{B} \right) \right] + \frac{\partial}{\partial t} \left(\vec{D} \times \vec{B} - \frac{1}{c^2} \vec{E} \times \vec{H} \right) \\ & + \rho \vec{E} + \vec{J} \times \vec{B} \end{aligned} \quad (\text{A.25})$$

If we assume the media to possess no free charge or current, then:

$$\rho = 0 \quad \text{and} \quad \vec{J} = 0 \quad (\text{A.26})$$

and thus our expression for the body force in Eq. (A.25) becomes:

$$\begin{aligned} \vec{f}_e = & \frac{1}{2} \left[\left(\vec{\nabla}^T \cdot \vec{E} \right) \vec{D} + \vec{D} \times \left(\vec{\nabla} \times \vec{E} \right) - \vec{E} \times \left(\vec{\nabla} \times \vec{D} \right) \right] + \\ & \frac{1}{2} \left[\left(\vec{\nabla}^T \cdot \vec{H} \right) \vec{B} + \vec{B} \times \left(\vec{\nabla} \times \vec{H} \right) - \vec{H} \times \left(\vec{\nabla} \times \vec{B} \right) \right] + \frac{\partial}{\partial t} \left(\vec{D} \times \vec{B} - \frac{1}{c^2} \vec{E} \times \vec{H} \right) \end{aligned} \quad (\text{A.27})$$

Now we wish to derive an expression for the time average of the body force under the conditions of Eq. (A.26) and the fact that the fields are periodic, i.e. the equalities of Eq. (A.10) hold. This derivation will most easily be seen if each term of Eq. (A.27) is considered separately:

$$\begin{aligned} \text{1st Term : } \left(\vec{\nabla}^T \cdot \vec{E} \right) \vec{D} & \quad \left(\vec{\nabla}^T \cdot \vec{E} \right) \vec{D} = \vec{D} \left(\vec{\nabla}^T \cdot \vec{E} \right) = \text{Re} \{ \vec{D} \} \text{Re} \left\{ \vec{\nabla}^T \cdot \vec{E} \right\} \\ \overline{\text{Re} \{ \vec{D} \} \text{Re} \left\{ \vec{\nabla}^T \cdot \vec{E} \right\}} & = \frac{1}{2} \text{Re} \left\{ \vec{D} \left(\vec{\nabla}^T \cdot \vec{E} \right)^* \right\} = \frac{1}{2} \text{Re} \left\{ \underline{\epsilon} \vec{E} \left(\vec{\nabla}^T \cdot \vec{E} \right)^* \right\} \end{aligned}$$

$$\begin{aligned} \text{From Maxwell's equations under the conditions of Eq. (26): } \quad \vec{\nabla}^T \cdot \vec{D} & = 0 \\ \Rightarrow \vec{\nabla}^T \cdot \vec{D} = \vec{\nabla}^T \cdot \underline{\epsilon} \vec{E} = \vec{E}^T \cdot \vec{\nabla} \underline{\epsilon} + \underline{\epsilon} \vec{\nabla}^T \cdot \vec{E} & = 0 \\ \therefore \vec{\nabla}^T \cdot \vec{E} & = -\frac{1}{\underline{\epsilon}} \left(\vec{E}^T \cdot \vec{\nabla} \underline{\epsilon} \right) \end{aligned}$$

$$\therefore \overline{\text{Re} \{ \vec{D} \} \text{Re} \left\{ \vec{\nabla}^T \cdot \vec{E} \right\}} = -\frac{1}{2} \text{Re} \left\{ \frac{\underline{\epsilon}}{\underline{\epsilon}^*} \vec{E} \vec{E}^T \cdot \vec{\nabla} \underline{\epsilon}^* \right\} \quad (\text{A.28})$$

$$\begin{aligned} \text{2nd Term : } \vec{D} \times \left(\vec{\nabla} \times \vec{E} \right) & \quad \vec{D} \times \left(\vec{\nabla} \times \vec{E} \right) = \text{Re} \{ \vec{D} \} \times \text{Re} \left\{ \vec{\nabla} \times \vec{E} \right\} \\ \overline{\text{Re} \{ \vec{D} \} \times \text{Re} \left\{ \vec{\nabla} \times \vec{E} \right\}} & = \frac{1}{2} \text{Re} \left\{ \vec{D} \times \left(\vec{\nabla} \times \vec{E} \right)^* \right\} \\ & = \frac{1}{2} \text{Re} \left\{ \vec{D} \times \left(-\frac{\partial \vec{B}}{\partial t} \right)^* \right\} = \frac{1}{2} \text{Re} \left\{ \vec{D} \times \left(i\omega \vec{B} \right)^* \right\} \\ & = \frac{1}{2} \text{Re} \left\{ -i\omega \underline{\epsilon} \vec{E} \times \underline{\mu}^* \vec{H}^* \right\} \\ & = -\frac{1}{2} \text{Re} \left\{ i\omega \underline{\epsilon} \underline{\mu}^* \vec{E} \times \vec{H}^* \right\} \end{aligned} \quad (\text{A.29})$$

$$\begin{aligned}
3^{\text{rd}} \text{ Term : } & -\vec{E} \times (\vec{\nabla} \times \vec{D}) \quad (\vec{\nabla} \times \vec{D}) \times \vec{E} = \text{Re}\{\vec{\nabla} \times \vec{D}\} \times \text{Re}\{\vec{E}\} \\
\overline{\text{Re}\{\vec{\nabla} \times \vec{D}\} \times \text{Re}\{\vec{E}\}} &= \frac{1}{2} \text{Re}\left\{(\vec{\nabla} \times \vec{D}) \times \vec{E}^*\right\} = \frac{1}{2} \text{Re}\left\{(\vec{\nabla} \times \underline{\epsilon}\vec{E}) \times \vec{E}^*\right\} \\
&= \frac{1}{2} \text{Re}\left\{(\vec{\nabla}\underline{\epsilon} \times \vec{E} + \underline{\epsilon}\vec{\nabla} \times \vec{E}) \times \vec{E}^*\right\} \\
&= \frac{1}{2} \text{Re}\left\{(\vec{\nabla}\underline{\epsilon} \times \vec{E}) \times \vec{E}^* + \underline{\epsilon}\left(-\frac{\partial\vec{B}}{\partial t}\right) \times \vec{E}^*\right\} \\
&= \frac{1}{2} \text{Re}\left\{-\vec{E}^* \times (\vec{\nabla}\underline{\epsilon} \times \vec{E}) + i\omega\underline{\epsilon}\vec{B} \times \vec{E}^*\right\} \\
&= \frac{1}{2} \text{Re}\left\{\left(\vec{E}^{\text{T}*} \cdot \vec{\nabla}\underline{\epsilon}\right)\vec{E} - \left(\vec{E}^{\text{T}*} \cdot \vec{E}\right)\vec{\nabla}\underline{\epsilon} + i\omega\underline{\epsilon}\underline{\mu}\vec{H} \times \vec{E}^*\right\} \\
&= \frac{1}{2} \text{Re}\left\{\vec{E}\vec{E}^{\text{T}*} \cdot \vec{\nabla}\underline{\epsilon} - |\vec{E}|^2\vec{\nabla}\underline{\epsilon} - i\omega\underline{\epsilon}\underline{\mu}\vec{E}^* \times \vec{H}\right\} \quad (\text{A.30})
\end{aligned}$$

$$\begin{aligned}
4^{\text{th}} \text{ Term : } & \left(\vec{\nabla}^{\text{T}} \cdot \vec{H}\right)\vec{B} \quad \left(\vec{\nabla}^{\text{T}} \cdot \vec{H}\right)\vec{B} = \vec{B}\left(\vec{\nabla}^{\text{T}} \cdot \vec{H}\right) = \text{Re}\{\vec{B}\} \text{Re}\left\{\vec{\nabla}^{\text{T}} \cdot \vec{H}\right\} \\
\overline{\text{Re}\{\vec{B}\} \text{Re}\left\{\vec{\nabla}^{\text{T}} \cdot \vec{H}\right\}} &= \frac{1}{2} \text{Re}\left\{\vec{B}\left(\vec{\nabla}^{\text{T}} \cdot \vec{H}\right)^*\right\} = \frac{1}{2} \text{Re}\left\{\underline{\mu}\vec{H}\left(\vec{\nabla}^{\text{T}} \cdot \vec{H}\right)^*\right\} \\
\text{From Maxwell's equations : } & \vec{\nabla}^{\text{T}} \cdot \vec{B} = 0 \\
\Rightarrow \vec{\nabla}^{\text{T}} \cdot \vec{B} = \vec{\nabla}^{\text{T}} \cdot \underline{\mu}\vec{H} = \vec{H}^{\text{T}} \cdot \vec{\nabla}\underline{\mu} + \underline{\mu}\vec{\nabla}^{\text{T}} \cdot \vec{H} = 0 \\
\therefore \vec{\nabla}^{\text{T}} \cdot \vec{H} &= -\frac{1}{\underline{\mu}}\left(\vec{H}^{\text{T}} \cdot \vec{\nabla}\underline{\mu}\right) \\
\therefore \overline{\text{Re}\{\vec{B}\} \text{Re}\left\{\vec{\nabla}^{\text{T}} \cdot \vec{H}\right\}} &= -\frac{1}{2} \text{Re}\left\{\frac{\underline{\mu}}{\underline{\mu}^*}\vec{H}\vec{H}^{\text{T}*} \cdot \vec{\nabla}\underline{\mu}^*\right\} \quad (\text{A.31})
\end{aligned}$$

$$\begin{aligned}
5^{\text{th}} \text{ Term : } \vec{B} \times (\vec{\nabla} \times \vec{H}) \quad \vec{B} \times (\vec{\nabla} \times \vec{H}) &= \text{Re}\{\vec{B}\} \times \text{Re}\{\vec{\nabla} \times \vec{H}\} \\
\overline{\text{Re}\{\vec{B}\} \times \text{Re}\{\vec{\nabla} \times \vec{H}\}} &= \frac{1}{2} \text{Re}\left\{ \vec{B} \times (\vec{\nabla} \times \vec{H})^* \right\} \\
&= \frac{1}{2} \text{Re}\left\{ \vec{B} \times \left(\frac{\partial \vec{D}}{\partial t} \right)^* \right\} = \frac{1}{2} \text{Re}\left\{ \vec{B} \times (-i\omega \vec{D})^* \right\} \\
&= \frac{1}{2} \text{Re}\left\{ i\omega \underline{\mu} \vec{H} \times \underline{\epsilon}^* \vec{E}^* \right\} \\
&= \frac{1}{2} \text{Re}\left\{ i\omega \underline{\mu} \underline{\epsilon}^* \vec{H} \times \vec{E}^* \right\} \tag{A.32}
\end{aligned}$$

$$\begin{aligned}
6^{\text{th}} \text{ Term : } -\vec{H} \times (\vec{\nabla} \times \vec{B}) \quad (\vec{\nabla} \times \vec{B}) \times \vec{H} &= \text{Re}\{\vec{\nabla} \times \vec{B}\} \times \text{Re}\{\vec{H}\} \\
\overline{\text{Re}\{\vec{\nabla} \times \vec{B}\} \times \text{Re}\{\vec{H}\}} &= \frac{1}{2} \text{Re}\left\{ (\vec{\nabla} \times \vec{B}) \times \vec{H}^* \right\} = \frac{1}{2} \text{Re}\left\{ (\vec{\nabla} \times \underline{\mu} \vec{H}) \times \vec{H}^* \right\} \\
&= \frac{1}{2} \text{Re}\left\{ (\vec{\nabla} \underline{\mu} \times \vec{H} + \underline{\mu} \vec{\nabla} \times \vec{H}) \times \vec{H}^* \right\} \\
&= \frac{1}{2} \text{Re}\left\{ (\vec{\nabla} \underline{\mu} \times \vec{H}) \times \vec{H}^* + \underline{\mu} \left(\frac{\partial \vec{D}}{\partial t} \right) \times \vec{H}^* \right\} \\
&= \frac{1}{2} \text{Re}\left\{ -\vec{H}^* \times (\vec{\nabla} \underline{\mu} \times \vec{H}) - i\omega \underline{\mu} \vec{D} \times \vec{H}^* \right\} \\
&= \frac{1}{2} \text{Re}\left\{ \left(\vec{H}^{\text{T}*} \cdot \vec{\nabla} \underline{\mu} \right) \vec{H} - \left(\vec{H}^{\text{T}*} \cdot \vec{H} \right) \vec{\nabla} \underline{\mu} + i\omega \underline{\mu} \vec{E} \times \vec{H}^* \right\} \\
&= \frac{1}{2} \text{Re}\left\{ \vec{H} \vec{H}^{\text{T}*} \cdot \vec{\nabla} \underline{\mu} - |\vec{H}|^2 \vec{\nabla} \underline{\mu} - i\omega \underline{\mu} \underline{\epsilon} \vec{E} \times \vec{H}^* \right\} \tag{A.33}
\end{aligned}$$

$$\text{Last term : } \frac{\partial}{\partial t} \left(\vec{D} \times \vec{B} - \frac{1}{c^2} \vec{E} \times \vec{H} \right)$$

$$\begin{aligned}
\frac{\partial}{\partial t} \left(\vec{D} \times \vec{B} - \frac{1}{c^2} \vec{E} \times \vec{H} \right) &\cong \frac{\partial \vec{D}}{\partial t} \times \vec{B} + \vec{D} \times \frac{\partial \vec{B}}{\partial t} = (\vec{\nabla} \times \vec{H}) \times \vec{B} - \vec{D} \times (\vec{\nabla} \times \vec{E}) \\
&= -\text{Re}\{\vec{B}\} \times \text{Re}\{\vec{\nabla} \times \vec{H}\} - \text{Re}\{\vec{D}\} \times \text{Re}\{\vec{\nabla} \times \vec{E}\}
\end{aligned}$$

$$\begin{aligned}
\overline{\frac{\partial}{\partial t} \left(\vec{D} \times \vec{B} - \frac{1}{c^2} \vec{E} \times \vec{H} \right)} &= -\frac{1}{2} \operatorname{Re} \left\{ \vec{B} \times \left(\vec{\nabla} \times \vec{H} \right)^* + \vec{D} \times \left(\vec{\nabla} \times \vec{E} \right)^* \right\} \\
&= -\frac{1}{2} \operatorname{Re} \left\{ \underline{\mu} \vec{H} \times \left(\frac{\partial \vec{D}}{\partial t} \right)^* + \underline{\varepsilon} \vec{E} \times \left(-\frac{\partial \vec{B}}{\partial t} \right)^* \right\} \\
&= -\frac{1}{2} \operatorname{Re} \left\{ \underline{\mu} \vec{H} \times \left(-i\omega \vec{D} \right)^* + \underline{\varepsilon} \vec{E} \times \left(i\omega \vec{B} \right)^* \right\} \\
&= -\frac{1}{2} \operatorname{Re} \left\{ i\omega \underline{\mu} \underline{\varepsilon}^* \vec{H} \times \vec{E}^* - i\omega \underline{\varepsilon} \underline{\mu}^* \vec{E} \times \vec{H}^* \right\} \tag{A.34}
\end{aligned}$$

Collecting Eqs. (A.28) – (A.34) together, we obtain for the time average of the body force as derived in Eq. (A.27):

$$\begin{aligned}
\overline{\vec{f}_e} &= -\frac{1}{4} \operatorname{Re} \left\{ |\vec{E}|^2 \vec{\nabla} \underline{\varepsilon} + |\vec{H}|^2 \vec{\nabla} \underline{\mu} + \frac{\underline{\varepsilon}}{\underline{\varepsilon}^*} \vec{E} \vec{E}^{\top*} \cdot \vec{\nabla} \underline{\varepsilon}^* - \vec{E} \vec{E}^{\top*} \cdot \vec{\nabla} \underline{\varepsilon} + \frac{\underline{\mu}}{\underline{\mu}^*} \vec{H} \vec{H}^{\top*} \cdot \vec{\nabla} \underline{\mu}^* \right\} - \\
&\quad \frac{1}{4} \operatorname{Re} \left\{ -\vec{H} \vec{H}^{\top*} \cdot \vec{\nabla} \underline{\mu} + i\omega \left(\vec{E}^* \times \vec{H} + \vec{E} \times \vec{H}^* \right) \underline{\varepsilon} \underline{\mu} \right\} \tag{A.35}
\end{aligned}$$

Eq. (A.35) may be expressed in slightly more compact form upon realizing the following:

$$\begin{aligned}
\vec{\nabla} \left(\frac{\underline{\varepsilon}}{\underline{\varepsilon}^*} \right) &= \frac{1}{\underline{\varepsilon}^*} \vec{\nabla} \underline{\varepsilon} - \frac{\underline{\varepsilon}}{\underline{\varepsilon}^{*2}} \vec{\nabla} \underline{\varepsilon}^* \\
\Rightarrow \underline{\varepsilon}^* \vec{\nabla} \left(\frac{\underline{\varepsilon}}{\underline{\varepsilon}^*} \right) &= \vec{\nabla} \underline{\varepsilon} - \frac{\underline{\varepsilon}}{\underline{\varepsilon}^*} \vec{\nabla} \underline{\varepsilon}^* \\
\therefore \frac{\underline{\varepsilon}}{\underline{\varepsilon}^*} \vec{E} \vec{E}^{\top*} \cdot \vec{\nabla} \underline{\varepsilon}^* - \vec{E} \vec{E}^{\top*} \cdot \vec{\nabla} \underline{\varepsilon} &= -\underline{\varepsilon}^* \vec{E} \vec{E}^{\top*} \vec{\nabla} \left(\frac{\underline{\varepsilon}}{\underline{\varepsilon}^*} \right) \\
\text{and similarly : } \frac{\underline{\mu}}{\underline{\mu}^*} \vec{H} \vec{H}^{\top*} \cdot \vec{\nabla} \underline{\mu}^* - \vec{H} \vec{H}^{\top*} \cdot \vec{\nabla} \underline{\mu} &= -\underline{\mu}^* \vec{H} \vec{H}^{\top*} \vec{\nabla} \left(\frac{\underline{\mu}}{\underline{\mu}^*} \right)
\end{aligned}$$

And thus the time average of the body force may be written:

$$\begin{aligned}
\overline{\vec{f}_e} &= -\frac{1}{4} \operatorname{Re} \left\{ |\vec{E}|^2 \vec{\nabla} \underline{\varepsilon} + |\vec{H}|^2 \vec{\nabla} \underline{\mu} - \underline{\varepsilon}^* \vec{E} \vec{E}^{\top*} \cdot \vec{\nabla} \left(\frac{\underline{\varepsilon}}{\underline{\varepsilon}^*} \right) - \underline{\mu}^* \vec{H} \vec{H}^{\top*} \cdot \vec{\nabla} \left(\frac{\underline{\mu}}{\underline{\mu}^*} \right) \right\} - \\
&\quad \frac{1}{4} \operatorname{Re} \left\{ i\omega \left(\vec{E}^* \times \vec{H} + \vec{E} \times \vec{H}^* \right) \underline{\varepsilon} \underline{\mu} \right\} \tag{A.36}
\end{aligned}$$

Now in the time average, the continuity equation for the electromagnetic momentum density becomes:

$$\overline{\vec{f}_e} = \overline{(\underline{\underline{\Pi}} \cdot \vec{\nabla})} \quad (\text{A.37})$$

With the choice of a symmetric Maxwell stress tensor according to Eq. (A.17), and with periodic electric and magnetic fields, the time average of the Maxwell stress tensor is:

$$\begin{aligned} \underline{\underline{\Pi}} &= \frac{1}{2} \cdot \frac{1}{2} \text{Re} \left\{ \vec{E} \vec{D}^{\text{T}*} + \vec{D} \vec{E}^{\text{T}*} + \vec{H} \vec{B}^{\text{T}*} + \vec{B} \vec{H}^{\text{T}*} - \left(\vec{D}^{\text{T}} \cdot \vec{E}^* + \vec{B}^{\text{T}} \cdot \vec{H}^* \right) \underline{\underline{\mathbf{U}}} \right\} \\ &= \frac{1}{4} \text{Re} \left\{ \underline{\underline{\epsilon}}^* \vec{E} \vec{E}^{\text{T}*} + \underline{\underline{\epsilon}} \vec{E} \vec{E}^{\text{T}*} + \underline{\underline{\mu}}^* \vec{H} \vec{H}^{\text{T}*} + \underline{\underline{\mu}} \vec{H} \vec{H}^{\text{T}*} - \left(\underline{\underline{\epsilon}} |\vec{E}|^2 + \underline{\underline{\mu}} |\vec{H}|^2 \right) \underline{\underline{\mathbf{U}}} \right\} \\ &= \frac{1}{4} \text{Re} \left\{ \left(\underline{\underline{\epsilon}}^* + \underline{\underline{\epsilon}} \right) \vec{E} \vec{E}^{\text{T}*} + \left(\underline{\underline{\mu}}^* + \underline{\underline{\mu}} \right) \vec{H} \vec{H}^{\text{T}*} - \left(\underline{\underline{\epsilon}} |\vec{E}|^2 + \underline{\underline{\mu}} |\vec{H}|^2 \right) \underline{\underline{\mathbf{U}}} \right\} \\ &= \frac{1}{4} \text{Re} \left\{ 2 \text{Re} \{ \underline{\underline{\epsilon}} \} \vec{E} \vec{E}^{\text{T}*} + 2 \text{Re} \{ \underline{\underline{\mu}} \} \vec{H} \vec{H}^{\text{T}*} - \left(\underline{\underline{\epsilon}} |\vec{E}|^2 + \underline{\underline{\mu}} |\vec{H}|^2 \right) \underline{\underline{\mathbf{U}}} \right\} \\ &= \frac{1}{4} \left[\text{Re} \{ \underline{\underline{\epsilon}} \} \text{Re} \left\{ \vec{E} \vec{E}^{\text{T}*} + \vec{E} \vec{E}^{\text{T}*} \right\} - \text{Re} \{ \underline{\underline{\epsilon}} \} |\vec{E}|^2 \underline{\underline{\mathbf{U}}} \right] + \\ &\quad \frac{1}{4} \left[\text{Re} \{ \underline{\underline{\mu}} \} \text{Re} \left\{ \vec{H} \vec{H}^{\text{T}*} + \vec{H} \vec{H}^{\text{T}*} \right\} - \text{Re} \{ \underline{\underline{\mu}} \} |\vec{H}|^2 \underline{\underline{\mathbf{U}}} \right] \\ &= \frac{1}{4} \text{Re} \{ \underline{\underline{\epsilon}} \} \left(\vec{E}^* \vec{E}^{\text{T}} + \vec{E} \vec{E}^{\text{T}*} - |\vec{E}|^2 \underline{\underline{\mathbf{U}}} \right) + \frac{1}{4} \text{Re} \{ \underline{\underline{\mu}} \} \left(\vec{H}^* \vec{H}^{\text{T}} + \vec{H} \vec{H}^{\text{T}*} - |\vec{H}|^2 \underline{\underline{\mathbf{U}}} \right) \quad (\text{A.38}) \end{aligned}$$

The conservation law for the total momentum density (both mechanical and electromagnetic) when no external forces are present is:

$$\frac{\partial}{\partial t} (\tau \vec{v} + \vec{p}_e) = \left(-\tau \vec{v} \vec{v}^{\text{T}} + \underline{\underline{\Pi}} - \underline{\underline{\mathbf{P}}} \right) \cdot \vec{\nabla} \quad (\text{A.39})$$

where $\underline{\underline{\mathbf{P}}}$ is the pressure tensor, \vec{v} the velocity, and τ the mass density. Substitution of Eq. (A.16) into Eq. (A.39) gives the material momentum density balance equation:

$$\frac{\partial}{\partial t} (\tau \vec{v}) = - \left(\tau \vec{v} \vec{v}^{\text{T}} + \underline{\underline{\mathbf{P}}} \right) \cdot \vec{\nabla} + \vec{f}_e \quad (\text{A.40})$$

In the time average, if no external forces are present, the material momentum density balance

equation becomes:

$$\overline{(\underline{\underline{P}} \cdot \vec{\nabla})} = \overline{\vec{f}_e} \quad (\text{A.41})$$

With an external force present that keeps the body at rest, Eq. (A.41) becomes:

$$\underline{\underline{P}} \cdot \vec{\nabla} - \overline{\vec{f}_e} = \vec{f}_{ex} \quad (\text{A.42})$$

where \vec{f}_{ex} is actually the external force density. Substitution of Eq. (A.37) into Eq. (A.42) gives:

$$(\underline{\underline{P}} - \underline{\underline{\Pi}}) \cdot \vec{\nabla} = \vec{f}_{ex} \quad (\text{A.43})$$

As the external force \vec{f}_{ex} is actually a force density, the external force is actually:

$$\int \vec{f}_{ex} dV_s = \int (\underline{\underline{P}}_s - \underline{\underline{\Pi}}_s) \cdot \vec{\nabla} dV_s \quad (\text{A.44})$$

where V_s is the volume of the solid body to which the external force acts and which is subject to an electromagnetic field. With both the Maxwell and the pressure tensors be selected so as to be symmetric we have:

$$\left((\underline{\underline{P}}_s - \underline{\underline{\Pi}}_s) \cdot \vec{\nabla} \right)^T = (\underline{\underline{P}}_s - \underline{\underline{\Pi}}_s) \cdot \vec{\nabla} = \vec{\nabla}^T \cdot (\underline{\underline{P}}_s - \underline{\underline{\Pi}}_s)$$

and from the divergence theorem of Gauss we know:

$$\int_V \vec{\nabla}^T \cdot \vec{A} dV = \int_a \vec{A} \cdot \vec{n} da$$

where \vec{n} is the unit normal vector to the surface and da an infinitesimal surface element; and thus the right hand side of Eq. (A.44) may be converted to give:

$$\int \vec{f}_{ex} dV_s = \int (\underline{\underline{P}}_s - \underline{\underline{\Pi}}_s) \cdot \vec{n}_s da_s \quad (\text{A.45})$$

At a surface of discontinuity, i.e. between a solid body (s) immersed in a liquid (l), there is a surface force density: \vec{t}_{sl} . For a surface that is stationary, the surface force density must be compensated by an external force density, and therefore: $\vec{t}_{ex} = -\vec{t}_{sl}$. From limit consid-

erations of Eqs. (A.37) and (A.41) applied on a small volume including the surface of discontinuity one obtains:

$$\vec{t}_{sl} = \left[(\underline{\underline{\Pi}}_l - \underline{\underline{P}}_l) - (\underline{\underline{\Pi}}_s - \underline{\underline{P}}_s) \right] \cdot \vec{n}_s \quad (\text{A.46})$$

Therefore, the total external force which maintains the body stationary in the time average is:

$$\vec{F}_{ex} = \int \vec{t}_{ex} da_s + \int \vec{f}_{ex} dV_s \quad (\text{A.47})$$

and with substitution of Eqs. (A.45) and (A.46) gives:

$$\begin{aligned} \vec{F}_{ex} &= - \int \left[(\underline{\underline{\Pi}}_l - \underline{\underline{P}}_l) - (\underline{\underline{\Pi}}_s - \underline{\underline{P}}_s) \right] \cdot \vec{n}_s da_s + \int (\underline{\underline{P}}_s - \underline{\underline{\Pi}}_s) \cdot \vec{n}_s da_s \\ &= \int (\underline{\underline{P}}_l - \underline{\underline{\Pi}}_l) \cdot \vec{n}_s da_s \end{aligned} \quad (\text{A.48})$$

Thus with Eq. (A.48) one is able to calculate the force acting on the center of mass of a solid body immersed in a liquid if both the Maxwell and pressure tensors are known for the liquid at the surface of the body. As the general problem involved in calculating the force in Eq. (A.48) is too complicated, several approximations have to be made in order to solve the problem analytically. We begin by assuming that the radius R of the particle is small compared to the distance separating the electrodes and that this distance is small compared to the wavelength of the external field in a vacuum. Under these assumptions the terms involving the magnetic field strength \vec{H} in the Maxwell stress tensor (A.17) can be neglected as they are small and thus the time average of the body force (Eq. (A.36)) becomes on the right hand side of Eq. (A.42):

$$\overline{(\underline{\underline{P}} \cdot \vec{\nabla})} = -\frac{1}{4} \text{Re} \left\{ |\vec{E}|^2 \vec{\nabla} \underline{\underline{\epsilon}} - \underline{\underline{\epsilon}}^* \vec{E} \vec{E}^T \cdot \vec{\nabla} \left(\frac{\underline{\underline{\epsilon}}}{\underline{\underline{\epsilon}}^*} \right) \right\} \quad (\text{A.49})$$

If the electric field strength is not too high then the dielectric losses in the media resulting

through the terms: $\vec{\nabla}_{\underline{\varepsilon}}$ and $\vec{\nabla}\left(\frac{\underline{\varepsilon}}{\underline{\varepsilon}^*}\right)$ may be neglected, resulting in a constant pressure tensor.

Now with these assumptions, Eq. (A.48) becomes:

$$\begin{aligned}\vec{F}_{ex} &= - \int (\underline{\underline{\Pi}}_l) \cdot \vec{n}_s da_s \\ &= - \frac{1}{4} \text{Re}\{\underline{\varepsilon}_l\} \iint \left(\vec{E}_l^* \vec{E}_l^T + \vec{E}_l \vec{E}_l^{T*} - |\vec{E}_l|^2 \underline{\underline{U}} \right) \cdot \vec{n}_s da_s\end{aligned}\quad (\text{A.50})$$

where in the last equality use has been made of Eq. (A.38). There are two boundary conditions pertinent to the problem as follows:

$$(1) \quad \vec{D}_l^T \cdot \vec{n}_s = \vec{D}_s^T \cdot \vec{n}_s \quad \Rightarrow \quad \underline{\varepsilon}_l \vec{E}_l^T \cdot \vec{n}_s = \underline{\varepsilon}_s \vec{E}_s^T \cdot \vec{n}_s \quad (\text{A.51})$$

$$(2) \quad \vec{E}_l^T \times \vec{n}_s = \vec{E}_s^T \times \vec{n}_s \quad (\text{A.52})$$

We wish to transform the integrand of Eq. (A.50) into electric field dependent terms inside the spherical body; and this may be accomplished through the boundary conditions of Eqs. (A.51) and (A.52). From Eq. (A.51) we have:

$$\vec{E}_l^T \cdot \vec{n}_s = \frac{\underline{\varepsilon}_s}{\underline{\varepsilon}_l} \vec{E}_s^T \cdot \vec{n}_s$$

and defining: $b \equiv \frac{\underline{\varepsilon}_s - \underline{\varepsilon}_l}{\underline{\varepsilon}_l}$; we have:

$$\vec{E}_l^T \cdot \vec{n}_s = (b + 1) \vec{E}_s^T \cdot \vec{n}_s \quad (\text{A.53})$$

And from the second boundary condition, i.e. Eq. (A.52):

$$\begin{aligned}\vec{n}_s \times \left(\vec{E}_l^T \times \vec{n}_s \right) &= \vec{n}_s \times \left(\vec{E}_s^T \times \vec{n}_s \right) \\ \left(\vec{n}_s^T \cdot \vec{n}_s \right) \vec{E}_l - \left(\vec{E}_l^T \cdot \vec{n}_s \right) \vec{n}_s &= \left(\vec{n}_s^T \cdot \vec{n}_s \right) \vec{E}_s - \left(\vec{E}_s^T \cdot \vec{n}_s \right) \vec{n}_s \\ \text{and thus from Eq.(53): } \vec{E}_l - (b + 1) \left(\vec{E}_s^T \cdot \vec{n}_s \right) \vec{n}_s &= \vec{E}_s - \left(\vec{E}_s^T \cdot \vec{n}_s \right) \vec{n}_s \\ \therefore \vec{E}_l &= \vec{E}_s + b \left(\vec{E}_s^T \cdot \vec{n}_s \right) \vec{n}_s\end{aligned}\quad (\text{A.54})$$

Substitution of Eqs. (A.53) and (A.54) along with there complex conjugated analogues into

Eq. (A.50) gives after some straight forward substitution:

$$\begin{aligned} \vec{F}_{ex} = & -\frac{1}{4}\text{Re}\{\underline{\epsilon}_l\} \iint \left[(b+1) \left(\vec{E}_s^T \cdot \vec{n}_s \right) \vec{E}_s^* + (b^*+1) \left(\vec{E}_s^{T*} \cdot \vec{n}_s \right) \vec{E}_s - |\vec{E}_s|^2 \vec{n}_s \right] da_s \\ & - \frac{1}{4}\text{Re}\{\underline{\epsilon}_l\} \int |b|^2 |\vec{E}_s^T \cdot \vec{n}_s|^2 \vec{n}_s da_s \quad (A.55) \end{aligned}$$

Before preceding to evaluate this integral a couple of points should be noted. Firstly, the integrand in Eq. (A.55) is real as expected, as the total external force must be real. It should also be realized that Eq. (A.55) is different than the derived analogue of Sauer's (Eq. (3.3)). Sauer's expression is complex and therefore must be incorrect as the external force can not be complex. Now in order to evaluate the integral of Eq. (A.55) some approximations must be implemented. If one assumes that the body is rigid and subjected to only a slightly inhomogeneous field then use may be made of the gradient approximation in expanding the electric field at the surface by means of a Taylor expansion around the center of the sphere up to first order terms, i.e.:

$$\vec{E}_s(R\vec{n}_s) = \vec{E}(0) + R(\vec{E}\vec{\nabla}^T)_0 \cdot \vec{n}_s \quad (A.56)$$

where the 0 indicates that the quantity is evaluated at the center of the sphere, i.e. where $R=0$; and where it is understood that all electric field quantities refer to the solid body (as opposed to the liquid in which the body is immersed) and hence the subscript s has been dropped. Evaluation of Eq. (A.55) involves four integrals and thus with the approximation made in Eq. (A.56), each integral will be considered separately:

$$\begin{aligned} \text{First integral : } \int (b+1) \left(\vec{E}_s^T \cdot \vec{n}_s \right) \vec{E}_s^* da_s &= (b+1) \int \left(\vec{E}_s^T \cdot \vec{n}_s \right) \vec{E}_s^* da_s \\ &= (b+1)V \left[(\vec{\nabla}\vec{E}^T)_0 \cdot \vec{E}^*(0) + (\vec{\nabla}^T \cdot \vec{E}^*)_0 \vec{E}(0) \right] \\ &= (b+1)V (\vec{\nabla}\vec{E}^T)_0 \cdot \vec{E}^*(0) \quad (A.57) \end{aligned}$$

where the last line of Eq. (A.57) is the result of the application of Maxwell's equations under conditions of no free charge and a homogeneous body ($\vec{\nabla}\underline{\epsilon} = 0$); and where V is the volume

of the sphere ($V = \frac{4}{3}\pi R^3$). The second integral is, of course, the complex conjugate of the first integral:

$$\text{Second integral : } \int (b^* + 1) \left(\vec{E}_s^{\text{T}*} \cdot \vec{n}_s \right) \vec{E}_s da_s = (b^* + 1) V (\vec{\nabla} \vec{E}^{\text{T}*})_0 \cdot \vec{E}(0) \quad (\text{A.58})$$

$$\text{Third integral : } \int |\vec{E}|^2 \vec{n}_s da_s = V \left[(\vec{\nabla} \vec{E}^{\text{T}})_0 \cdot \vec{E}^*(0) + (\vec{\nabla} \vec{E}^{\text{T}*})_0 \cdot \vec{E}(0) \right] \quad (\text{A.59})$$

And finally the last integral:

$$\begin{aligned} \text{Fourth integral : } \int |b|^2 |\vec{E}^{\text{T}} \cdot \vec{n}_s|^2 \vec{n}_s da_s &= |b|^2 \int |\vec{E}^{\text{T}} \cdot \vec{n}_s|^2 \vec{n}_s da_s \\ &= \frac{2}{5} |b|^2 V \left[(\vec{\nabla} \vec{E}^{\text{T}})_0 \cdot \vec{E}^*(0) + (\vec{\nabla} \vec{E}^{\text{T}*})_0 \cdot \vec{E}(0) \right] \end{aligned} \quad (\text{A.60})$$

Hence, with substitution of Eqs. (A.57) – (A.60) into Eq. (A.55) gives after cancellation of some terms:

$$\begin{aligned} \vec{F}_{ex} &= -\frac{1}{4} \text{Re}\{\underline{\epsilon}_l\} V \left[b (\vec{\nabla} \vec{E}^{\text{T}})_0 \cdot \vec{E}^*(0) + b^* (\vec{\nabla} \vec{E}^{\text{T}*})_0 \cdot \vec{E}(0) \right] \\ &\quad - \frac{1}{4} \text{Re}\{\underline{\epsilon}_l\} V \left[\frac{2}{5} b b^* \left((\vec{\nabla} \vec{E}^{\text{T}})_0 \cdot \vec{E}^*(0) + (\vec{\nabla} \vec{E}^{\text{T}*})_0 \cdot \vec{E}(0) \right) \right] \end{aligned}$$

which may be written:

$$\vec{F}_{ex} = -\frac{V}{20} \text{Re}\{\underline{\epsilon}_l\} \left[b^* (2b + 5) (\vec{\nabla} \vec{E}^{\text{T}})_0 \cdot \vec{E}^*(0) + b (2b^* + 5) (\vec{\nabla} \vec{E}^{\text{T}*})_0 \cdot \vec{E}(0) \right] \quad (\text{A.61})$$

Now it is clear from the derivation with its approximations thus far, that the electric field in Eq. (A.61) is the actual electric field at the center of the sphere or body. The electric field in the sphere may be expressed in terms of the external electric field, \vec{E}_{ex} , through a multipole expansion about the center of the sphere:

$$\vec{E}(0) = \frac{3}{b+3} \vec{E}_{ex} \quad (\text{A.62})$$

$$\text{and } (\vec{\nabla} \vec{E}^T)_0 = \frac{5}{2b+5} \vec{\nabla} \vec{E}_{ex}^T \quad (\text{A.63})$$

Substitution of these relations into Eq. (A.61) gives for the total external force:

$$\vec{F}_{ex} = -\frac{3}{16} V(\underline{\epsilon}_l^* + \underline{\epsilon}_l) \left[\frac{b^*}{3+b^*} + \frac{b}{3+b} \right] \vec{\nabla} |\vec{E}_{ex}|^2 \quad (\text{A.64})$$

Now from the definition of the permittivities ratio b , we know:

$$\begin{aligned} \frac{b}{3+b} &= \frac{\underline{\epsilon}_s - \underline{\epsilon}_l}{\underline{\epsilon}_l} \times \frac{1}{3 + \frac{\underline{\epsilon}_s - \underline{\epsilon}_l}{\underline{\epsilon}_l}} \\ &= \frac{\underline{\epsilon}_s - \underline{\epsilon}_l}{\underline{\epsilon}_l} \times \frac{\underline{\epsilon}_l}{3\underline{\epsilon}_l + \underline{\epsilon}_s - \underline{\epsilon}_l} \\ &= \frac{\underline{\epsilon}_s - \underline{\epsilon}_l}{\underline{\epsilon}_s + 2\underline{\epsilon}_l} \\ &= \underline{K}_e \end{aligned} \quad (\text{A.65})$$

where \underline{K}_e is, of course, the complex Clausius–Mossotti factor; and thus Eq. (A.64) may be written:

$$\begin{aligned} \vec{F}_{ex} &= -\frac{3}{16} \left(\frac{4}{3} \pi R^3 \right) 2 \operatorname{Re}\{\underline{\epsilon}_l\} 2 \operatorname{Re}\{\underline{K}_e\} \vec{\nabla} |\vec{E}_{ex}|^2 \\ &= -\pi R^3 \operatorname{Re}\{\underline{\epsilon}_l\} \operatorname{Re}\{\underline{K}_e\} \vec{\nabla} |\vec{E}_{ex}|^2 \end{aligned} \quad (\text{A.66})$$